dynamic software & engineering

Master Thesis

Determination of Production Characteristics and Temperature Distribution of a Hot Dry Rock Geothermal Reservoir

Animesh Ranjan

Master Thesis 2015 "Applied Computational Mechanics"
Landshut University of Applied Sciences and Technical University of Ingolstadt

Landshut University of Applied Sciences

Technical University of Ingolstadt

Applied Computational Mechanics

European School of Computer Aided Technology

Master Thesis

Determination of Production Characteristics and Temperature Distribution of a Hot Dry Rock Geothermal Reservoir

Author : Animesh Ranjan

Issued on : 25.05.2015

Submitted on : 20.11.2015

First examiner : Dr. -Ing. Johannes Will

Second Examiner : Prof. Dr. -Ing. Tim Rödiger

CERTIFICATION

I certify that I have read this report and that in my opinion it is fully adequate, in scope and in quality, as partial fulfillment of the degree of Master of Engineering in Applied Computational Mechanics.

_____

Dr Ing Johannes Will

(Prinicipal Supervisor)

Acknowledgements

I would like to thank my advisor Dr Stefan Eckardt for the support and direction, along with the assistance of principal supervisors, Dr Ing. Johannes Will and Prof Dr Ing Tim Rödiger. I would also like to express my heartful gratitude to the engineering team at Jena-GEOS and the Department of Earth Sciences, TU Bergakadmie Freiberg for supporting the research work by providing valuable data and information. Additionally, I would like to recognize the efforts of the staff at Technische Hochschule Ingolstadt and Fachhochschule Landshut.
Lastly, I would like to appreciate the support of my colleagues and my family who encouraged me to fulfill my goals timely.

Animesh Ranjan

Abstract

The thesis focuses on simulation of the fracturing process and the post-fracturing production characteristics of a Hot Dry Rock Geothermal reservoir. Most of currently explored geothermal resources are embedded in dry and impermeable rock which can only be exploited through the process of hydraulic stimulation. Post stimulation phase, a production cycle is employed, which is the primary cycle, used in the extraction of useable energy. The profitability of a hot dry rock Geo-thermal reservoir is dependent on the location of the injection and production wells, the corresponding heat exchanger area and the temperature profile developed over the designated life cycle of the reservoir. The study focuses on an integrated simulation procedure of the complete operation cycle of such a Geo-thermal reservoir, based on Dynardo's hydraulic fracturing simulator. The fracturing simulation is based on a homogenized continuum approach for fluid flow in jointed rock, supplemented by a production cycle which involves an unloading cycle and re-injection and extraction through the production and injection well respectively. The production characteristics such as heat exchanger area, connected height of the fractures and pressure losses are estimated through the production cycle. Additionally, a 3D transient thermal simulation is carried out to estimate the temperature distribution over a period of 30 years. The basis of the thermal simulation is the application of a heat/mass transport scheme with a developed artificial diffusivity algorithm. Considering the homogeneity assumption and the uncertainties in procuring reservoir data for the simulator, the study will be backed by a Design of Experiments and Sensitivity study. Proposed software include ANSYS in conjunction with MultiPlas and optiSlang, a material model library and a stochastic analysis software respectively.

Keywords : Geothermal Simulation, Enhanced Geothermal Systems, Thermo-hydro-mechanical Analysis

KURZFASSUNG

Die vorliegende Masterarbeit beschäftigt sich mit dem Risserzeugungsprozess und den Produktionseigenschaften eines Hot-Dry- Rock-Geothermischen Reservoirs. Die meisten der neuentdeckten Reservoire befinden sich in trockenen und undurchlässigen Gesteinen, die nur durch eine hydraulische Wasserinjektion aktiviert werden können. Nach dem Risserzeugungsprozess erfolgt der Produktionsvorgang, bei dem die nutzbare Energie extrahiert werden kann. Die Effektivität der Energiegewinnung hängt von der Position der Injektions- und Produktionsbohrlöcher, durch hydraulische Stimulierung erzeugten Wärmetauschergebiet und dem unterirdischen Temperaturübergang während der Betriebsdauer des Reservoirs ab. Die vorliegende Untersuchung stellt einen integrierten Simulationsansatz der Stimulierung sowie des gesamten Betriebsdurchlaufs eines geothermischen Kraftwerks nach dem homogenisierten Kontinuumsansatz der Wasserströmung in geklüfteten Felsgestein einschließlich des Wärmetransportes vor. Die Produktionseigenschaften, z.B. das Wärmetauschergebiet, die Ausdehnung der Risse und Druckverluste, werden rechnerisch ermittelt und mittels Sensitivitätsstudien untersucht. Alle Simulationen werden mit ANSYS+Dynardos Erweiterungen für Rissentwicklung und Wasserströmung im geklüfeten Felsgestein sowie optiSLang durchgeführt.

Schlüsselwörter: Geothermische Simulation, Hydraulisch-Mechanisch-Thermische Analyse, Enhanced Geothermal System

Contents

Nomenclature

J	Hydraulic Conductivity Matrix [m/s]
ε	Plastic Strain Vector [dimensionless]
λ	Plastic multiplier [dimensionless]
Q	Plastic Potential [Pa]
κ	Hardening/Softening Modulus [Pa]
q	Darcy Flux Vector [m/s]
R	General source-sink term [s^{-1}]
S_s	Specific Storage [m^{-1}]
h	Hydraulic Height [m]
K	Conductivity matrix [m/s]
γ	Specific Gravity [dimensionless]
μ	Dynamic Viscosity [cP]
S	Joint Distance [m]
R_c	Joint Roughness Coefficient [dimensionless]
ρ	Density [kg/m^3]
c_p	Heat Capacity [J/kg K]
$\vec{u}$	Velocity vector [m/s]
Φ	Porosity [dimensionless]
EGS	Enhanced Geothermal Reservoir
APDL	Ansys Parametric Design Language
HDR	Hot Dry Rock

List of Figures

List of Tables

Chapter 1

Introduction

1.1 Energy Consumption

Energy consumption in the world has seen an ever increasing upward trend since the early part of the 20^{th} century. According to a key report by the International Energy Agency published in 2014 (IEA, 2014 [12]) the world energy consumption has doubled from 4672 Mtoe in 1973 to 8979 Mtoe in 2012 (1Mtoe = 41.87 Million Gigajoules). A major chunk of the total energy supply comes from non-renewable energy resources with approximately 66% supplied only by crude oil, natural gas and coal reserves. The large share of these resources are not just restricted to developing economies such as China, Brazil, etc but also economic powerhouses such as USA and the European Union. This has further led to an exponential rise of CO_2 emissions, which have doubled from 15,633 Million Tonnes (MT) to 31,734 MT in the last 40 years. Incidentally, the aforementioned energy resources are responsible for 99.5% of the total emissions. Although, new energy policies aim at restricting the average global temperature increases to 2 degree centigrade, the emission level is expected to rise upto 37, 242 MT by 2035 i.e. much higher compared to 21,568 MT to restrict it to desired level.

Hence, in the wake of global warming, there is a growing need to harness energy resources which do not produce greenhouse gases. Consequently, there is a greater focus on alternative resources such as Geothermal Energy, Wind En-

ergy, etc. The major challenge, however, is to maintain global energy needs and develop safe, economical and environmental friendly technologies for wider acceptance of such energy resources.

1.2 Hot Dry Rock/Enhanced Geothermal Systems

Geothermal Power systems aim to extract the inexhaustible heat available beneath the earth's surface. Since the early part of the 20^{th} century, when the first geothermal power generator was tested at Larderello dry steam field, the utilization of Geothermal energy for power generation has increased manifolds, leading to 11,700 MW of effective power available in 2013 (Geothermal Capacity, BP Global 2013 [3]). Geothermal Power benefits from having a very high load factor since it is barely influenced by seasonal effects which gives it a distinct advantage over other renewable sources like solar energy, wind energy, etc. Moreover, the emissions resulting from a Geothermal Power System is minimum and the cost is highly competitive in the range of 4-10 cent/KW.hr (Bertani et al, 2007 [2]). Despite distinct advantages, Geothermal Energy suffers from the following disadvantages :-

- Viable sources of Geothermal Energy are sparse
- Initial cost of plant installation, including skilled labour costs are very high.
- Fluid Pumping rate into the wells should be optimal to allow extraction for extended periods of time.
- Open-Loop Geothermal systems, where emissions are exposed to the atmosphere, can also contribute to greenhouse gases. Although, the overall

percentage of harmful fumes from a Geothermal reservoir are much lower compared to coal plants.

An alternative to reducing dependence on naturally occuring hydrothermal reservoirs is using Hot Dry Rock/Enhanced Geothermal Systems (EGS). EGS reservoirs are set-up by drilling wells beneath the earth's surface and creating an artificial permeable fracture network between the wells. Fluid flowing through the permeable fracture network, captures heat from the in-situ rock and escapes the reservoir through the installed Production wells. In a closed loop system, the fluid reaching the surface and subsequently leaving the power plant is re-injected through the injection wells, leading to no emissions. A schematic figure is shown in figure 1.1.

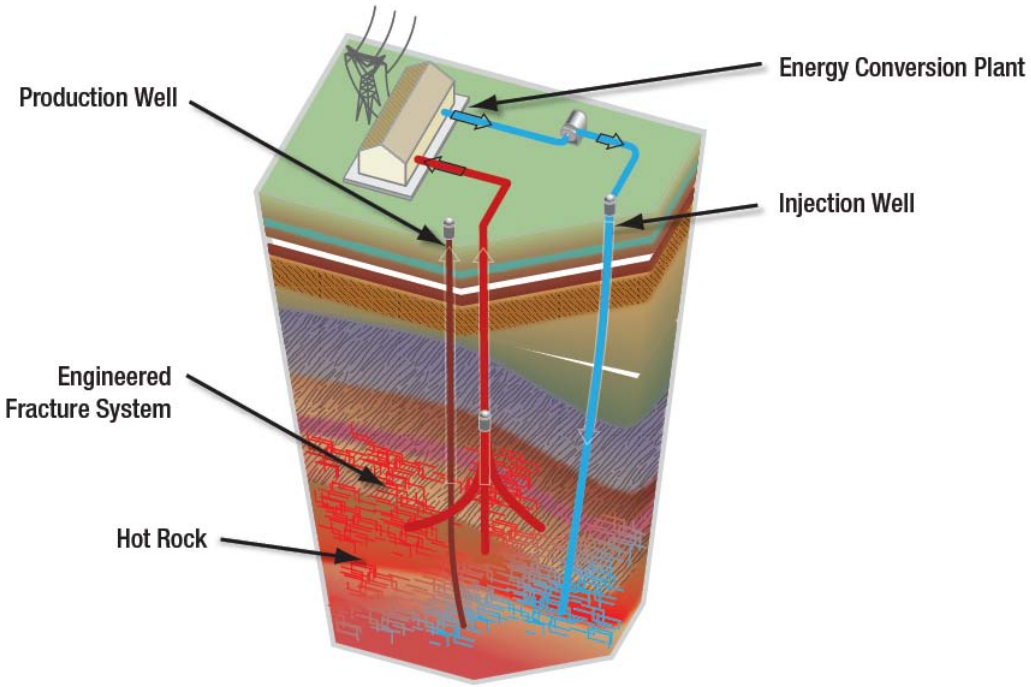

Figure 1.1: Schematic figure of an EGS system

The EGS process has two main major subprocesses :-

- *Hydraulic Fracturing Cycle*
- *Production Cycle*

1.2.1 Hydraulic Fracturing Cycle

Hydraulic Fracturing is a well-stimulation technique used for creating artificial reservoirs by creating a network of permeable fractures between injection and production wells. The process has been successfully applied over decades on oil and gas reservoirs located in layered rock formations with low permeability like the Barnett Shale in Texas, United States. With the development of new fracturing techniques, the production of natural gas has increased over 50 times in a period of 10 years and it continues to make otherwise unfeasbile shale reservoirs economically productive.

A typical hydraulic fracturing cycle involves water injection at a suitable flow rate, leading to a higher pressure level than the initial pore pressure gradient in the reservoir. The injected fluid percolates through fault lines and fractures within the rocks, thereby creating a permeable fracture network in and around the borehole. In order to prevent the fractures from collapsing and the resulting fracture openings from closing, a proppant is placed into the stimulated reservoir which allows oil or gas to flow up to the well. The process is carried out using cased boreholes while the fluid injection regions are generated by creating perforations in the casing. The injection fluids used are typically a mixture of water, proppant materials such as sand, ceramics or special gels or foam and other chemicals. The fracturing fluid also influences the extent and intensity of generated fractures. With a higher flow rate and a lower viscosity, the distribution of fractures is wider in contrast to a fracturing cycle with a

fluid of a higher viscosity which leads to large dominant fractures. Monitoring a hydraulic fracturing process is based on measurements of fluid flow rate and pressure levels. There are other tracking techniques such as radiotracers and the more widely used microseismic monitoring which can be used to estimate the size and orientation of induced fractures.

The Fracturing cycle in an EGS reservoir is a bit different to fracturing in an oil or gas reservoir. The process, more commonly referred to as Hydro-shearing(Pierce, 2010 [21]) aims to generate slips between rocks by inducing shear failure in contrast to Hydraulic Fracturing in oil or gas reservoirs where fluid is injected at a very high pressure, along with a proppant mixture, to break the rock and maintain the created openings.

1.2.2 Production Cycle

The Production Cycle directly follows the fracturing cycle with a prescribed unloading time in a stimulated reservoir. During the Production cycle, the injection process is repeated but at a much lower flow rate, comparable to fluid flow rates in conventional geothermal reservoirs. The injection procedure allows fluid to flow through the permeable fracture network, absorbing heat from the surrounding rocks. During the Production cycle, there is a significant pressure loss due to flow resistance in the reservoir. This flow resistance also referred to as the impedence is a function of the fracture opening which further depends on overall pressure levels in the fracture network, temperature of surrounding rock and other geo-physical effects such as sliding of fracture planes along the faces of the fracture surface(Hirakawa, 2012 [19]).

During Fracturing and Production, there is a loss of fluid depending on the pressure gradient in the reservoir, the fluid flow rate and the permeabiliity of the rock layers itself. This loss, coined as the Leak-off volume plays a major role in determining the overall pumping efficiency of the reservoir and is hereby a useful measure in EGS calculations. Test runs of the first EGS reservoirs were

carried out in the early part of 1970s at Fenton Hill, New Mexico and subsequent activities were carried out in other parts of Europe and Australia. The largest EGS plant is currently being supervised by Geodynamics Ltd in the Cooper Basin, north eastern South Australia (Bendall, 2012 [1]).

1.3 Disadvantages and Associated Risks

The functional efficiency of a EGS reservoir is dependent on the individual efficiencies of the Fracturing and Production Cycles. Using efficient drilling techniques and advanced well completions, an EGS reservoir could achieve its true potential with minimal losses. However, the challenges and risks associated with establishing an EGS system and its continual functioning, serve as a deterrent to widespread usage of the technique.

- **Initial Costs** - EGS reservoirs are typically located at a depth of 3-10 km below the earth's surface. The initial cost of drilling wells at such low depths leads to very high establishment costs. In order to make it an economically profitable avenue, an EGS reservoir should be able to provide continuous output over a period of 30-50 years. Lower lifecycles would lead to tremendous losses for firms and associated contractors.
- **Well Connection** - Estimation of reservoir characterisitics is an intensive R&D exercise in an EGS reservoir. Insufficient and improper reservoir data may lead to poor connections between the Injection and Production wells. Hence, even though the Fracturing cycle might have successfully finished, the Production cycle may not provide expected output.
- **Induced Seismicity** - The stimulation process leads to seismic activities below the earth's surface. The seismic waves, induced due to such a process, are generally low and are usually not felt at the earth's surface. However, instances of earthquakes due to induced seismicity from

the stimulation process have been recorded at several places. These include the HDR geothermal project in Basel (Glanz, 2009 [7]) which caused several tremors, the largest one measuring 3.4 on the Richter scale. The project was terminated in light of potential future earthquakes.

- **Short Circuiting** - In order to save costs, supplemented with unavailability of good prediction tools, EGS reservoirs are often used with open hole wells. Open hole wells have larger uncased sections which lead to localized, dynamic effects near the borehole. This pressure and temperature distortion (Deo, 2013 [4]) near the borehole is also referred to as short-circuiting of the well.

1.4 Thesis Objective

In the thesis work, an effort has been made to analyse a prospective Enhanced Geothermal System in Meiningen and Suhl, South-west Thüringen. The project is being carried out as a co-operative study between Das Deutsche-Brennstoffinstitut (DBI), Bergakademie TU-Freiberg, Jena-Geos GmbH and Dynardo GmbH. Experiments and simulation parameter data have been obtained from trials by Jena-Geos GmbH or through reliable literature data. The project follows the aforementioned operation cycles :

- Hydraulic Fracturing Process (Hydro-shearing)
- Reservoir-Unloading & Production Cycle
- Energy output estimation over a stipulated Geothermal life-cycle

Figure 1.2 illustrates the stress field map in the regions around Meiningen - Suhl. The legends denote various categories representing the quality of measured stress gradients at these regions with Category A having the highest quality or most

accurate results (within ± 15°) and C having the lowest quality or least accurate results (within ± 20-25°). Tunnel-hill indicate presence of a tunnel which implies modified stress regimes at these regions and and stress trajectories represent stress isolines across which the stress gradients are equal. (*For more details, refer to Appendix A*)

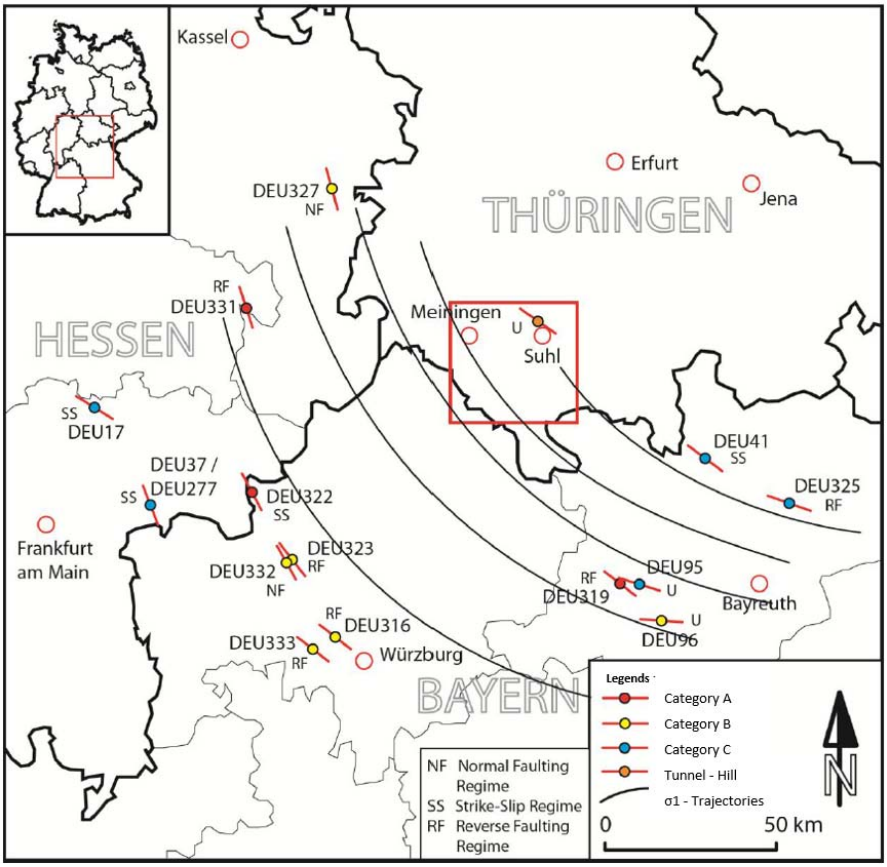

Figure 1.2: Stress-field map of South Thüringen, North-east Bayern and East Hessen (Heidbach, 2008 [11])

Chapter 2

Reservoir Stimulation

Advanced measurement technologies such as micro-seismic mapping are reliable tools to estimate well performance in the stimulation process. However, measurement tools are not a medium for prediction and considering the exaggerated costs and risks to life and property, there has been a growing demand for reliable mathematical modelling and computer simulations of the fracturing process. A hydraulic fracturing simulator is a cost-effective tool for evaluating different loading conditions, perforation cluster combinations, stage spacing, etc. The ability to forecast the growth and extent of fractured volume is, however, dependent on the reliability of well log data and the intricate modelling of various physical effects involved in the process.

2.1 Physical Phenomena

The modelling of a physical phenomena is largely influenced by the prevalent stress-state and associated material characteristics. In case of complex reservoirs, where the stress states are anisotropic, the structure is layered and contains jointed rock formations, the need for a 3D simulation is recognized by the oil and gas community. According to a technical report (Weijers, 2007 [27]), a simulation program should possess the following three characterisitics :-

- A 3D simulation model should incorporate the anisotropic stress distribution, anisotropic material properties and joint/fracture orientation.
- Fracture extension through layered reservoirs and along layer interfaces should be well simulated.
- The fracture model should incorporate reservoir parameters such as in-situ stresses, initial pore pressure distribution and mechanical rock parameters like strength of intact and jointed rocks.

Hence, the three major physical phenomena occuring in the stimulation process described in the following section need to be well represented :-

- Fluid Flow in Jointed Rocks
- Rock permeabilitiy and Hydraulic conductivity update due to fluid flow
- Opening and closure of in-situ rocks or fractures created during the stimulation cycle.

2.2 Rock Mechanics - Homogenized Continuum

The jointed rock framework in a layered reservoir represents a highly discrete phenomena in nature. However, modelling the individual layers and the intact & jointed rocks as a discrete model is not only a modelling nightmare but also computationally expensive. Discrete element models have been developed which are based on the discrete modelling approach (Meyer, [17]) but in most cases, such simulators need fracture dimensions as a pre-requisite besides being computationally uneconomical. This rules out the possibility of using such simulators as a predictive tool for the stimulation phase. Hence, a homogenized continuum approach resolving intact rock and joints in a smeared manner, holds the key for an economical and accurate simulation tool. The translation of such

a discrete fracture network to a homogenized element is shown in figure 2.1. The continuum approach, used initially in dam engineering, does not model joints in a discrete manner. In contrast, a representative volume element is assumed containing a matrix (intact rock) and zones of weakness (joint sets). The computation of the intact rock and the joints are evaluated at each discretization point with each joint set having its own orientation and strength definitions.

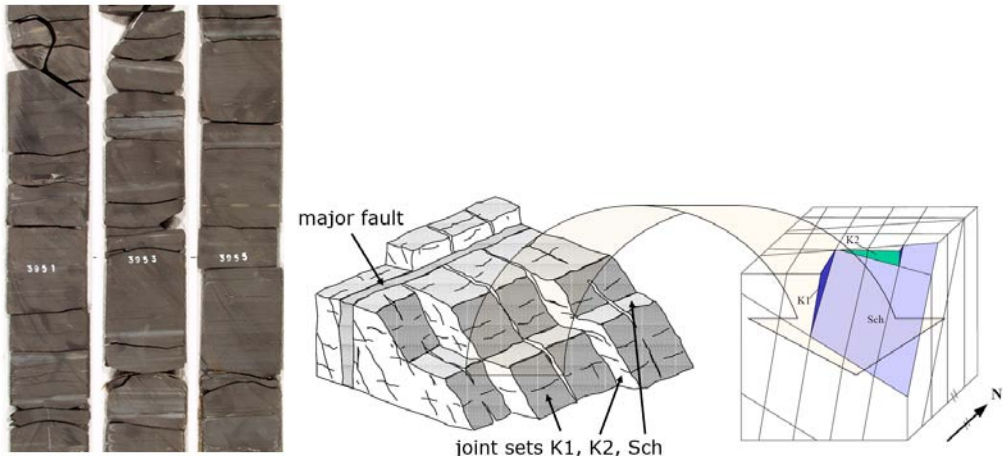

Figure 2.1: Planes of Weakness and Joint Modelling. Taken from Wittke, 1990 [31]

The constitutive model for jointed rock is available with multiPlas, a multi-surface plasticity material library. Using rate-independent plasticity models (mulitPlas, 2015 [18]), the material model for jointed rocks divides the total strain into an elastic and plastic part.

$$\{\epsilon\}^{total} = \{\epsilon\}^{el} + \{\epsilon\}^{pl} \tag{2.1}$$

where

$\{\epsilon\}^{el}$- elastic strain vector

$\{\epsilon\}^{pl}$- plastic strain vector

The plastic strain increment is calculated after the stress exceeds the yield criteria using the following flow rule :

$$d\epsilon^{pl} = \lambda \frac{\partial Q}{\partial \sigma} \tag{2.2}$$

where

λ - plastic multiplier

Q - Plastic Potential [Pa]

The yield criteria itself is given by :

$$F\left(\{\sigma\}, \kappa\right) \leq 0 \tag{2.3}$$

where

$\{\sigma\}$ - stress vector [Pa]

$\varkappa$ - hardening or softening parameter [Pa]

The definition of the plastic multiplier and the concept of plasticity implies that plastic flow can only take place only if the material is in a plastic state. This is given by the condition :

$$\dot{\lambda} f\left(\sigma, q\right) = 0 \tag{2.4}$$

Equation 2.4 has two inherent implications (Jirásek, 2000 [13]). Materials in their elastic state fulfill the criteria $f < 0$ but the plastic strain and hardening variables assume a constant value. On the other hand, under plasticity, the yield criteria is fulfilled through $f = 0$ but there is no restriction on the plastic multiplier itself. Yet, the plastic multiplier can never assume a negative value which leads to additional constraint equations, given by Kuhn-Tucker condition (*see eq 2.7*).

The yield condition, (*see eq* 2.3) is only a single additional equation for the determination of six individual components of plastic strain. Hence additional rules need to be formulated such as the flow rule given in eq 2.2. The most basic assumption of the flow rule is an associative one with a convex yield surface that obeys the normality rule, i.e. the direction of plastic strain is normal to the yield surface, as shown in figure 2.2.

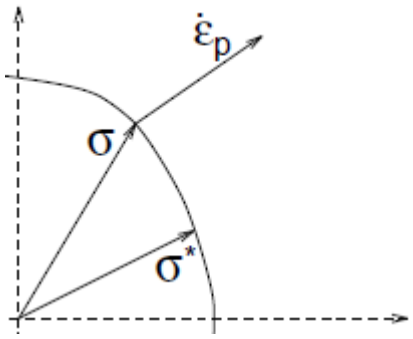

Figure 2.2: Normality and Convexity in associative Flow rule

The above assumptions imply that the plastic strain always grows in the direction normal to the yield surface. It is represented mathematically by :

$$\dot{\epsilon_p} = \dot{\lambda}\frac{\partial f}{\partial \sigma} \tag{2.5}$$

Although associative flow rule eases mathematical complexity in terms of model implementation, materials obeying pressure dependent laws do not exhibit associative rule behaviour. Infact, associative rules tend to over-estimate volumetric strains which led to development of a non-associative flow rule. Dilatancy effects, which are especially influential during shear failure can be introduced using the non-associative flow rule, i.e.

$$\dot{\epsilon}_p = \dot{\lambda}\frac{\partial q}{\partial \sigma}; \quad Q \neq F$$

The hardening/softening functions describe the eventual movement and growth of the yield surface within the stress space. Yet, due to lack of reliable experimental data, complicated relationships are avoided and following formulation is used :

$$d\kappa = d\kappa\left(\epsilon^{pl}\right) = d\epsilon^{pl}_{eq}$$

In the implementation of the algorithm itself, firstly a trial state of stress is computed based on the known parameters. When this computed trial stress state violates the yield surface criteria, a return-mapping algorithm (Simo, 1998 [26]) is used which re-traces the trial stress to the yield surface. The two-step process is outlined as follows :

1. $\sigma^{\mathbf{trial}} = \mathbf{C}\left[\epsilon^{\mathbf{total(n)}} + \mathbf{\Delta}\epsilon^{\mathbf{tot(n+1)}} - \epsilon^{\mathbf{pl(n)}}\right]$, where $\boldsymbol{\varepsilon}^{\mathbf{total(n)}}$ and $\boldsymbol{\varepsilon}^{\mathbf{pl(n)}}$ are total strains and plastic strains respectively at a known, previous step and $\mathbf{\Delta}\boldsymbol{\varepsilon}^{\mathbf{total(n+1)}}$ is a given strain increment.
2. $\frac{\mathbf{d}\sigma}{\mathbf{d}\lambda} = -\mathbf{D}\frac{\partial \mathbf{Q}}{\partial \sigma}$, denotes the plastic corrector step which is responsbile for returning the stress path back to the yield surface.

The material failure phenomena falls under the purview of multi-surface plasticity since the yield surface is built up considering failure mechanisms of the intact rock and different joint sets (Will, 2010 [30]). This leads to a non-smooth, complex yield surface in the stress space (see figure 2.3) . The flow rule and hardening/softening rule, when combined with the various individual yield criteria, is rewritten as :-

$$\mathbf{\Delta}\epsilon^{\mathbf{pl}} = \sum_{\alpha=\mathbf{1}}^{\mathbf{n_{YC}}} \mathbf{\Delta}\lambda^{\alpha}\frac{\partial \mathbf{Q}_{\alpha}}{\partial \sigma}, \qquad \Delta\kappa = \sum_{\alpha=1}^{n_{YC}} \Delta\lambda^{\alpha} h^{\alpha} \tag{2.6}$$

where

n_{YC} represents the total number of yield surfaces and h represents the hardening/softening modulus.

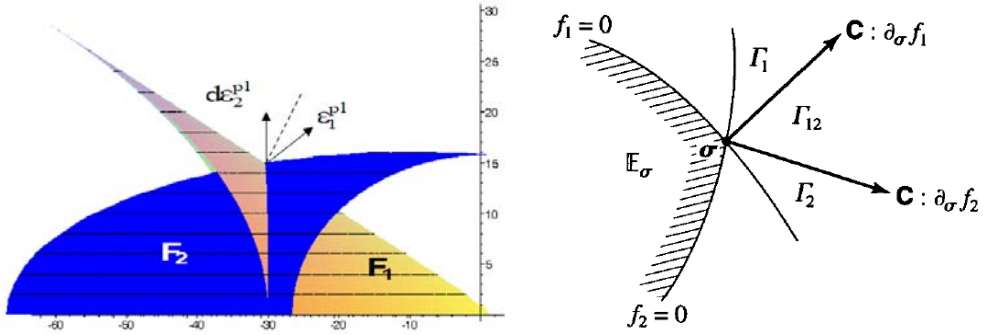

Figure 2.3: Multi-surface Plasticity - Intersection of Individual Yield Surfaces

Every individual yield criteria has to satisfy the Kuhn-Tucker conditions

$$F_\alpha(\sigma, \kappa) \leq 0 \quad \Delta\lambda^\alpha F_\alpha = 0 \quad \Delta\lambda^\alpha \geq 0 \quad \alpha = 1...n_{YC} \tag{2.7}$$

Not all yield surfaces remain active at the same time. Yield surfaces that are inactive do not contribute to eq 2.6. A similar rule is applied to the hardening equations. The choice of active yield surfaces is hence based on the number of positive plastic multipliers. In the end, all active yield functions have to be zero.

$$F_\alpha(\sigma, \kappa) = 0 \qquad \forall \alpha : F_\alpha \in \mathcal{L}$$

where $\mathcal{L}$ is the set of active yield surfaces

The above equations lead to a non-linear system of equations, including several singularities at interesections between the yield surface. Compared to single surface plasticity, under multi-surface plasticitiy, the plastic multiplier has to be additionally positive for every time-step along with the stress state meeting the yield criteria for an active joint set. A stress - return algorithm, responsible for the correction step in the predictor-corrector step, needs to be implemented. The closest point projection and the cutting plane algorithm are implicit and

explicit return algorithms repsectively that have been employed in multiPlas. The material laws used in the hydraulic fracturing simulation is shown in figure 2.4

$$\Delta\lambda^{\alpha} \geq 0 \qquad\qquad \alpha = 1...n_{YC}$$

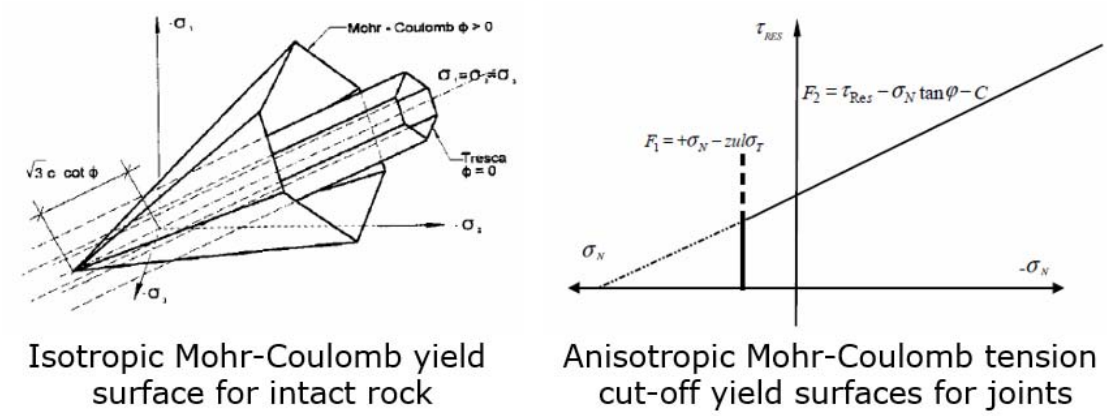

Figure 2.4: Multiple flow criteria under multi-surface Plasticity

2.3 Fluid Flow in Porous Medium

The hydraulic analysis in the stimulation process deals with simulation of fluid flow in the fracture network. The flow is laminar in nature and mainly occurs in the initiated or re-opened joint system. Hence, this process can be simulated using Darcy's law for porous media (see figure 2.5). However, to capture the complete flow behavior, fluid flow in intact rock and jointed rocks need to be super-imposed. This leads to the definition of an anisotropic hydraulic conductivity. Consequently, along with the mass and momentum balance equation, the groundwater flow equation could be used to solve and simulate fluid flow in porous media.

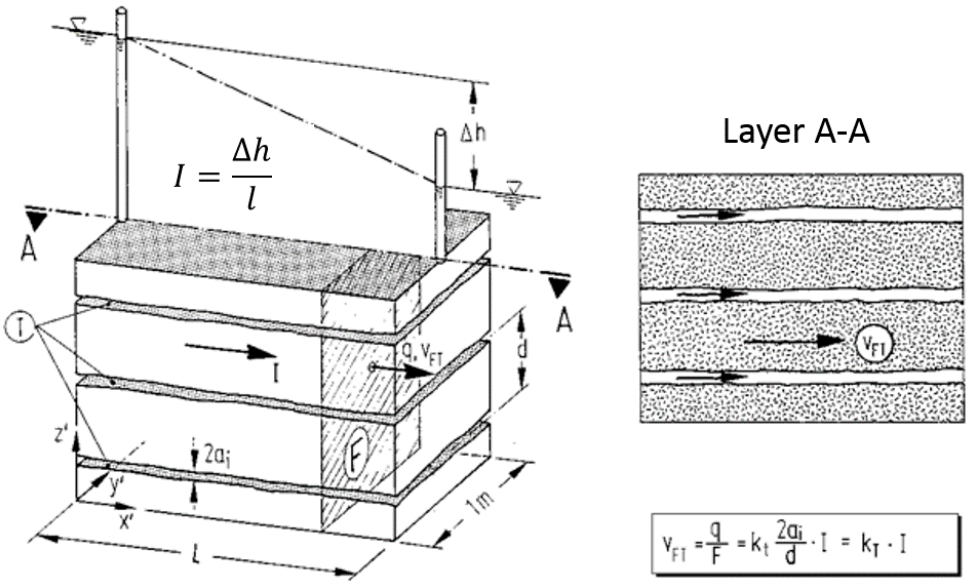

Figure 2.5: Laminar Flow in Multiple parallel plates (Wittke, 1990)

The governing equations for fluid flow are given below :-

Mass balance

$$-\nabla.\mathbf{q} + R = S_s \frac{\partial h}{\partial t} \tag{2.8}$$

Momentum Balance (Darcy's law)

$$\mathbf{q} = -\mathbf{K}.\nabla h \tag{2.9}$$

Groundwater Flow Equation

$$\frac{\partial}{\partial x}\left(\mathbf{K}_{xx}\frac{\partial h}{\partial x}\right)+\frac{\partial}{\partial y}\left(\mathbf{K}_{yy}\frac{\partial h}{\partial y}\right)+\frac{\partial}{\partial z}\left(\mathbf{K}_{zz}\frac{\partial h}{\partial z}\right)+R=S_s\frac{\partial h}{\partial t} \tag{2.10}$$

where **q** represents the Darcy flux [m/s],

R is the general source/sink term [1/s],

K is the hydraulic conductivity [m/s],

$S_s$is the specific storage [1/m] &

h is the hydraulic height [m].

The actual flow velocity is given by :

$$v_{FT}=\frac{\mathbf{q}}{A}=k_{TF}\frac{2a_i}{d}I, \qquad \{v_{FT}\}=\mathbf{K}\{\mathbf{I}\}$$

where V_{FT}- Flow velocity [m/s],

K - anisotropic permeability tensor of rock mass [m/s]

$2a_i$- Joint thickness / Joint opening [m]

A - cross-section [m^2]

d - Joint frequency

The anisotropic hydraulic conductivity tensor is a combination of transverse isotropic hydraulic conductivity matrix of the intact rock $(\boldsymbol{K_{Rh}})$ which is diagonal in the global co-ordinate system and transverse isotropic joint hydraulic conductivity matrix $(\boldsymbol{K_{Jk(\alpha k,\beta k)}})$ which no longer remains diagonal when transformed into the global space.

$$\underbrace{\begin{bmatrix} K_{xx} & K_{xy} & K_{xz} \\ K_{xy} & K_{yy} & K_{yz} \\ K_{xz} & K_{yz} & K_{zz} \end{bmatrix}}_{TotalConductivity} = \underbrace{\begin{bmatrix} K_{Rh} & 0 & 0 \\ 0 & K_{Rh} & 0 \\ 0 & 0 & K_{Rh} \end{bmatrix}}_{IntactRock} + \underbrace{\begin{bmatrix} K_{J1(\alpha_1,\beta_1)} & 0 & 0 \\ 0 & K_{J1(\alpha_1,\beta_1)} & 0 \\ 0 & 0 & K_{J1(\alpha_1,\beta_1)} \end{bmatrix}}_{JointConductivity1} + \begin{bmatrix} K_{J2(\alpha_2,\beta_2)} & 0 & 0 \\ 0 & K_{J2(\alpha_2,\beta_2)} & 0 \\ 0 & 0 & K_{J2(\alpha_2,\beta_2)} \end{bmatrix} + ... \quad (2.11)$$

2.4 Coupling Equations

The hydraulic and mechanical models represent the fluid flow phenomena and the jointed rock failure mechanism respectively. Yet, the two systems are not standalone in nature since each process has a significant impact on the other. As a result, coupling equations are required to connect the two phenomena and complete the system of equations. The coupling mechanism illustrated in the following section is explicit in nature which allows for an easier implementation in the finite-element environment. To maintain the stability of the coupling equations, it has to be ensured that the change of state variables of a given model over a particular time-step is small enough. This is, however, fulfilled in each of the systems since the change in pore-pressure gradient or the stress-state is not very large except for the initialization phase where lower time-steps are necessary.

2.4.1 Hydraulic - Mechanical Coupling

The hydraulic fracturing process begins with a transient fluid analysis which leads to variation of the prescribed initial pore pressure gradient in the reservoir field. The change in the hydraulic height leads to normal and shear forces on the joint walls, also referred to as flow forces which has 3 directional components. The summation of the 3 components provides a global force which is further

applied to the mechanical model as a Neumann boundary condition.

$$\sum_{3}^{i=1} \tau_i = V \sum_{3}^{j=1} -\Delta h_j . \gamma \tag{2.12}$$

where τ_i - i^{th} component of flow force [N]

Δh_j - j^{th} component of component of hydraulic height gradient

γ - Specific gravity [N/m^3]

V - Element Volume [m^3]

2.4.2 Mechanical - Hydraulic Coupling

Flow forces resulting from the hydraulic analysis, when transferred to the mechanical model, result in plastic strains and stresses in the model. Normal plastic strains from the mechanical model result in a joint opening which, in-turn, impact the fluid flow through a joint set. In other words, altering the fluid flow based on the joint opening requires a dependence between joint opening and joint hydraulic conductivity. Such a relationship has been established by Louis C, 1969 [16] and is redefined for the fracturing phase. It is given by

$$K_{J0} = \frac{\gamma e^3}{\mu 12 S R_c} \tag{2.13}$$

where,

K_{J0} - Stress-independent Hydraulic conductivity [m/s]

γ - Specific weight of fluid [N/m^3],

μ - Viscosity of fluid [cP]

e - Hydraulic opening[m],

S - Joint Distance [m] &

R_c - Joint Roughness Coefficient

Here, e and K_{J0} represent the hydraulic opening and the stress-independent component of Joint hydraulic conductivity respectively. A reasonable assumption for hydraulic opening is $\left(\frac{Mechanical Opening}{2}, Mechanical Opening\right)$. The joint hydraulic conductivity comprises of two parts :

- Stress-independent hydraulic conductivity or K_{J0}- The distribution of the stress-independent part is defined by the cubic law (Louis, 1969) while the maximum value is bounded by a maximum hydraulic conductivity calculated from a corresponding maximum hydraulic opening.

$$0 \leq K_{J0} \leq K_{max} \qquad K_{max} = \frac{\gamma e_{max}^3}{\mu 12 S R_c}$$

- Stress-dependent hydraulic conductivity - With increasing compressive stress, the hydraulic conductivity of the joint increases. Such a relationship (Gangi, 1978 [6]) incorporates the effect of stress state on the hydraulic conductivity more effectively. Figure 2.6 illustrates the relationship between normalized stress and normalized conductivity values.

$$K_J = K_{J0} \begin{cases} 1 & \sigma_N \gtrsim 0 \\ \left[1 - \check{K}_{min}\left[1 - \left(\frac{\sigma_N}{D}\right)^{\frac{1}{n}}\right]^2 + \check{K}_{min}\right] & D \leq \sigma_N \leq 0 \\ \check{K}_{min} & \sigma_N \lesssim D \end{cases} \tag{2.14}$$

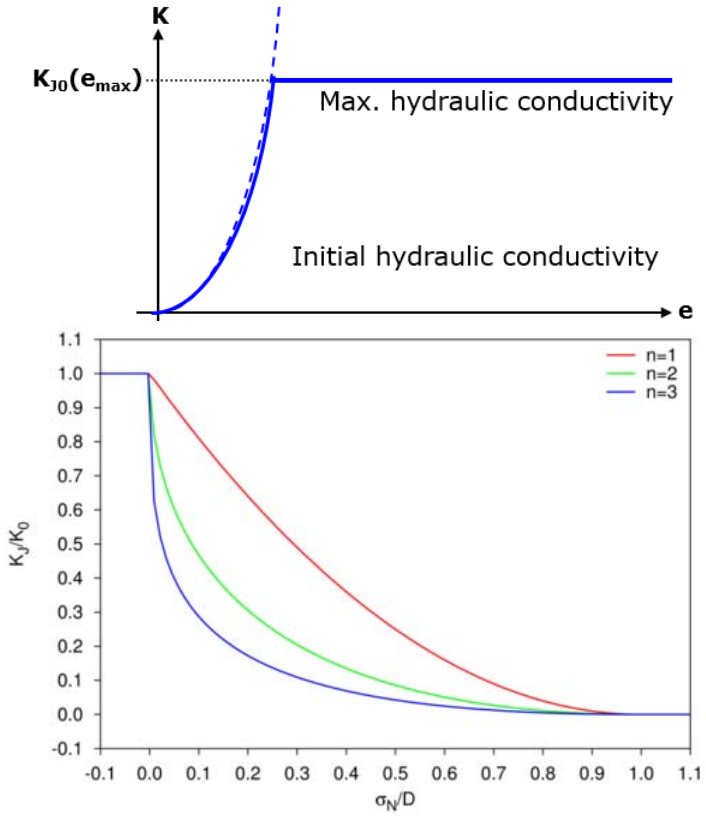

Figure 2.6: Stress-independent and Stress-dependent hydraulic conductivity

Chapter 3

Hydraulic Stimulation Cycle

The stimulation process, illustrated in figure 3.1, is carried out using a 3-D coupled hydro-mechanical simulator with each of the governing equations representing a physical phenomena in the hydraulic fracturing process. The process chain includes three major steps :

- Initialization
- Transient Analysis
- Reservoir-relevant Post Processing

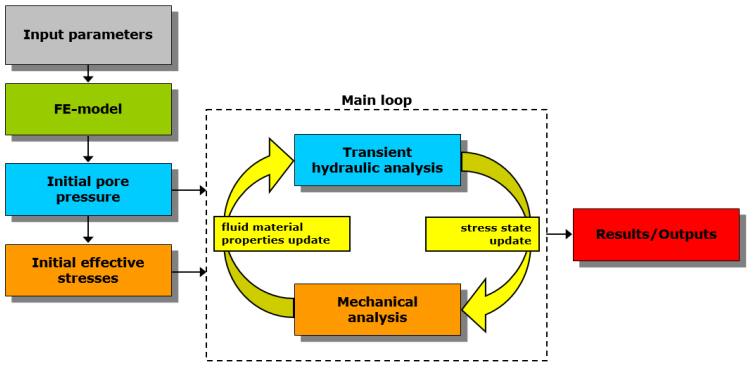

Figure 3.1: Hydraulic Fracturing Process Chain

3.1 Meiningen - Suhl Reservoir Model

The Meiningen - Suhl reservoir model is based on a 1 Well - 3 Stage model. The landing depth is defined at 4500 m with a single fracture perforation. A schematic is illustrated in figure 3.2. The conglomerate formation beyond 3000 m is not modelled in the FE-environment in order to reduce complexity, assuming that vertical fracture extension is not longer than 1500 m (See figure 3.3).

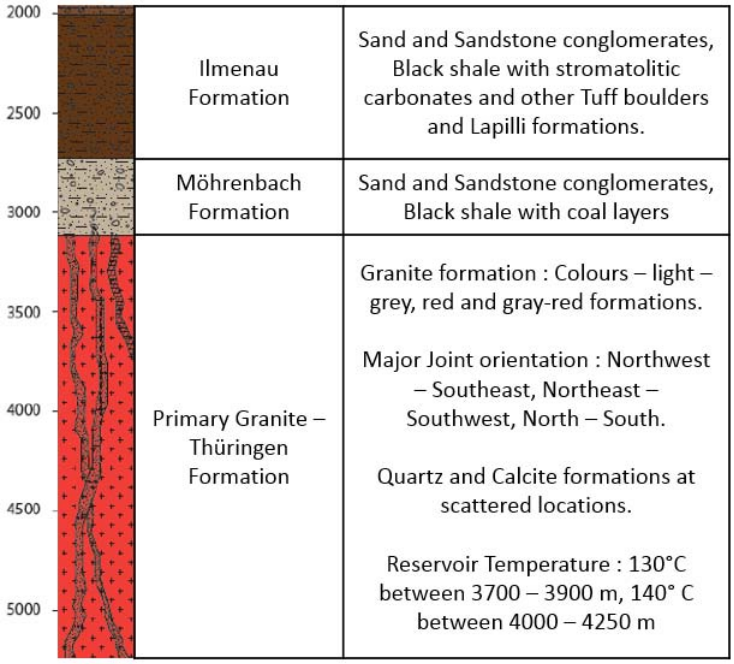

Figure 3.2: A schematic of reservoir layers in Meiningen/Suhl (DBI Input Sheet, 2013)

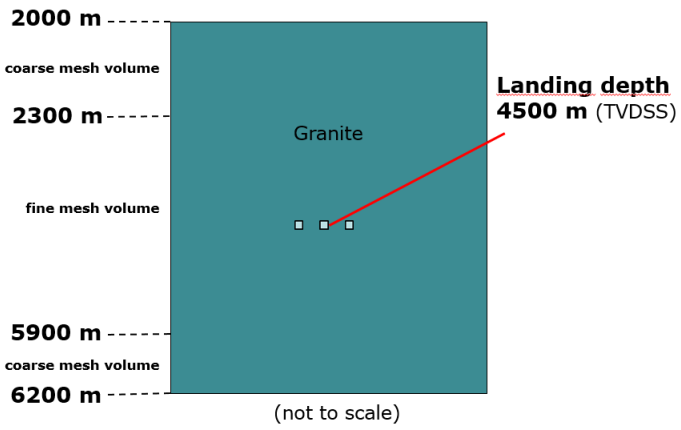

Figure 3.3: A schematic of reservoir layers in Meiningen/Suhl - FE Model

A list of important reservoir and operational parameters obtained from experiments and/or literature data is tabulated in Table 3.1 and Table 3.2.

Parameter	Value	Units
Operational Parameters		
Water Injection Rate	0.0833	m^3/s
Injection Time/Stage	1000	min
Dynamic Viscosity	1	cP
Well Azimuth	70.0	^{o}(deg)
Well Dip	0.0	^{o}(deg)
Reservoir Parameters		
Initial Pore Pressure Gradient	10.66	kPa/m
Total Vertical Stress Gradient	35.10	kPa/m
Minimum Total Horizontal Stress Gradient	29.80	kPa/m
Maximum Total Horizontal Stress Gradient	60.90	kPa/m
Minimum Horizontal Stress Direction	60	^{o}(deg)
Maximum Horizontal Stress Direction	90	^{o}(deg)

Table 3.1: Reservoir & Operational Parameters for Meiningen/Suhl

Parameter	Value	Units
Material Parameters - Granite		
Youngs' Modulus	77.62	MPa
Poissons' Ratio	0.1	-NA-
Friction Angle	41.8	^{o}(deg)
Dilatancy Angle	15	^{o}(deg)
Cohesion - Intact Rock	31.96	MPa
Tensile Strength - Intact Rock	14.2	MPa
Cohesion - Jointed Rock	5.11	MPa
Tensile Strength - Jointed Rock	2.2	MPa
Initial Permeability	8.97E-18	m^2
Bedding Plane - Dip Direction, Magnitude	0, 0	^{o}(deg)
Vertical Joint Set 1 - Dip Direction, Magnitude	45, 45	^{o}(deg)
Vertical Joint Set 2 - Dip Direction, Magnitude	225, 90	^{o}(deg)
Vertical Joint Set 3 - Dip Direction, Magnitude	180, 90	^{o}(deg)

Table 3.2: Material Parameters for Meiningen/Suhl

3.2 Numerical Modelling & Simulation

The stimulation process is carried out in several stages depending on the reservoir permeability and in-situ conditions. The number of wells itself may depend on the reservoir formation and the physical footprint of operations. In the current study, the number of well and stages per well have been restricted to 1 and 3. The model is designed to be a reference point for addition of further complexities in the near future. The modelling and description of stages have been illustrated in figure 3.4.

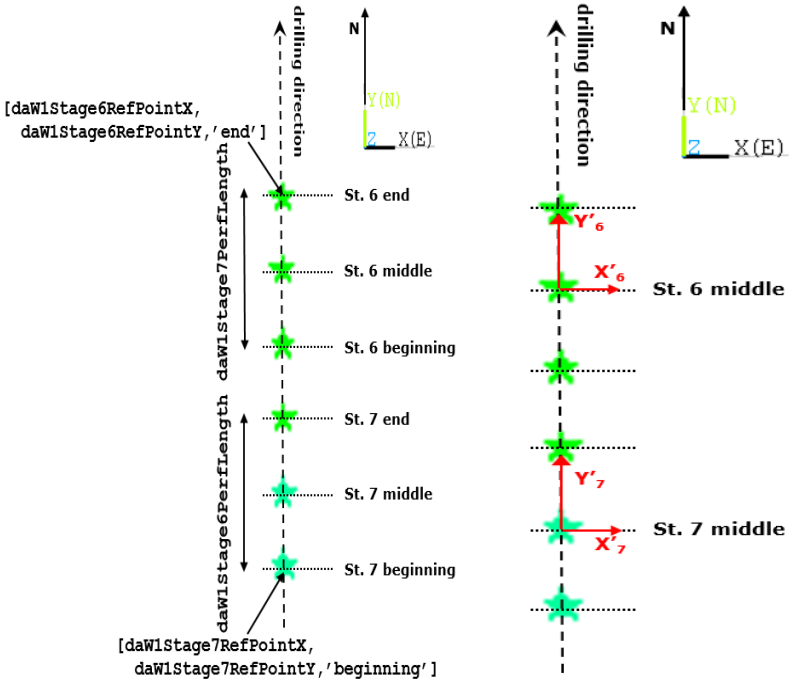

Figure 3.4: Definition of Stages using Reference Points along the Drilling direction

The beginning, middle and end points refer to individual locations in space, in relation to which the stage definition is established. Definition of a single point, i.e. 'beginning', 'middle' or 'end' along with the well orientation or drilling direction and the perforation length can be used to model a given well-stage location. It should be noted here that the current study assumes a single-perforation model, i.e. each stage has only one perforation through which the fluid is pumped in. The FE-model with mesh-size definitions, well-stage parameters is illustrated in figure 3.5.

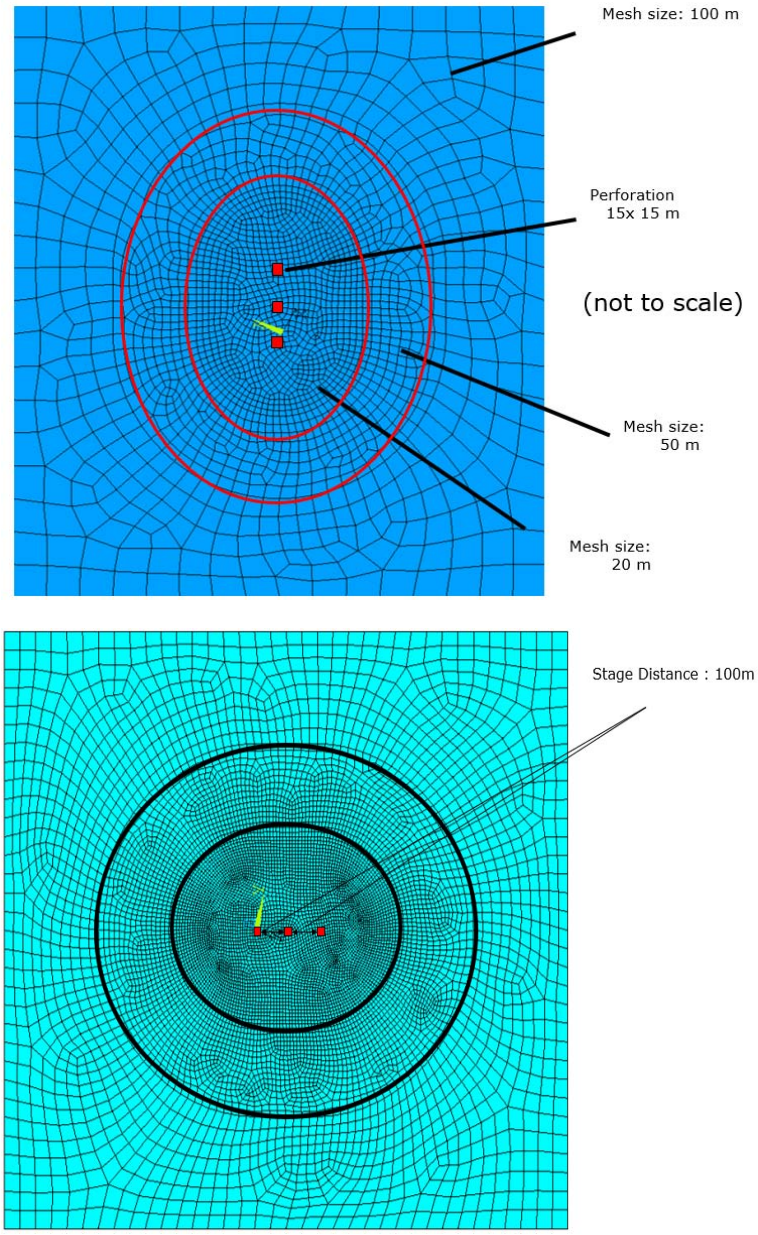

Figure 3.5: Mesh characteristics and Well - Stage parameters for the Mechanical model (top) and Hydraulic model (bottom)

At the end of the stimulation cycle, due to injected volume the pressure levels in the reservoir are much higher compared to the applied initial pore pressure gradient. Figure 3.6 depicts the reservoir balance and Bottom Hole Pressure lev-

els for Meiningen/Suhl (Wk-STy represents stage k of well y) using simulation parameters described in Table 3.1 and Table 3.2

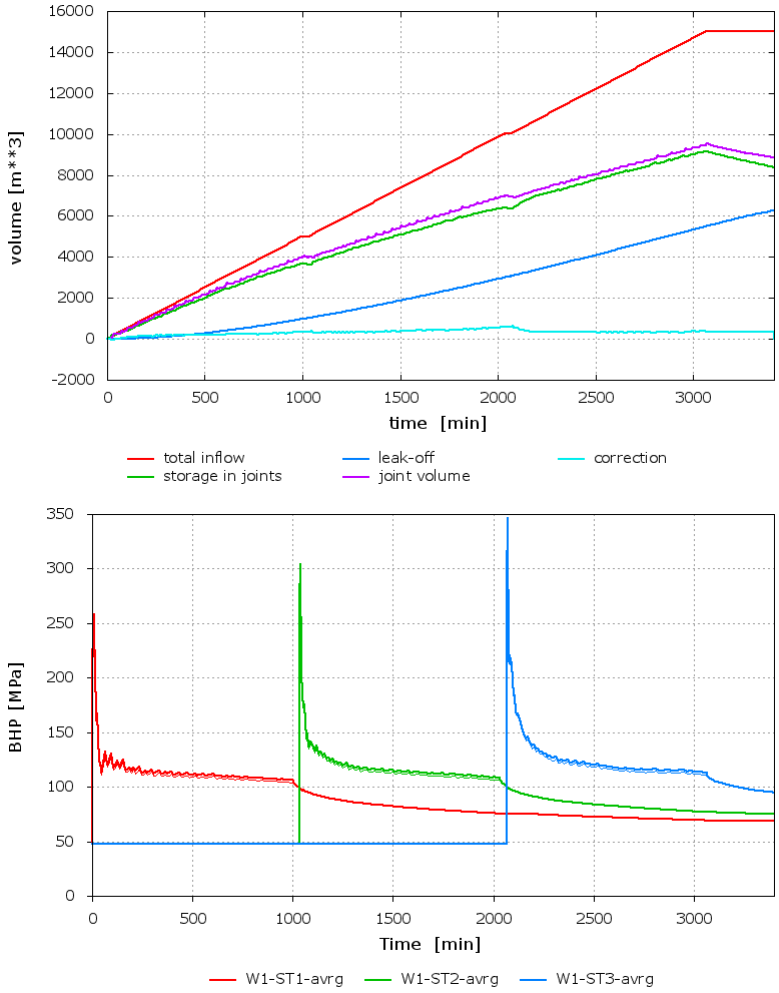

Figure 3.6: Reservoir Volume Balance and Bottom Hole Pressure levels for Meiningen/Suhl

The various terms introduced in the above plots are detailed in the following section :

- **Total Inflow** - The total inflow is the total amount of fluid injected into the reservoir. It is calculated based on the applied Slurry rate (m^3/s) and summed over all time-steps.
- **Storage in Joints** - Storage in joints represents the total amount of fluid stored in fractured elements in the hydraulic domain. In order to correlate the storage volume in the fluid model with the fractured volume of the mechanical domain, the global storativity value needs to be calibrated.
- **Leak - off** - The leak-off volume is the amount of fluid stored in elastic elements. It is described as leak-off since the leak-off volume is the fluid volume that could not be utilized to induce plasticity and contribute to fracture extension.
- **Joint - volume** - The amount of fluid stored in joints is calculated based on the joint openings and the total extension of the fracture system in the mechanical domain. Assuming low permeabilities however, it should be should be close to pumped fluid volume and therefore the storativity term of the flow equation should be calibrated..
- **Correction** - In order to account for the difference between the storage in joints and the joint volume, an explicit correction volume is applied. The simulator has a capability to ensure a certain fluid efficiency by introducing volume corrections at the element level. As observed, the correction volume amounts to $< 1\%$ of the storage volume in joints which indicates that using a pre-calibrated global storativity value, the volume correction applied is indeed negligible.
- **Wk-STy-avrg** - The average pressure value in well k, stage y during the course of the simulation.

Further results of the simulation, using the parameter set in Table 3.1 and Table 3.2, is available in Chapter - Results and Discussion - 6.

Chapter 4

Unloading and Production Cycle

The fracturing process is followed by an unloading interval during which the reservoir pressure is allowed to relax with the relaxation pressure depending on the treatment of the pressure in the fracture system . The unloading process directly precedes the production cycle, where an injection slurry is applied to the production well to allow the slurry to flow through the fracture network and get heated up in the process. The orientation of production well may depend on several factors such as the total extension of the fractures, orientation of the fracture network and the conductivity of the fractured elements. The orientation of the injection well and the stress gradient in the reservoir might also play a big role in determination of the position and orientation of the production well. However, in general, two possible well scenarios in an Unloading/Production cycle could be visualized. They are illustrated in figure 4.1

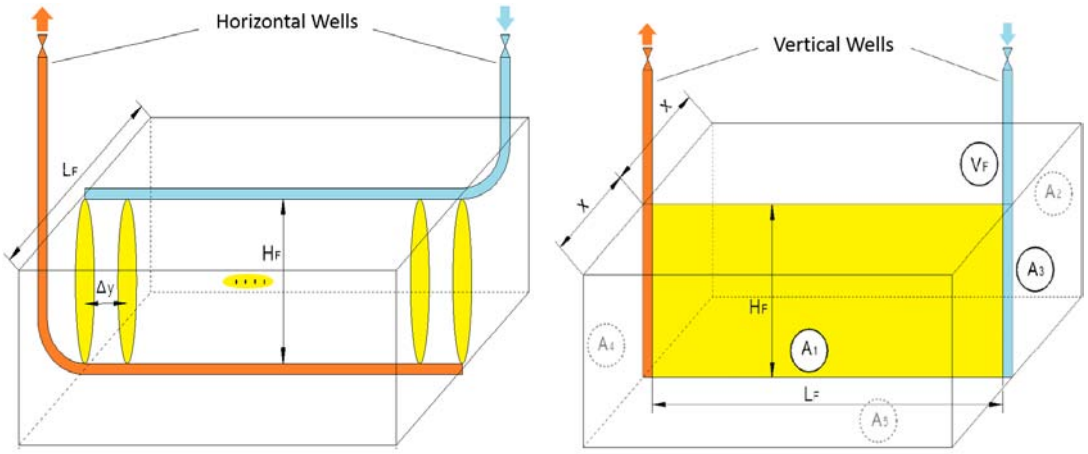

Figure 4.1: Possible well-setup scenarios in EGS (DBI, 2015)

The red well here represents the Stimulation well and the blue well represents the Production well, Δy is the stage distance, H_F is the heat exchanger height, A_k is the area of face k and L_F represents the total model width in horizontal-well construction and the total fracture depth in the vertical-well set-up. Horizontal wells are prefered since the resulting heat exchanger area from the generated fractures are much larger compared to the vertical well set-up.

The placement of the Production well, in practice, is a bit ambiguous. It is not clearly understood whether the production well is drilled before or after the fracturing process. It would be more profitable to introduce the Production well after the stimulation procedure is finished since the probability of connecting the two wells with a high permeable fracture network would be much higher and the available heat exchanger area would be maximized. In order to estimate the most optimum production well position, best available measurements about fracture extension and orientation (such as micro-seismic measurements (MSE) during stimulation process) and available simulation results tools used to forecast the fracture extention and conductivity should be combined. In the current study using FE environment, the well selection algorithm is based on

the practical assumption that the dip and orientation of the production well is similar to the injection well in use and the heat-exchanger area is maximized. (*Refer 4.2 for more details*)

4.1 Unloading cycle

The purpose of the simulation of unloading cycle is to account for the time-gap between the fracturing and production cycles observed in real-world applications. Unloading is simulated by applying a pressure boundary condition to the injection well corresponding to the initial pore-pressure at the given depth. The loading is ramped in order to avoid sudden gradients and numerical errors in the model. It must be ensured though that the applied pressure gradient is larger than or equal to the recorded bottom hole pressure gradient at the end of the stimulation process. Applying a lower gradient, would imply a slurry in-flow in the reservoir model which is unphysical. Based on the conductivity and pressure level of individual fractures, one or the other stages may undergo a slower or faster relaxation. This is clearly illustrated in figure 4.2 where Stage 3 fracture shows larger out-flow rates compared to the other two fracture networks since stage 3 has a higher pressure level at the end of the stimulation cycle.

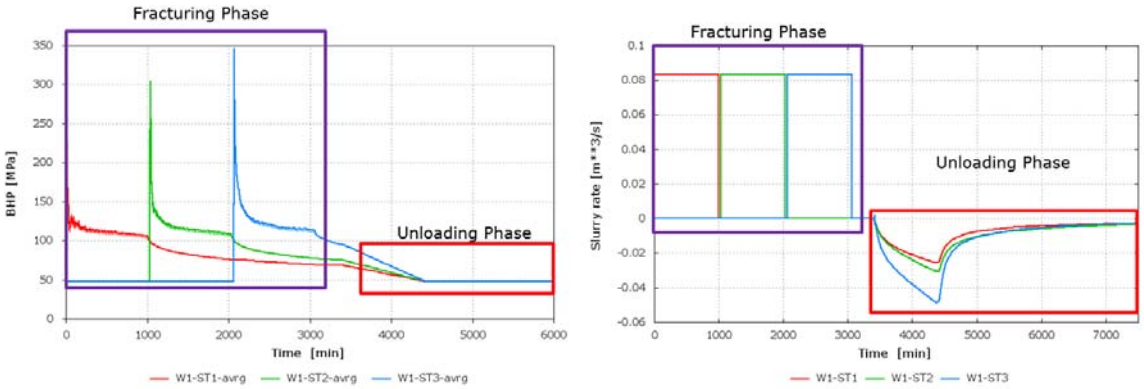

Figure 4.2: Fracturing + Unloading - Pressure Gradients & Slurry Volumes

Assuming a large time for unloading, the unloading cycle has to be continued until there is almost zero outflow rate or the reservoir reaches equilibrium or steady-state condition. Hence, it needs to be ensured that there is bare minimum outflow in the model. However, achieving a zero outflow rate requires a long unloading time since the pressure gradient is constantly reducing. This, in turn, allows for larger yet ramped time-steps to reduce the overall simulation time. The outflow rate and the corresponding time-step scheme is illustrated in figure 4.3

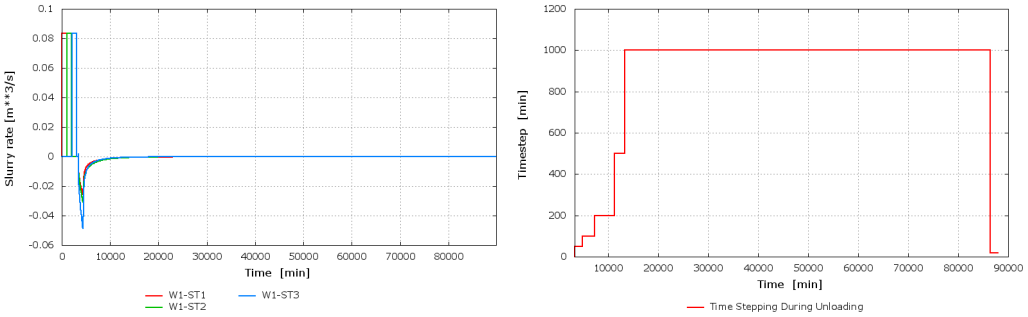

Figure 4.3: Outflow Rate and Time-Stepping during Unloading

4.2 Production Well Selection algorithm

An optimal location of the Production Well in terms of maximal heat exchanger area depends on the height and orientation of the generated fractures. Consequently, the exact location cannot be determined at the beginning of the fracturing simulation. Based on practical assumptions, a well-selection algorithm is developed, which considers the dip and orientation of the injection well and the maximum heat exchanger area. Besides, there are other factors which need to be considered such as the hydraulic conductivity of the connected fractures and its impact on overall pressure change during the production cycle. The algorithm, therefore, considers the following connection scenarios :-

- The lowest maximum height, second lowest maximum height and the height of the largest fracture among the three fractures is determined. This ultimately leads to three possible connection scenarios : a) All Fractures Connected - Production Well, b) Two Fractures Connected - Production Well, c) One Fracture Connected Production Well.

- The available heat exchanger area due to a single well connection, two well connections and all three well connections is calculated. The maximum available area out of the three connection scenarios results in the corresponding well selection. This is an important factor in cases where the height of one or two of the three fractures is much lower than the height of the other fracture/fractures. This may lead to a scenario where the connected area due to one/two fracture connections is much larger compared to when all three fractures are connected.

- The final height of the connected Production well is reduced by 200 m, in order to ensure that the connected fracture elements are conductive enough to facilitate the production cycle. This is done to ensure that there is no further failure/shearing of the granite layer which would lead to an unreasonable pressure change and an inefficient Production cycle.

The three possible well connection scenarios are illustrated in figure 4.4. The dark blue well represents the injection/fracturing well and the light orange coloured wells represent the observation lines used to track pressure at designated heights of 200 m, 400 m, 600 m and 800 m from the injection wells. The red well illustrates the well connection scenario when all three wells are connected while the sky blue represents the scenario when the two highest wells are connected. Lastly, the yellow well highlights the connection scenario when only one well is used to carry out the unloading/production process. In the current simulation method, only one of the connection scenarios will be utilitzed to carry out the unloading and production processes, with the selection being

based on the largest available surface area, also denoted as the heat exchanger area. Post execution of the production well algorithm in the reference model, the all fractures - connected production well, located at a height of 814 m from the injection well, was selected as the best Production well position.

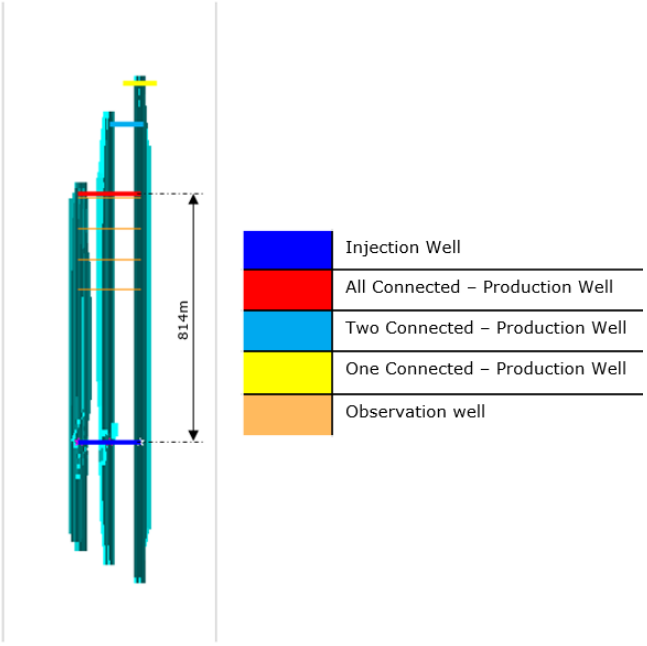

Figure 4.4: Production well - Stage Connection scenarios

4.3 Production Cycle

The Production cycle in the simulation process follows after nearly equilibrium or steady-state conditions are reached. No additional fracturing occurs either in the Unloading or the Production cycle. The process in the numerical model, is not carried out by explicitly introducing a well or pipe element after the unloading process. This is because the simulation procedure works on restarting the fracturing + unloading models and any addition of new elements would

lead to modification of the stiffness matrix and the total number of degrees of freedom in the original result files. The solution is to directly apply an equivalent injection rate boundary condition on the nodes of exisiting solid elements. At the injection well, the fracturing slurry rate is applied as a volumetric heat generation rate but in the production cycle, the production rate is applied as individual nodal heat rate on nodes of the solid model (see figure 4.5).

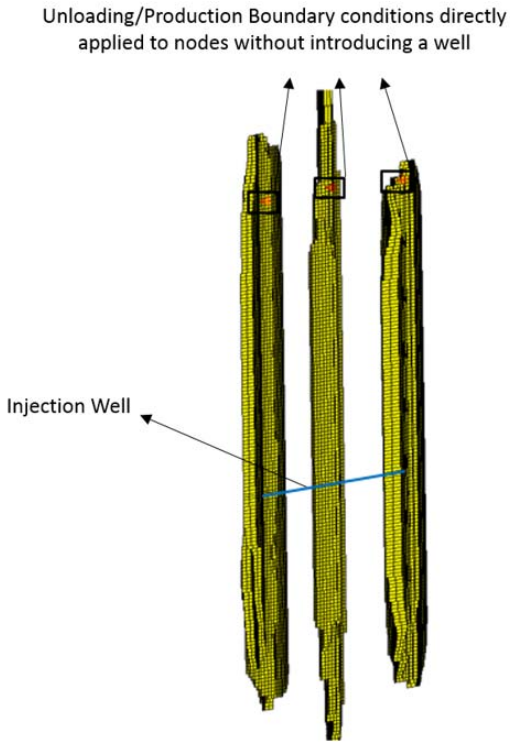

Figure 4.5: Production Boundary Conditions - Injection Rate applied to Nodes

The objective of the Production cycle is to predict the following :

- **Pressure Loss** - The pressure loss during Production cycle occurs due to two primary factors, a) pressure loss due to fluid flow in pipes, b) flow resistance in reservoir which determines the necessary pressure levels in

the injection pump. Flow resistance in the fracture network leads to losses in pipe system and heat exchanger, which in turn, is influenced by friction effects and fluid rheology/viscosity. Since the prevalent resistance in the heat exchanger needs to be calibrated after finalizing the EGS system, a low pressure value is targeted which ultimately corresponds to low flow resistance.

- **Volumetric Efficiency & Leak-off -** The volumetric efficiency is defined as $= \frac{Outflow\ Volume}{Inflow\ Volume}$. In other words, the outflow volume needs to be estimated by measuring the amount of fluid lost in the reservoir, i.e. the leak - off volume.

In the current version of the Hydraulic fracturing simulator, pipe modeling has been limited to represent the injection process. Moreover, due to the aforementioned approach of direct application of Production influx boundary conditions to nodes, the complex pipe system in the model need not be modelled. The resistivity in the pipe system, however, can be easily re-integrated. The reformulation is based on varying the conductivity of the system and calibrating the pressure change to desired/prescribed pressure levels. As a part of a global objective, the pressure values are tracked in order to simultaneously minimize the fracture resistivity and maximize the heat exchanger area. The hydraulic conductivity is calculated using (*see eq 2.13 for more details)* :

$$K_{J0} = \frac{\gamma e^3}{\mu 12 S R_c}$$

Apart from specific gravity and dynamic viscosity, all other parameters are geometrical parameters and should not be altered with. In the next section, the pressure loss mechanism and leak-off calculation will be discussed in detail.

4.3.1 Reservoir Flow Resistance - Viscosity Modelling

Pressure loss during Production can be modelled using the Darcy flow equation by a correlated fluid viscosity in the system. The desired change in pressure level in the Meiningen/Suhl reservoir is 20 - 30 bar which is also a target value for the reference design in the production simultation. In the current numerical simulation procedure, the overall pressure change is also dependent on the orientation of generated fractures, well connection and the conductivity of the system but reservoir-resistivity minimization will be dealt as a single-objective optimization. Figure 4.6 illustrates how the variation in fluid viscosity from 1 to 5 cP leads to a change of pressure levels in the reservoir. Production Node k represents the pressure distribution at node k ($k \in 1..3$), defined in figure 4.5 and Wk-STy illustrates the pressure distribution at well 1, stage 1 of the initial injection well. Intermediate results are available in *Appendix A*.

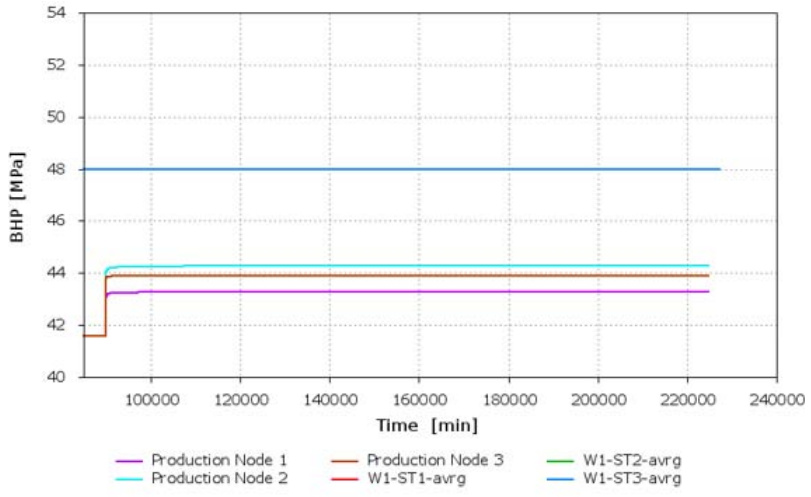

Viscosity 1.0 cP

Avg Δ Pressure = 22.40 bar

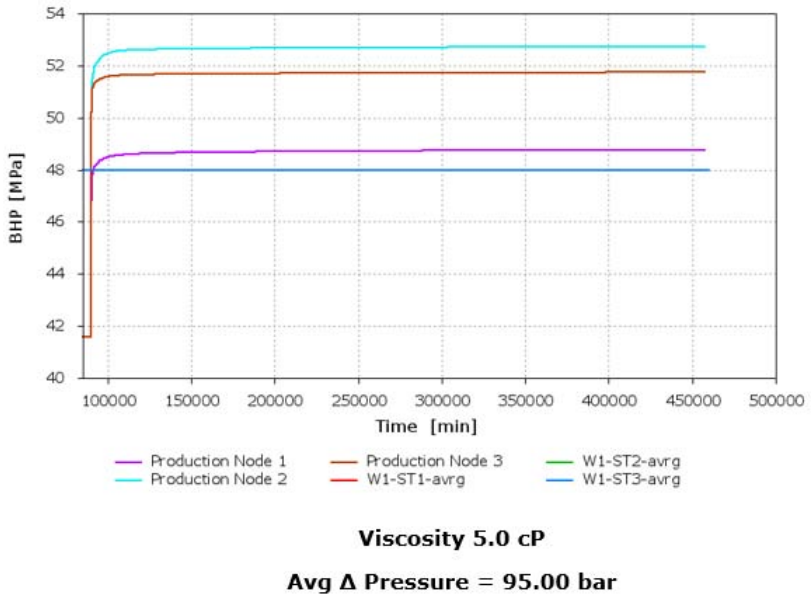

Figure 4.6: Change in Pressure Levels - Viscosity effects

For convenience purposes and to account for high pressure levels due to influx boundary conditions being applied on nodes , a viscosity value of 1 CP is selected which amounts to a reference average pressure change of 2.24 MPa or 22.40 bar. As mentioned earlier, the experimental values of pressure change in the general reservoirs are estimated between 20-30 bar.

4.3.2 Volumetric efficiency - Leak-off

Fluid flow loss takes place during each of the injection cycles, i.e Fracturing & Production. The estimation of fluid flow losses is extremely vital for determination of Fracturing or Production cycle efficiency. The calculation of fluid leak-off is estimated through the determination of storage volume in elastic elements. This can be inferred since the total storage volume represents the total fluid stored in the model due to fluid injection. The joint volume represents the fluid

volume in plastic elements and the leak off would hence represent the remaining volume in the elastic elements.

$$Total\ Fluid\ Volume\ Injected = Total\ Storage\ Volume \equiv$$
$$Leak\ Off + Joint\ Volume + Outflow_{Fluid\ Boundaries}$$
$$Total\ Storage\ Volume = Total\ Elastic\ Volume + Total\ Plastic\ Volume$$
$$\because \quad Total\ Plastic\ Volume = Joint\ Volume$$
$$\therefore \quad Leak\ Off = Total\ Elastic\ Volume + Outflow_{Fluid\ Boundaries}$$

In order to estimate the leak-off during the Production cycle, the Production simulation has to be run long enough until the in-flow rate through the Production well becomes equal to out-flow rate from the Injection well. Due to variation of viscosity, the time needed for the system to achieve equilibrium increases as shown in figure 4.7. Production Node k represents the slurry rate at node k ($k \in 1..3$), defined in figure 4.5 and Wk-STy illustrates the slurry rates at well 1, stage 1 of the initial injection well. Intermediate results are available in *Appendix A*.

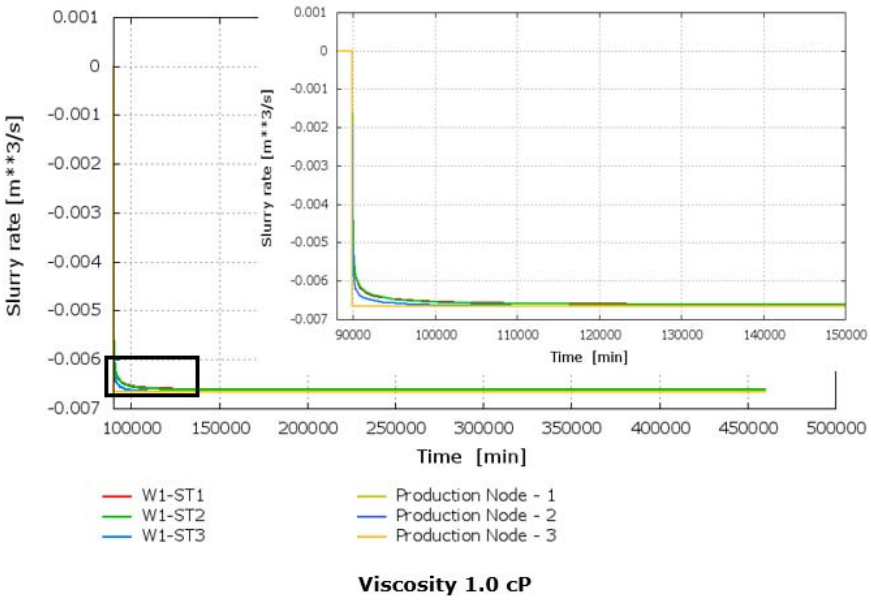

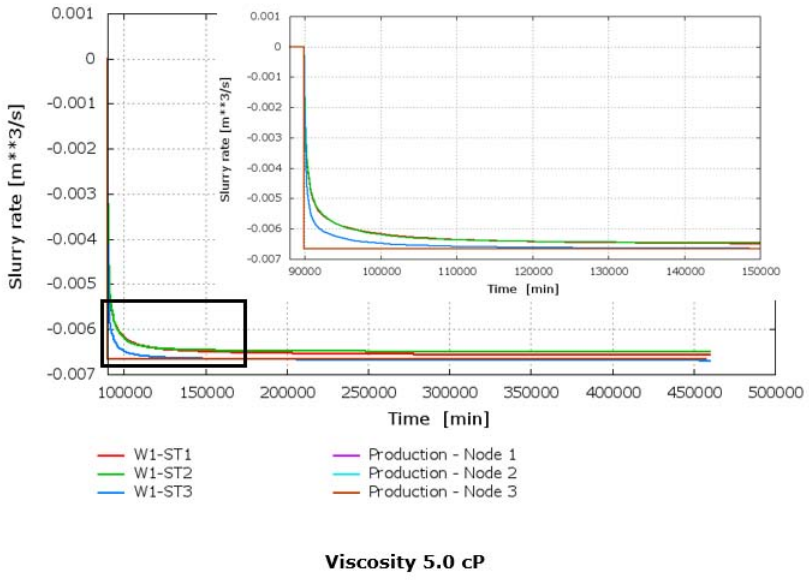

Figure 4.7: Inlet - Outlet Flow Rate Variations - Viscosity effects

The leak-off volume is calculated after the initial dynamic effects have subsided and the reservoir reaches a state of equilibrium. Thereafter, it is assumed that the variation in leak-off volume is largely linear in nature. Leak-off calculation is shown in figure 4.8.

$$Leakoff\ Gradient = \frac{\Delta Leakoff\ Volume}{\Delta Time} \quad [m^3/s]$$

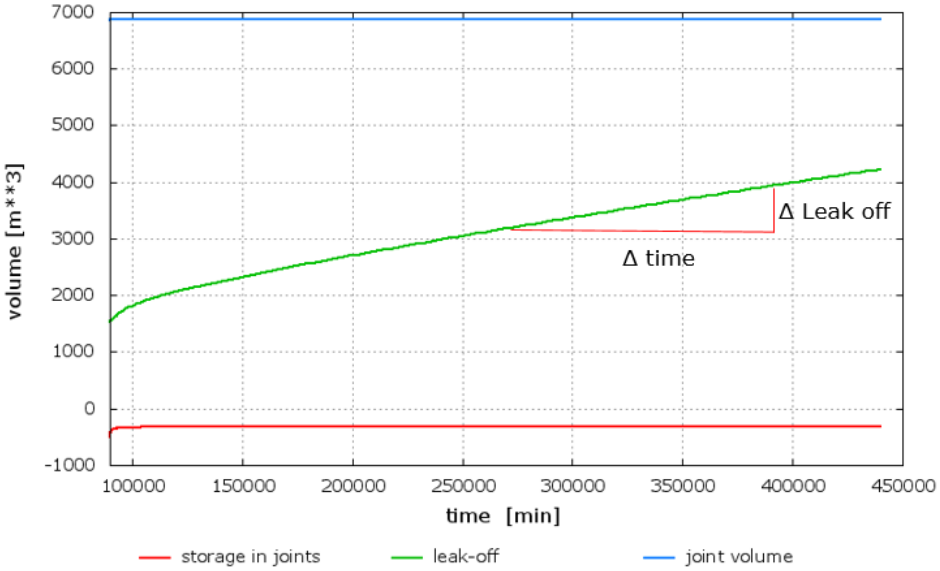

Figure 4.8: Leak off volume calculation

The leak-off is computed for all aforementioned viscosity iterations. Table 4.1 shows change in pressure level iterations.

Viscosity Iterations (cP)	Average Pressure Change (bar)
1.0	**22.40**
1.5	31.90
2.0	42.00
2.5	51.66
5.0	95.00

Table 4.1: Summary of all Viscosity Iterations

The viscosity value of **1 cP**, leading to a pressure change of **22.40 bar** and leak-off gradient of **0.0048 $\mathbf{m^3/min}$**, is chosen as the reference result for the Meiningen/Suhl reservoir.

The pressure level estimation and leak-off calculation complete the evaluation of Production cycle in an Enhanced Geothermal System. Most of the above calculations have been automated using APDL macros or Python scripts and are currently also a part of the EGS simulation process chain.

A secondary objective of the current study is the investigation of uncertain parameters in the reservoir and analysis of possible variations assigned to operational parameters, used in practice. The following section outlines such a study carried out for the fracturing and production cycle and will also be used to arrive at a set of optimum parameter values.

4.4 Sensitivity Study

The goal of the sensitivity study is estimation of the variation of all relevant responses and identification of sensitivity of uncertain and operational parameters within the paradigms of a defined design space. The parameters used for building up a design space is based on observed uncertainities in reservoir characteristics and operational conditions (*see Section* 6.1). The selected parameters, along with the parameter ranges, for establishing a design space is tabulated below :-

Parameter Name	Reference Value	Minimum Value	Maximum Value
Stage Distance [m]	100	100	200
Well Azimuth [°]	70	40	100
Well Dip [°]	0	-20	0
Pore Pressure Gradient [Pa/m]	10660	5000	11000
Youngs' Modulus [Pa]	7.8E+10	6.5E+10	8.5E+10
Friction Angle [°]	41.8	35	42
Uniaxial Compressive Strength [Pa]	1.43E+08	1.1E+08	1.8E+08
Dilatancy Angle [°]	20	15	25
Relative Joint Strength	0.16	0.1	0.3
Vertical Stress Ratio	0.8	0.75	0.85
Horizontal Stress Ratio	6.41	6.0	7.0
Slurry Volume [m^3/s]	5000	2500	7500
Stimulation Rate [m^3/s]	5	5	10
Production Rate [m^3/s]	100	80	120
Horizontal Well Length [m]	1500	1000	2000

Table 4.2: Sensitivity Parameters and Parametric Space

The design space is created using above parameter ranges and an Advanced Latin Hypercube Sampling (ALHS) scheme. A total of 100 design points are created and simulated subsequently. A noteworthy outcome of the sensitivity analysis is also the estimation of parameters sensitive to the connected fracture surface area (*See Section* 4.2). The connected fracture surface area needs to be interpreted in terms of the total available heat exchanger area by the following equation :

$$Heat\ Exchanger\ area = \frac{Connected\ Fracture\ Surface\ area \times Horizontal\ Well\ Length}{Number\ of\ Stages \times Stage\ Distance} \tag{4.1}$$

The other critical responses include the total height of the connected fracture network and the total height of the complete fracture network (*see Appendix*

A). The estimate of parameter importance is based on the measure of Coefficient of Optimal Prognosis (COP) for the generated Metamodel of Optimal Prognosis (MOP) (Will, 2009 [28] [29]). COP is a mathematical measure of the ability of a given metamodel to predict response values which are not a part of the metamodel raw data, with correlations to input parameter variations. Consequently, a metamodel with a high COP can be used to predict responses as a result of unknown combinations of input parameter values and allows for further optimization within the investigated design space. The metamodel for the available heat exchanger area and the connected height for the connected fracture surface area is illustrated in figure 4.9.

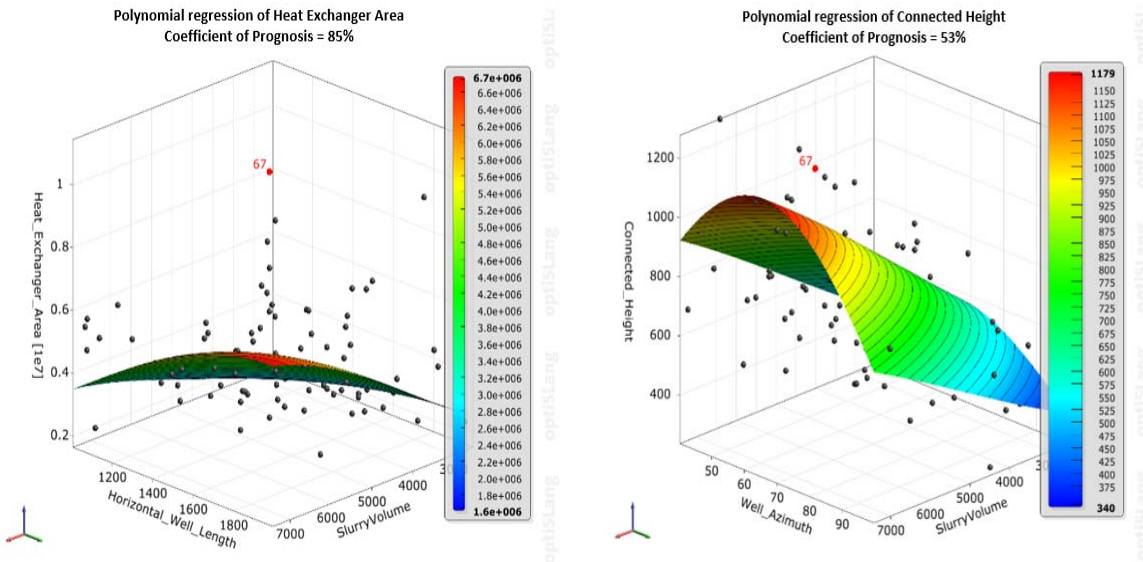

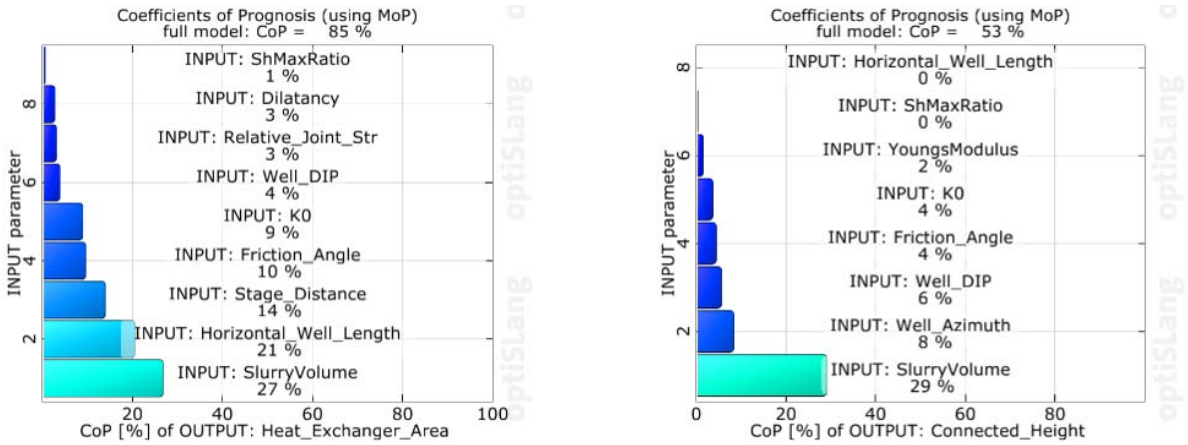

Figure 4.9: Metamodel and COP for Heat Exchanger Area & Connected Height

Other responses such as total vertical fracture extension, reservoir balance, etc are available in *Appendix I*. As pointed out earlier, a higher COP of a given metamodel indicates a higher overall prognosis ability. A COP value of $>$ 70%-75% indicates a reliable metamodel, especially for highly non-linear simulation models such as the one in consideration here. A lower COP value might indicate either too few design points to build up a reliable metamodel or numerical approximation difficulties which affect the response apart from the variation in the design space itself. As observed in figure 4.9, the COP plots also highlight the significance of a single input parameter variation window to the resulting response variation. The low COP for the Connected height-metamodel is owing to the numerical noise created by the production well selection algorithm which is not considered in any form with the design parameters. (*See 4.2*). Best design, based on the largest heat exchanger area is design 67. Responses value are given in table 4.3.

The design points are simulated further to the next phase of the EGS-cycle, i.e. the Unloading and Production cycle. As already highlighted (*See 4.3*), the most

critical responses during the Production cycle are the leak-off gradient and the average pressure change in the reservoir and they are subsequently evaluated with the available design parameters as seen in figure 4.10.

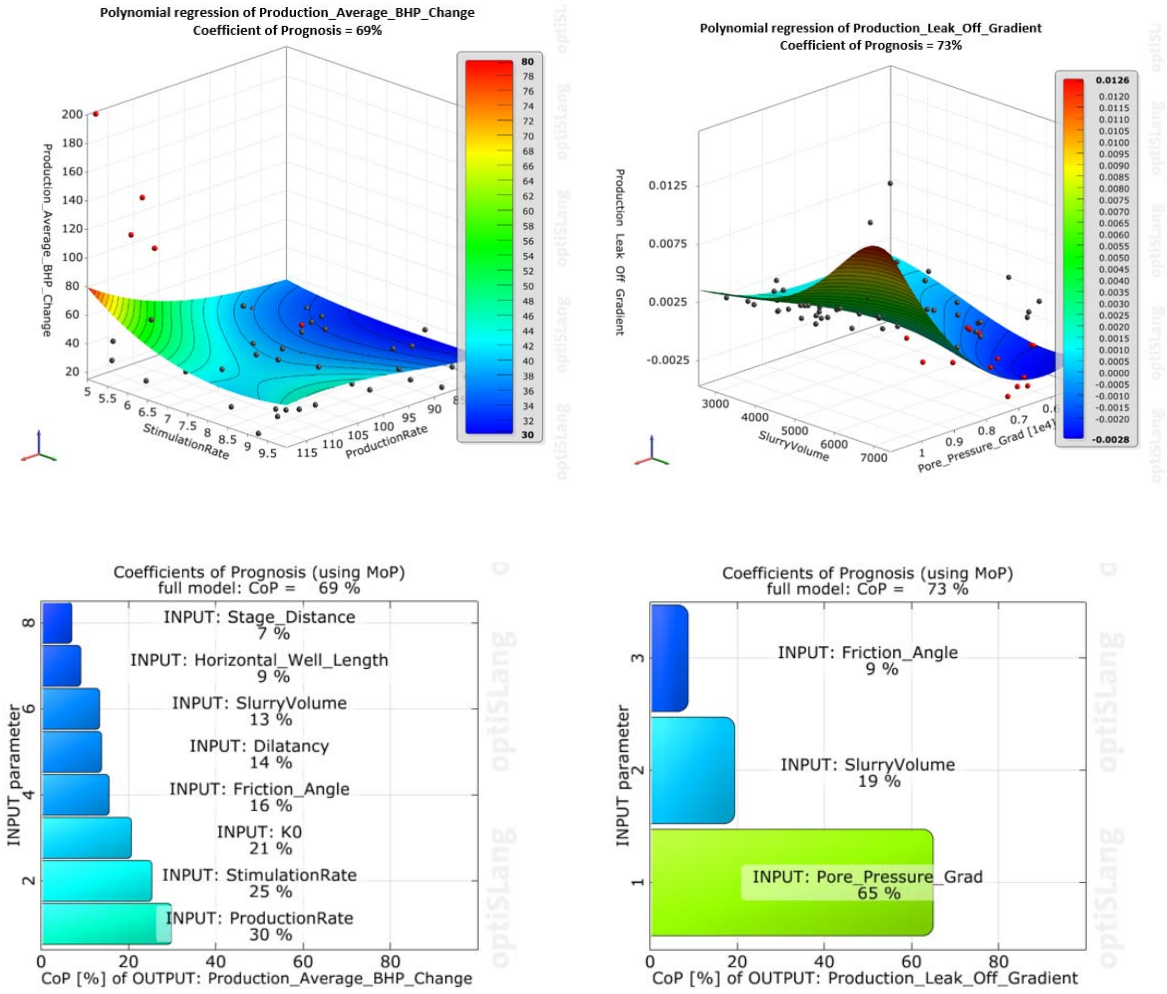

Figure 4.10: Metamodel and COP for Average Production Pressure Change & Leak-off Gradient

As per the metamodel evaluation, the average change in pressure values during Production is directly influenced by the the applied production flow rate and

the preceding stimulation flow rate. The leak-off is dependent primarily on the initial pore pressure gradient since the leak-off gradient is influenced by the pressure gradient in the fractured and unfractured elements and the initial pressure gradient in the model is defined throught the Initial Pore Pressure Gradient.

Response Name	**Reference**	**Best Design - 67**
Connected Heat Exchanger Area [m^2]	0.62E7	1.15E7
Connected Height [m]	831	1198.12
Average Pressure Change - Production [bar]	22.45	35.52

Table 4.3: MOP Responses - Reference & Best Design

The sensitivity study identifies the best possible metamodel resulting in highest forecast quality for important reservoir responses such as leak-off, total heat exchanger area, average pressure change, etc. The metamodel responses could be used to isolate sensitive parameters to an otherwise highly non-linear model. It could also be used to run an optimization cycle based on single or multiple objectives. Based on the current study, the reservoir parameters have been analyzed to arrive at the best design parameter set.

The last step in the simulation of an Enhanced Geothermal System is prediction of temperature distribution in the reservoir and the resulting overall power capacity of a potential EGS power-plant. The next chapter highlights the integration of such a coupled fluid-thermal temperature simulation with the EGS process chain. The end of the Production cycle marks the beginning of the thermal simulation in the overall process and hence is an absolutely integral part of the entire work-flow.

Chapter 5

Thermal Simulation

A crucial part of any EGS simulator is the ability to predict the possible power carrying capacity of the resulting EGS power-plant. The knowledge of available power can be helpful in critical analysis of economic feasibility of such a reservoir. In addition, since an EGS reservoir requires significant large investments to execute the hydro-shearing process, government agencies and companies are wary of initiating such cost-intensive projects despite their potential environmental benefits. The current section, however, focusses on simulation of the prevalent coupled fluid-heat phenomena during Production cycle of an EGS reservoir.

5.1 Conjugate Heat Transfer Analysis

A coupled fluid - thermal flow analysis is also referred to as a conjugate heat transfer (CHT) analysis. The main characteristic of a CHT analysis is the transport phenomenon where the dominant mode of heat flow is accompanied by fluid flow. Heat conduction plays a negligible or rather insignificant role (when thermal conductivity is low compared to applied velocities). Such transport or convection-dominated phenomenon is represented by the following equation :-

$$\rho c_p \cdot \left(\frac{\partial T}{\partial t} + \vec{u} \cdot \nabla T \right) = \nabla \cdot (k \nabla T) + Q_h \tag{5.1}$$

where ρc_p - Overall heat capacity of medium [J/m^{3}K],

T - Temperature [K],

t - Time [sec],

$\vec{u}$ - Fluid velocity vector [m/s],

k - Thermal conductivity [W/m K] &

Q_h - Heat source/sink [W/m^3]

As evident from the above relationship, the coupled fluid-heat transfer process is a combination of conduction terms, k and fluid transport terms, $\vec{u}$. CHT analysis is a practical analysis tool available with most modern Computational Fluid Dynamics (CFD) software such as Ansys CFX, Openfoam, etc. However, the fundamentals of the homogenization approach in the current approach limits the application of CFD software. This is described further in the next section.

5.1.1 CFD & Homogenized approach

The application of homogenized approach implies that the discrete geometrical modelling of joints in the reservoir is no longer mandatory. Yet, it imposes a modeling restriction since the fluid velocity field (a result of the solution of the Darcy's flow equation) does not represent the velocity in discrete flow channels but the Darcy flow in the homogenized continuum.

The aforementioned restriction demands investigation of a new approach where the simulation process uses a prescribed steady-state Darcy velocity field from the Production cycle described in Chapter 3. Heat transfer models need to be coupled with the velocity field, without resulting in any variation of the velocity field. Nevertheless, the challenges involved in such a process are similar to the

implementation of a CHT tool in CFD applications and understanding them is essential for solving the 3-D heat transport equation.

5.1.2 Problem Identification - 1D Scalar Transport

In order to clearly demonstrate numerical modelling difficulties in a convection-dominated fluid flow problem, a 1D scalar transport Dirichlet problem is described in the current section (Gravemeier, 2015 [8]). The general scalar transport (convection - diffusion) equation is represented by

$$\frac{\partial \phi}{\partial t} + \mathbf{a}\nabla \cdot \phi - \nabla \cdot (k \nabla \phi) = f \quad in\ \Omega \times (0, T) \tag{5.2}$$

$$\text{Dirichlet Boundary condition : } \phi = \phi_D \quad on\ \Gamma_D \times (0, T)$$
$$\text{Neumann Boundary condition : } k\nabla\phi \cdot \vec{n} = h \quad on\ \Gamma_n \times (0, T)$$
$$\text{Initial condition : } \phi = \phi^o \quad in\ \Omega \times \{0\}$$

where a - velocity vector

Φ - scalar quantitiy (temperature, concentration, etc)

k - kinematic diffusivity

f, h, Φ_D, Φ^o- source term, Neumann flux, Dirichlet scalar, initial scalar

When compared to the 3D thermal conduction - convection equation (eq 5.1), the following similarities are observed :

$$\varphi \equiv T,\ a \equiv u,\ f \equiv Q_h$$

In order to distinguish between convection and diffusion - dominated flows, a dimensionless number known as Péclet number has been defined as the ratio of the rate of advection to the rate of diffusion in fluid flow. This is numerically defined as

$$Pe = \frac{\mathbf{A}L}{k}$$

where **A** - characteristic velocity [m/s]

L - characteristic length [m]

In terms of flow ranges, fluid flow with Peclet numbers higher than 1 are **convection-dominated** and those lower than 1 are **diffusion-dominated**. The 3D scalar transport can be reduced to a stationary, single dimension equation to analyze the numerical implications in a convection dominated flow. The 1D formulation is given by

$$a\frac{\partial \phi}{\partial x} - \kappa\frac{\partial^2 \phi}{\partial x^2} = 0 \quad for\ x \sqsupset 0, L \sqsubset$$

along with

$$\phi = \phi^o \quad for\ x = 0$$

$$\phi = \phi_L \quad for\ x = L$$

The general analytical solution is given by

$$\phi(x) = \phi^o + \frac{e^{Pe\frac{x}{L}} - 1}{e^{Pe} - 1}(\phi_L - \phi_o) \tag{5.3}$$

where Pé - Peclet number,

x, L - Boundary condition scalars [m]

The numerial solution, approximated with finite difference scheme with central differentiation (figure 5.1) leads to the following numerical solution at a given nodal point A.

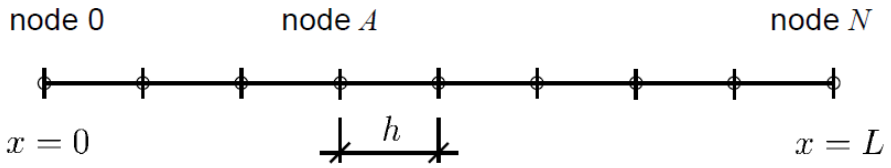

Figure 5.1: Numerical discretization of 1D Scalar transport problem (Gravemeier, 2015)

Equation for numerical solution :

$$\phi_A = \phi_0 + \frac{\left(\frac{1+Pe_i}{1-Pe_i}\right)^A - 1}{\left(\frac{1+Pe_i}{1-Pe_i}\right)^N - 1} (\phi_L - \phi_0) \tag{5.4}$$

where $Pé_i = \frac{ah_i}{2\kappa}$ also known as the Grid Peclet number,

h_i - discretized length [m]

The graphical representation of the analytical and numerical solution is given in figure 5.2

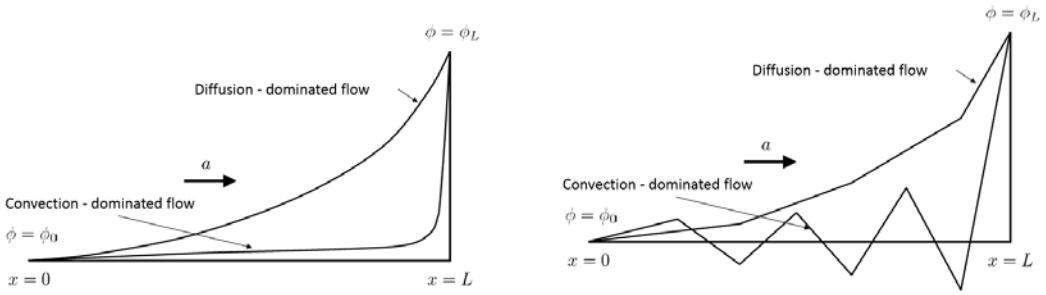

Figure 5.2: Analytical and Numerical solution with Central-difference scheme (Gravemeier, 2015)

As observed, the central-difference numerical scheme is dependent on the Grid Peclet number of the model and leads to spurious oscillations in convection - dominated flows. Such solutions are unacceptable and need to be resolved.

5.1.3 Upwind scheme / Artificial diffusivity

The central-difference discretization scheme leads to the following approximation of the stationary 1D scalar transport equation via finite differencing :

$$a\frac{\phi_{A+1} - \phi_{A-1}}{2h} - \kappa\frac{\phi_{A+1} - 2\phi_A + \phi_{A-1}}{h^2} = 0 \tag{5.5}$$

when used with an upwind (against flow-direction) scheme, the equivalent equation assumes the following :

$$a\frac{\phi_A - \phi_{A-1}}{h} - \kappa\frac{\phi_{A+1} - 2\phi_A + \phi_{A-1}}{h^2} = 0 \tag{5.6}$$

The upwind scheme can hence also be interpreted with an equivalent artificial diffusion with central-differencing scheme as illustrated by the following equation

$$a\frac{\phi_{A+1} - \phi_{A-1}}{2h} - (\kappa + \kappa^{art})\frac{\phi_{A+1} - 2\phi_A + \phi_{A-1}}{h^2} = 0 \tag{5.7}$$

where,

$\kappa^{art} = \frac{ah}{2} = \kappa Pe_i$, is the applied artificial diffusivity

The artificial diffusivity used here represents a stabilization scheme applied to filter out spurious oscillations in transport-dominated problems (Courant, 1952 [22]). As a result of the upwind scheme/artificial diffusivity, the Peclet number is always reduced to a value lower than 1. Figure 5.3 illustrates the impact of stabilization with refined mesh sizes.

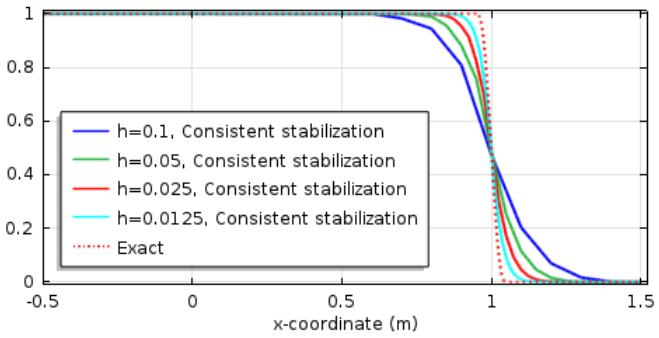

Figure 5.3: Impact of Stabilization on resulting numerical solutions with varying mesh size

The application of upwind schemes/artificial diffusivity helps to stabilize the numerical solution by filtering out spurious numerical oscillations. In 3D scenarios, however, the usage of artificial conductivity leads to various possibilities of application. Consistent stabilization (Schlegel, 2014 [25]) refers to application of artificial diffusion to upwind and cross-wind directions of fluid flow. In the current approach, the application of artificial diffusivity is restricted to streamline direction.

5.2 Lauwerier Formulation

The coupled fluid-heat transfer phenomena along with related challenges and solutions have been discussed in the previous section. The application of the discussed approach, in relevance to EGS reservoirs, needs to be compared with an already existing analytical solution. Such a solution was developed by Lauwerier, 1955 [15] to determine the temperature distribution due to convective heat transport in porous media.

5.2.1 Model Description & Mathematical Formulation

The Lauwerier problem is essentially a two dimensional heat convection problem with a permeable layer bounded by a surrounding inpermeable layer. The model illustrated in fig 4.4 is reduced, being axisymmetric about the z-axis and symmetric about the r-axis. The schematic diagram is illustrated in figure 5.4

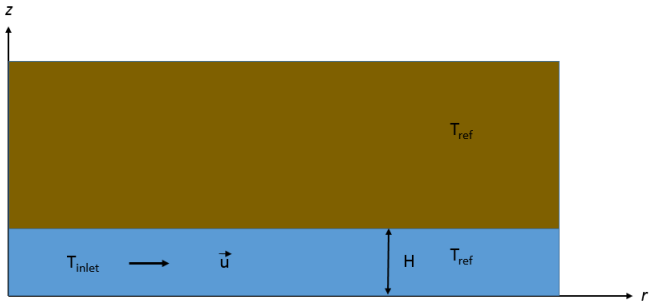

Figure 5.4: Lauwerier Problem - Schematic Diagram

The mathematical formulation is given by the following relations (Saeid, 2009 [24]):

Porous Layer

$$D\frac{\partial^2 T}{\partial r^2} - \nu\frac{\partial T}{\partial r} + \frac{Q}{H} = \frac{\partial T}{\partial t} \tag{5.8}$$

where r $>$ 0, t $>$ 0

Impervious Layer

$$D'\frac{\partial^2 T}{\partial z^2} = h\frac{\partial T'}{\partial t} \tag{5.9}$$

where z $>$ 0, t $>$ 0

Other terms represent :

$$D = \frac{\lambda}{\rho c},\ D' = \frac{\lambda'}{\rho c},\ h = \frac{(\rho c)'}{\rho c} \tag{5.10}$$

$$\rho c = (\phi \rho_{fluid} c_{fluid} + (1 - \phi)\, \rho_{rock} c_{rock}) \tag{5.11}$$

$$\lambda = \phi \kappa_{fluid} + (1 - \phi)\, \kappa_{rock} \tag{5.12}$$

$$(\rho c)' = (\phi' \rho_{fluid} c_{fluid} + (1 - \phi')\, \rho'_{rock} c'_{rock}) \tag{5.13}$$

$$\nu = \frac{q}{\phi} \tag{5.14}$$

where T - Temperature [K],

Q - Heat source [mK/s]

H - Reservoir height [m]

T_i - Injected Temperature [K]

T_0 - Initial Temperature [K]

λ - Heat conductivity [J/(msK)]

ϱ - Density [kg/m^3]

c - Specific heat capacity [J/kgK]

q - Darcy velocity [m/s]

φ - Porosity (Ganji et al, 1978 [5]) [dimensionless]

D - Thermal diffusivity of aquifer [m^2/s]

ν - Real velocity [m/s]

Additional assumptions and boundary conditions include :

- Heat transfer in the fluid channel by convection and in the adjacent layers by vertical conduction.
- Initial heat distribution is uniform.

- $\lambda = \lambda'$, $\varphi = \varphi'$: Heat conductivity and Porosity of pervious and impervious layers are alike.
- T = T' = T, r > 0, z =H, t > 0 : Interface temperature is constant
- $T = T_c$, for (r, z $\rightarrow \infty$, t > 0). : Model extends to infinity in r & z-direction.
- Q = 0, for r > 0, t > 0 : No additional source/sink terms

5.2.2 Analytical Solution

The analytical solution for the Lauwerier problem is given by the following relationship :

$$T = T_{ref} + (T_{inlet} - T_{ref})\, erfc\left(\frac{\frac{\pi r^2}{H^2}}{\sqrt{\frac{\vartheta}{H^2}(\vartheta Dt - h\pi r^2)}}\right) \tag{5.15}$$

where $\vartheta = \frac{\tilde{V}(\rho c)_{fluid}}{\lambda H}$, $\tilde{V}$ is the injected volume flow rate and *erfc* represents the complementary error function given by $erfc = \frac{2}{\sqrt{\pi}} \int_x^\infty e^{-t^2} dt$

The variation of temperature distribution can be well understood by plotting the analytical solution at a given measuring point with changes in input volume flow rate (figure 5.5). The inputs for the analytical solution are given as follows [DBI, 22] :

- Aquifer Height, H - 8 mm
- Measuring Point Distance from Inlet, r - 366 m
- Rock Temperature, T_{ref} - 423 K
- Injected Water Temperature, T_{inlet} - 353 K
- Rock Conductivity, λ_{rock} - 3 W/mK
- Water Conductivity, λ_{water} - 0.6 W/mK
- Rock Heat Capacity, c_{rock} - 860 J/kg K
- Water Heat Capacity, c_{water} - 4186 J/kg K
- Rock Density, ρ_{rock}- 2600 kg/m^3
- Water Density, ρ_{water} - 1000 kg/m^3

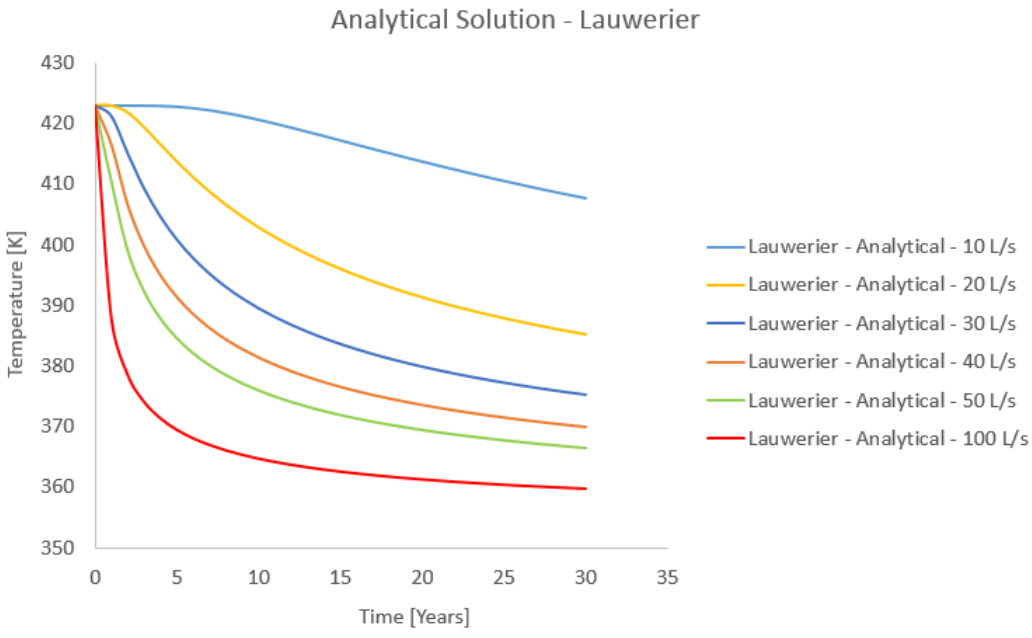

Figure 5.5: Variation of analytical solution with change in Flow Rates

5.2.3 Numerical Modelling and Simulation

The analytical solution for the Lauwerier Model has been well-established. In order to arrive at a simulation process for EGS simulation, it is imperative that the Lauwerier solution is correlated with simulation results. The current section discusses the modelling and simulation aspects of the Lauwerier Solution using ANSYS and coupled fluid-heat transfer. The results are validated with 2D axisymmetric and 3D models. Energy/Power balance is developed in order to verify the implemented physics in the model.

5.2.3.1 Model and Meshing - 2D axisymmetric

The simulation of Lauwerier Model is based on similar physical properties as described in Section 5.2.2. However, the definition of Porosity is altered here since in the simulation environment, it is based on the homogenization of the aquifer thickness over a given element size, i.e mesh dimensions are much larger than the aquifer height itself. This leads to modification of the real velocity field to a Darcy velocity definition and the corresponding material properties of the aquifer are also modified based on the current definition of Porosity. Table 5.1 and 5.2 outlines the model and material properties of the Lauwerier model respectively [DBI, 22].

$$\phi = \frac{Actual\ \ Aquifer\ \ Thickness}{Mesh\ \ Size\ \ of\ \ Aquifer} \equiv \frac{Joint\ \ Volume}{Element\ \ Volume} \tag{5.16}$$

Model Properties	Value
Total Radius	800 m
Total Model Width	200 m
Measuring Distance	366 m
Aquifer Thickness / Element Size	0.008 m

Table 5.1: Model Properties for Simulation of Lauwerier Model

Material Properties	Value
Impervious Rock Heat Capacity	860 J/kg K
Impervious Rock Density	2800 kg/m^3
Impervious Rock Conductivity	3 W/m K
Aquifer Heat Capacity**	863.175 J/kg K
Aquifer Density	2800 kg/m^3
Aquifer Conductivity**	2.98 W/m K
Water Heat Capacity	4186 J/kg K
Water Density	1000 kg/m^3
Water Conductivity	0.6 W/m K

Table 5.2: Material Properties for Simulation of Lauwerier Model

***The aquifer properties are determined from homogenous properties calculation as described in eqns 5.11, 5.12 and 5.16*

The model is illustrated in figure 5.6. The initial and boundary condtions are as follows:

- An initial temperature of 150°C (423 K) is applied to the entire model. The external nodes at the boundary are constrained at a temperature of 150°C (423 K). *See Section* 5.2.1
- The r- & z-axis have no additional boundary conditions. This is in consideration with the axi-symmetric, symmetric model assumption. A temperature boundary condition of 80°C (353 K), corresponding to inlet fluid temperature is applied on the inlet nodes.

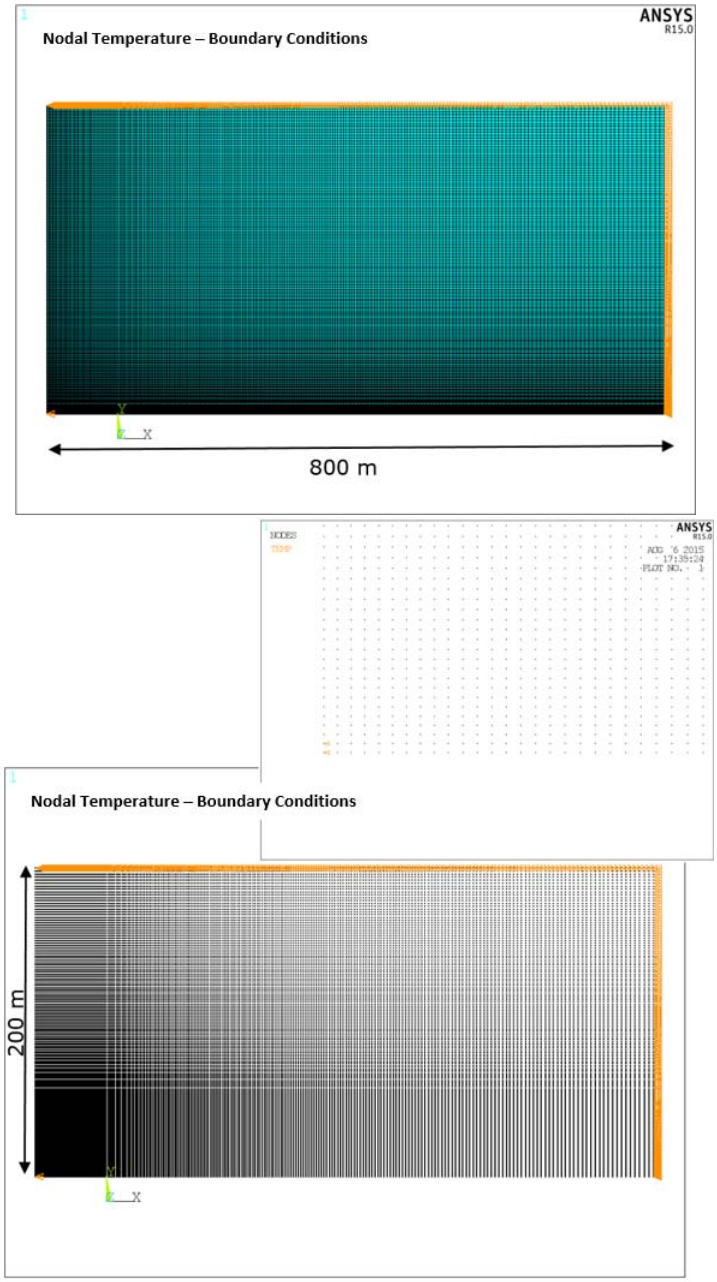

Figure 5.6: Model dimensions with Boundary Conditions

5.2.3.2 Element Formulation - Mass Transport

The heat transport component in the governing equation, (*See eq* 5.1) $\vec{\nu} \cdot \nabla T$ cannot be modelled with a general 2D or 3D heat transfer element. ANSYS provides with a 2D Plane or axisymmetric element, Plane 55, with mass transport capabilities. The element allows velocity input definitions in the element co-ordinate system. For a defined control volume (ANSYS, 2014 [9]), the governing equation is represented as :

$$\rho c \left(\frac{\partial T}{\partial t} + \{v\}^T \{L\} T \right) + \{L\}^T \{q\} = \ddot{q} \tag{5.17}$$

where ρ - Density [kg/m^3]

c - specific heat capacity [J/kg K]

T - Temperature [K]

t - Time [sec]

$$\{L\} = \begin{Bmatrix} \frac{\partial}{\partial x} \\ \frac{\partial}{\partial y} \\ \frac{\partial}{\partial z} \end{Bmatrix} \text{ [1/m] and}$$

$$\{v\} = \begin{Bmatrix} v_x \\ v_y \\ v_z \end{Bmatrix} \text{ [m/s]}$$

{q} - Heat flux vector [W/m^2]

$\ddot{q}$ - Heat generation rate per unit volume [W/m^3]

The problem can be extended to 3D problems using Solid 70. The application of mass transport in Plane 55 or Solid 70 in Ansys is restricted on the basis of physical flow characterisitics by the grid Peclet number, which needs to be < 1. Due to high overall heat capacity of water, the grid Peclet number turns out to be > 1 when used along with velocity and conductivity definitions of the Lauwerier model. This can be overcome using artficial diffusivity/upwind method already described earlier. *See Section* 5.1.3. The Grid Peclet number

is defined as

$$Pe = \frac{\rho c V L}{2\lambda} \tag{5.18}$$

where ρ - Density [kg/m^3]

c - Specific heat capacity [J/kg K]

V - Magnitude of velocity vector [m/s]

L - Element dimension along velocity vector [m]

λ - Equivalent thermal conductivity along velocity vector [W/m K]

In the Lauwerier Model, the thermal conductivity is scaled in the flow-direction, corresponding to a Peclet number lower than 1. L, or the characteristic element length, is given by

$$\mathbf{L} = \mathbf{l}, \ldots l - \textit{Element length for 2D axisymmetric elements}$$
$$\mathbf{L} = \sqrt{\mathbf{a^2 + b^2}}, \ldots a - \textit{Element length \& } b - \textit{Element width for 3D Solid elements}$$

5.2.3.3 Velocity Definitions and Energy Balance

Plane 55 or Solid 70 allows for mass transport input definitions as a part of its element formulation. Apart from the input material definitions, the velocity profile in the aquifer also needs to be generated. The velocity value for a given aquifer element is given by :

$$\nu_{radial} = \frac{\tilde{V}}{2\pi r H} \tag{5.19}$$

where ν_{radial} - Radial velocity in aquifer [m/s]

r - radial distance of element centroid from inlet [m]

In order to verify the implementation of mass-transport terms and estimate the total energy/power available in the system, it is necessary to compute the

total fluxes and their contribution to the total energy. There should also be a relation between a computed theoretical energy and the energy calculated due to the total fluxes in the model. The various energy components in the given problem are :

- Theoretical Energy - The theoretical energy gives an estimate of the total heat absorbed by the injected fluid as it flows through the aquifer. It is given by $Q_{theoretical} = \rho_{fluid} c_{fluid} \tilde{V} (T_{outlet} - T_{inlet})$.
- Convection Energy** - Convection energy is derived out of the transport term and the corresponding convective flux in the model. It is given as $Q_{convective} = \rho_{fluid} c_{fluid} (\nu_i \cdot \frac{\partial T}{\partial x_i}) Vol_{elem}$
- Diffusion Energy - The total energy due to heat conduction is represented by Diffusion energy. It is given as $Q_{diffusive} = \Delta (\lambda \Delta T) Vol_{elem}$.
- Stored Energy - The internal energy in the model, which is the sum of total heat exchanged or released in the model, is given by $Q_{internal} = \rho c Vol_{elem} \Delta T$, where Vol_{elem} is the element volume.

** *Convection flux in Ansys is not available as a post-processing entitiy. In order to calculate the convection energy, the convection flux needs to be manually re-calculated for each element of the aquifer.*

5.2.3.4 Results and Discussion

The Lauwerier Model is analyzed using model and material properties tabulated in Section 5.2.3.1. The results for 10 L/s and 100 L/s are illustrated in figure 5.7 (*Refer Appendix A for more results*)

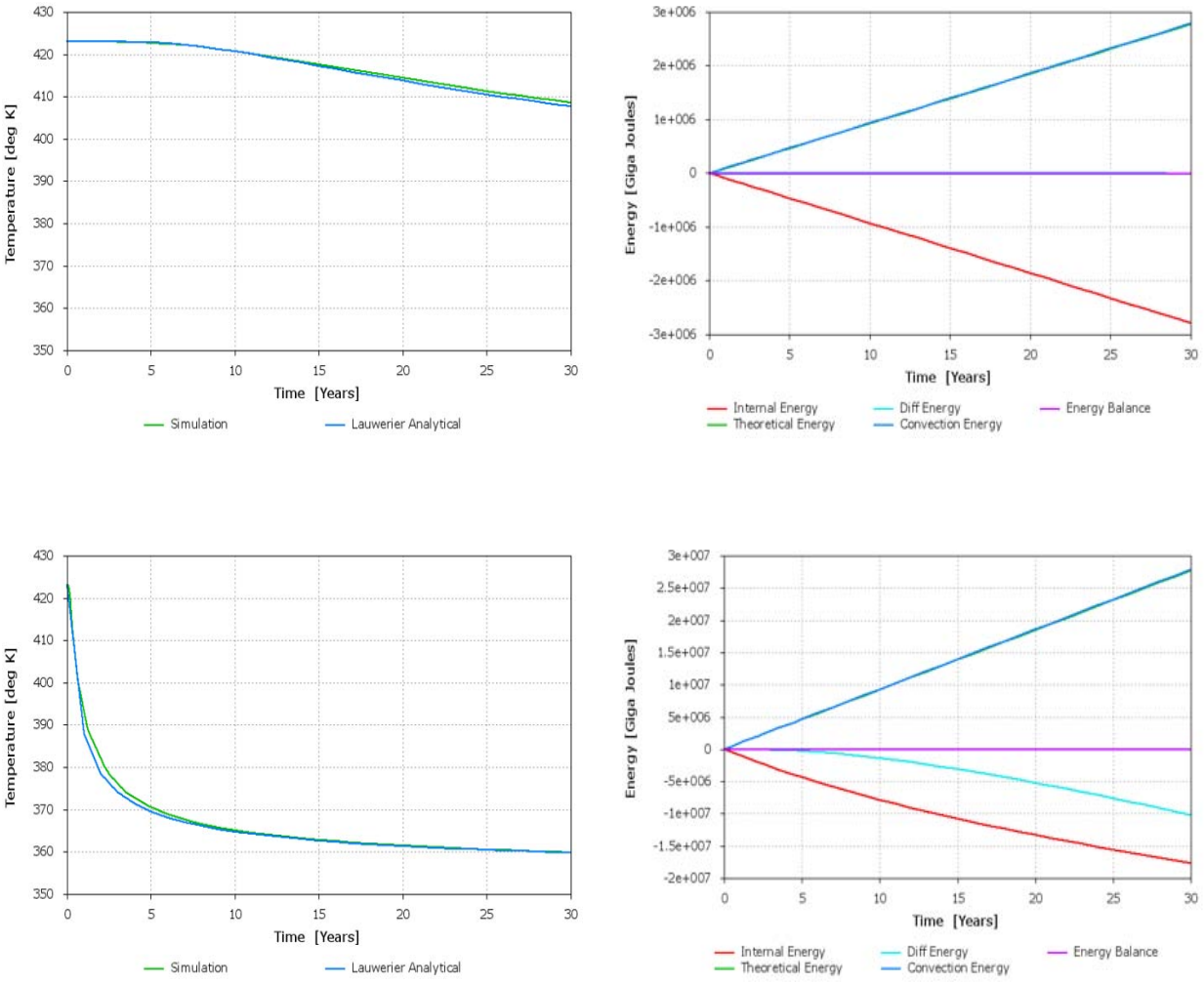

Figure 5.7: Results for 10 L/s and 100 L/s

The simulation results show good correlation with the analytical results. The minor differences in simulation and analytical solution can be attributed to spatial discretization of the model. The energy balance in both cases can be used to verify the model correctness. The high diffusive flux in the 100 L/s case corresponds to heat outflow from the model. This is owing to the fluid/heat flow outside model boundaries and should be rectified by increasing the model

dimensions since it violates the infinite boundary assumption. This, however, has no impact on the temperature measured by the probe which is located at 366 m from the inlet and not at the outlet boundary.

A major difference between the Lauwerier model and the derived Hydraulic Fracturing model for Production and Thermal simulation is the spatial discretization in the flow direction. In the 2D axisymmetric Lauwerier model, the mesh is refined close to the the inlet region and the element size becomes larger with lower velocities away from the inlet. However, the unstructured nature of the mesh in the 3D Hydraulic Fracturing model is only observed in the well plane, i.e. the mesh size in the vertical/flow direction is uniform. In order to overcome such spatial discretization constraints, the Lauwerier problem is recalculated with a 3-D model (using ANSYS - Solid 70 with mass transport) but similar properties as given in table 5.1 and 5.2. The quarter solid model has 960,000 elements and is illustrated along with the in-plane velocity profile in figure 5.8.

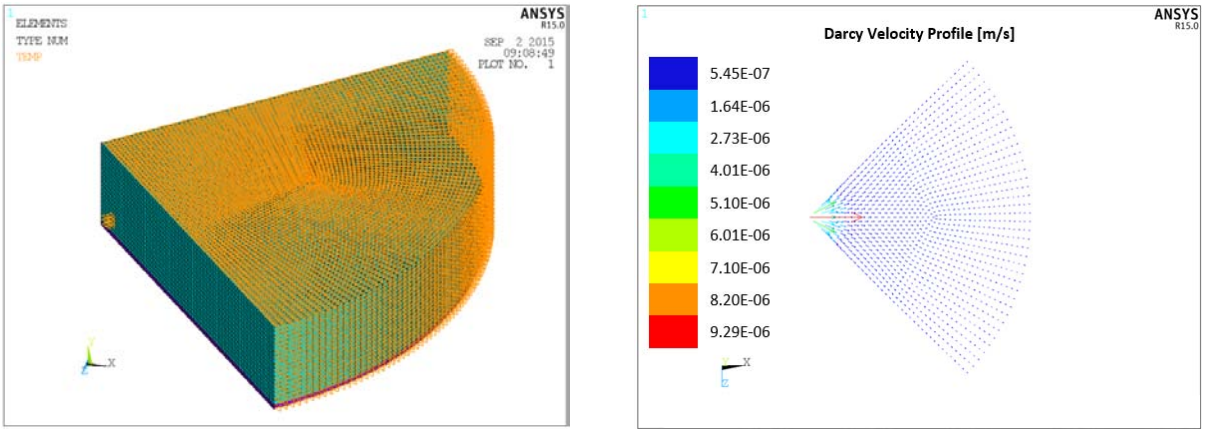

Figure 5.8: Quarter model - Lauwerier with corresponding Darcy Velocity profile

The model is analyzed for varying flow rates between 10 L/s and 100 L/s. The Energy Balance is computed here which is similar to the one shown in figure 5.7. The results for 10 L/s and 100 L/s are illustrated in figure 5.9 & 5.10 respectively.

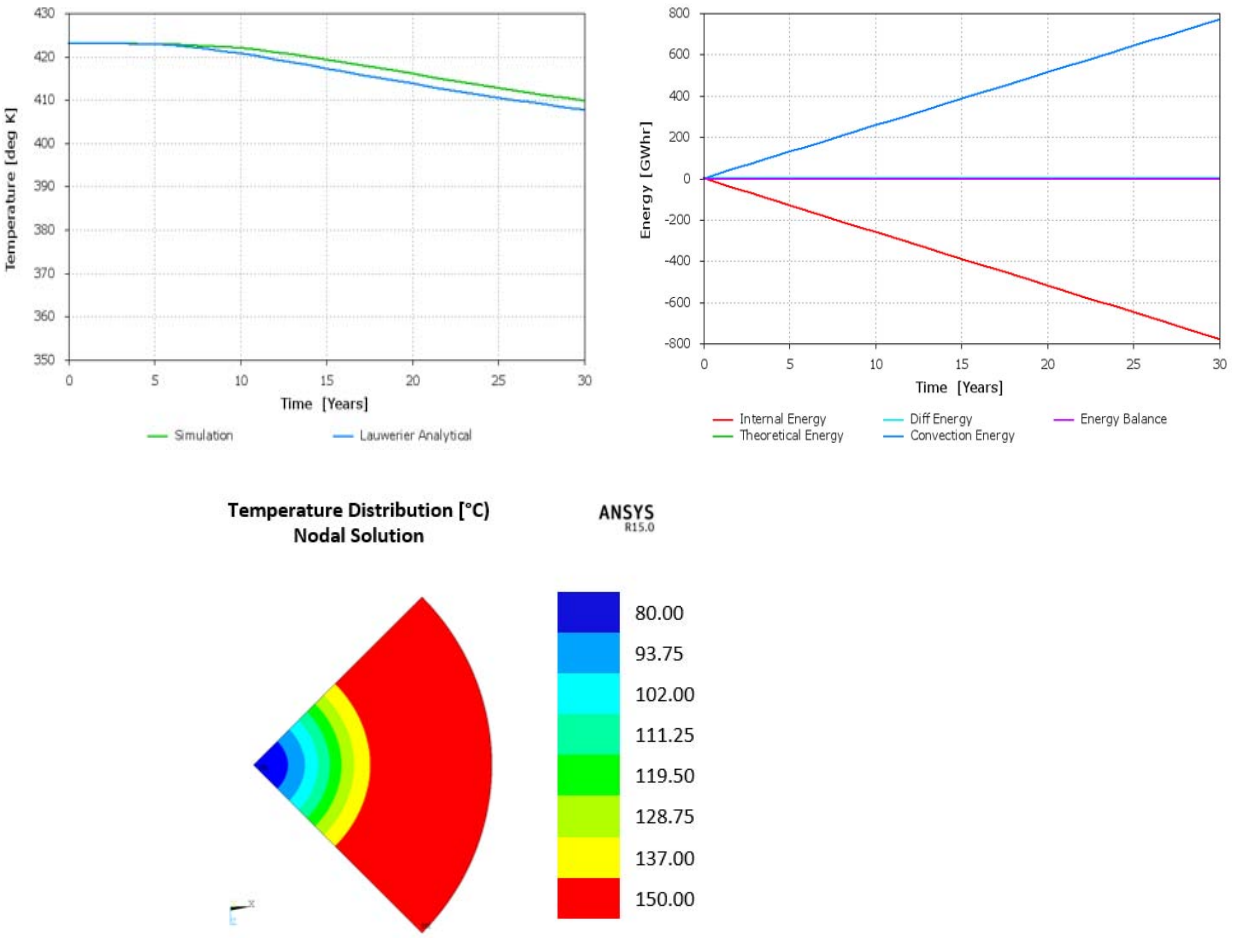

Figure 5.9: Outlet Temperature, Energy Distribution and Temperature Distribution - 10 L/s

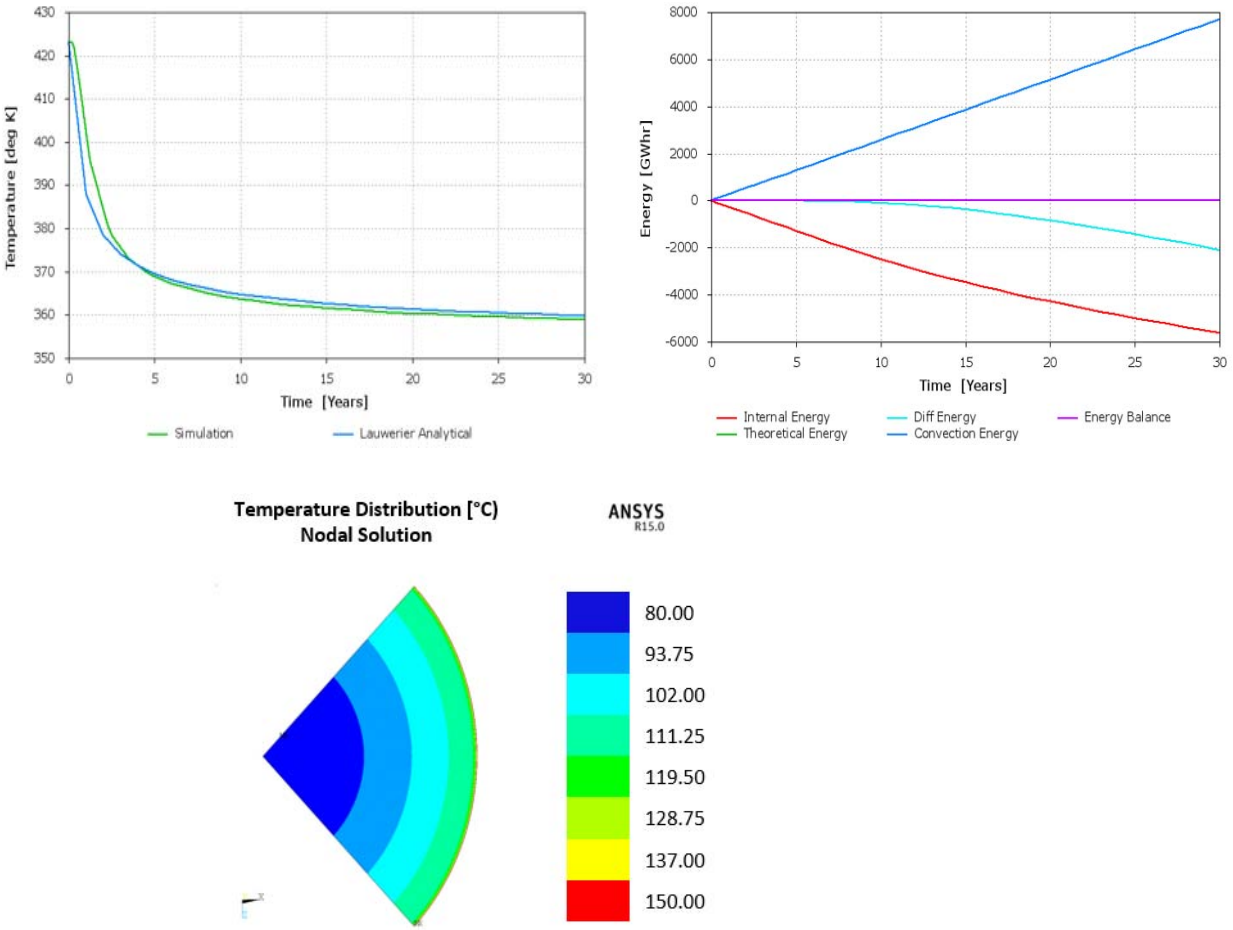

Figure 5.10: Outlet Temperature, Energy Distribution and Temperature Distribution - 100 L/s

The 3D simulations show reasonable correlation with the analytical results. The errors with the 3D simulation are much larger than the 2D axisymmetric model, which is largely due to the uniform mesh size of the model. The energy balance shows that the total energy exchanged in the model is in balance. The initial jump (*see figure* 5.11) in the diffusive energy is due to sudden temperature gradients, arising from a constant 80°C temperature boundary condition at the inlet nodes. It can be controlled using a gradual ramp-down of temperature from the initial temperature to the applied temperature and applying the inlet temperature boundary conditions to nodes of the entire element and not just

the ends. The out-flow from model boundaries observed at high flow rates can be resolved using extended model boundaries but it would have no impact on the temperature distribution which is not the model outlet but a probe location, situated at a distance of 366 m from the model.

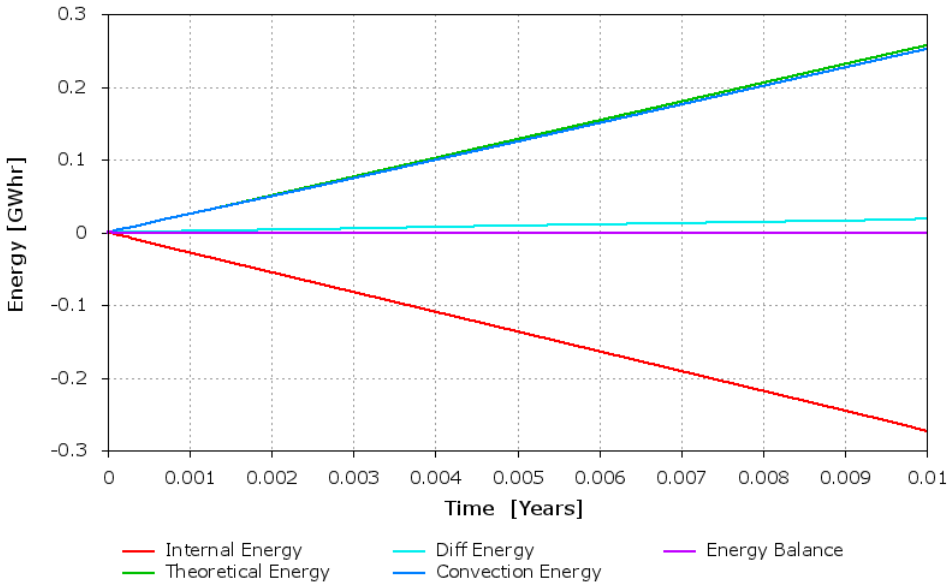

Figure 5.11: Jump in Diffusive Energy - Beginning of Simulation

The implemented mass-tranport scheme, with a simplified streamline upwind scheme/artificial diffusivity and aquifer homogenization, shows agreeable correlation with the analytical solution for reasonable mesh-sizes. The results of the 3-D simulation highlight the ill - effects of applying sudden temperature loading at certain nodes of the inlet element, leading to severe temperature gradients with an element. The energy/power balance further validate the physics and the implementation of inlet conditions along with a convective flux resulting due to heat-transport. It should be further stated that the deviation of simulation results from the analytical solution is a combined effect of the homogenization principle and space discretization measures.

5.3 Idealized Reservoir 3D model

The successful implementation of the developed mass-transport scheme to the Lauwerier Model, paves its way towards application in a real reservoir model. However, before the new scheme is tested with an actual 3D fracturing model with an arbitrary fracture network,its performance is evaluated with an idealized reservoir model. The same has also been tested with COMSOL Multiphysics (DBI, 2014 [23]) and a similar model is evaluated and compared here. The reservoir model is shown in figure 5.12.

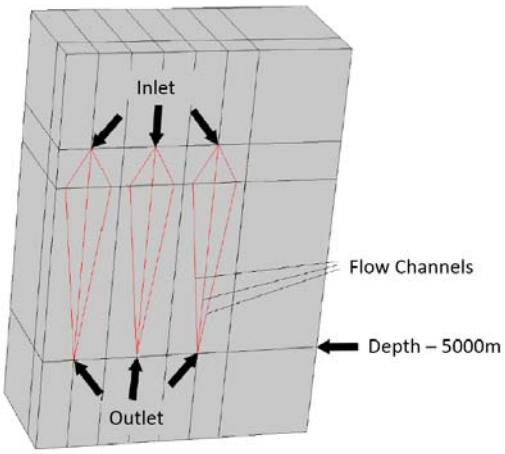

Figure 5.12: Idealized Reservoir Model - COMSOL (DBI, 2014)

The COMSOL - DBI model has the following assumptions :

- **The fracture network is idealized** - The fracturing simulation was carried out using MFRAC by DBI (Kretzschmar, 2013 [14]). However, COMSOL does not allow the direct import of MFRAC models to its simulation environment. The diamond-shape of fractures illustrated in figure 5.12 is owing to the assumed velocity profile in the generated fracture models.
- **The magnitude of velocity profile is unknown** - The resulting veloc-

ity profile in the reservoir is a function of hydraulic conductivity and joint opening values of the reservoir. The only available information with respect to joint openings in the reservoir is the average opening value which will be used to generate the velocity distribution in the reservoir.

- **Energy Balance** - There is no information about the energy exchange in the model. Hence, it is not clear which physical models of heat energy distribution are used in the model. The implemented heat-transfer model in COMSOL is the non-isothermal fluid flow with heat transport which has similarities to the implemented simplified upwind mass-transport scheme in ANSYS.

5.3.1 Reservoir Model - ANSYS

A 3D reservoir model is generated based on inputs from the COMSOL model. Instead of a diamond-shaped fracture network, a rectangular fracture is assumed with the surface area equal to the modelled diamond shaped fracture by COMSOL. The model is illustrated in figure 5.13

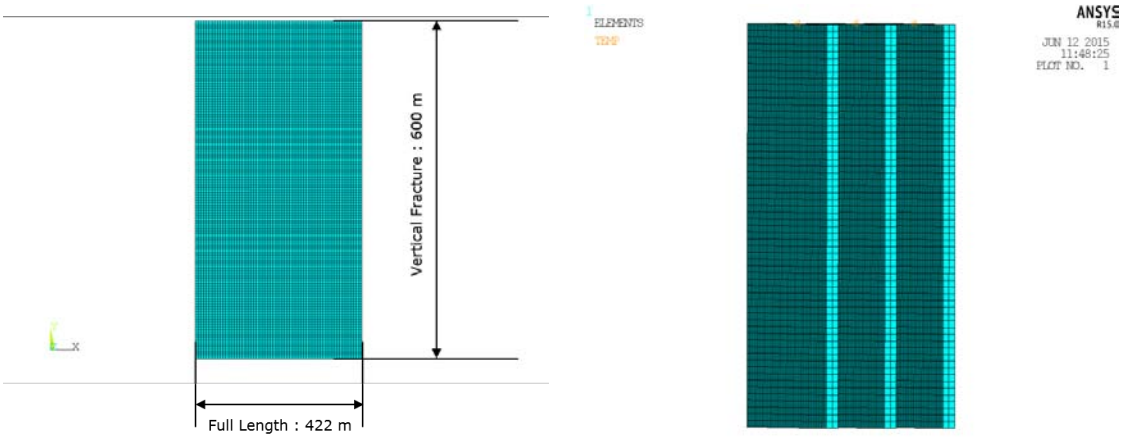

Figure 5.13: Idealized Reservoir model with ANSYS

The surface area of the model corresponds to 3.8E6 m^2 which is also the as-

sumed surface area of the COMSOL - DBI model and contains 780,000 elements. The velocity is generated adopting an initialized steady state Production cycle using simulation process described in Section 4.3. The boundary conditions are illustrated in figure 5.14.

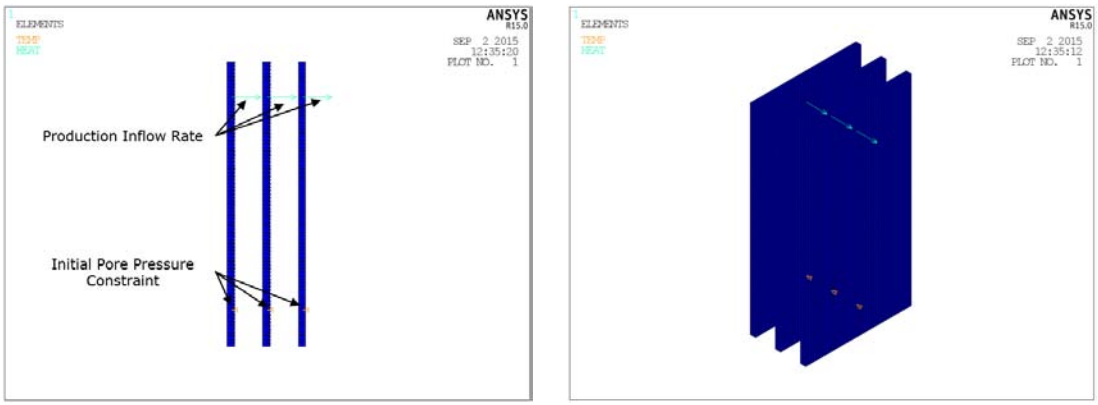

Figure 5.14: Boundary Conditions - Velocity Initialization steady-state Production cycle

5.3.1.1 Velocity Vectors and Reynolds' Number

The velocity vectors in the reservoir are initialized using Production boundary conditions in the idealized reservoir model. In order to successfully carry out the steady state analysis, the fracture network needs to be initialized by a hydraulic conductivity value. This is done using an average opening value of 8 mm and using the conductivity - opening relation used in eq 2.13. For simplification purposes, the overall conductivity matrix is assumed to be orthotropic, i.e high in-plane and low out-of-plane conductivities (*See eq* 2.11). The resulting velocity profile and Reynolds' number is represented in figure 5.15.

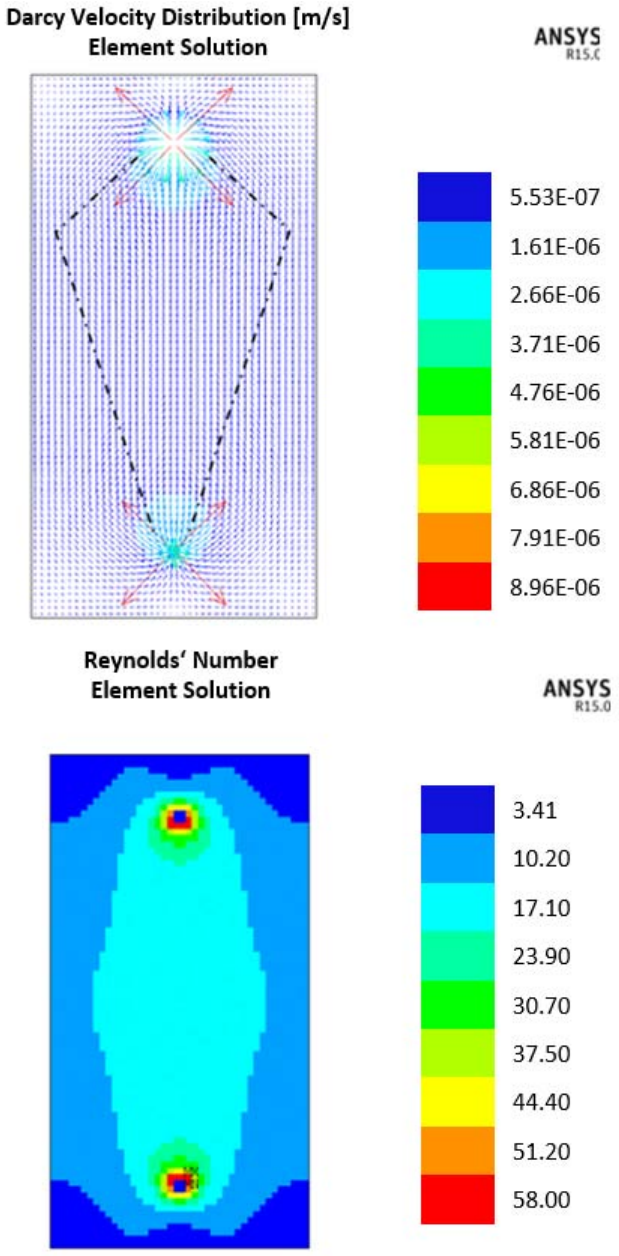

Figure 5.15: Velocity and Reynolds' number Distribution in Fracture Network

The outline along the velocity vector shows an idealized velocity vector profile, similar to one used by COMSOL. The Reynolds' number is used to identify the flow - characteristics. Restricted to a low value, the flow in the reservoir is lami-

nar (also assumed by the theory of Porous Media) which based on the employed mesh sizes always results in a Grid Peclet number < 1 and doesn't require a different time-step discretization scheme or artificial diffusivity for heat-transport. The maximum Peclet Number for the idealized reservoir model was noted to be **0.88**. It is important to note that the above velocity is a representative velocity or Darcy velocity based on the homogenization assumption. However, it does not cause any conflicts since the developed mass-transport scheme also works on Darcy velocities and not real velocities.

5.3.1.2 Loading Scenarios & Stability

As noted during 3D modelling of the Lauwerier problem (*see Section* 5.2.3.4), sudden application of the inlet temperature conditions may lead to large diffusive fluxes and over-estimated Energy values. Ramping of inlet boundary conditions is not the only problem faced during the 3D Reservoir simulation to achieve a stable solution. Accumulation of velocity fluxes at inlet and outlet regions and out-of-plane Darcy velocities lead to either unconvergent or incorrect solutions, as illustrated in figure 5.16

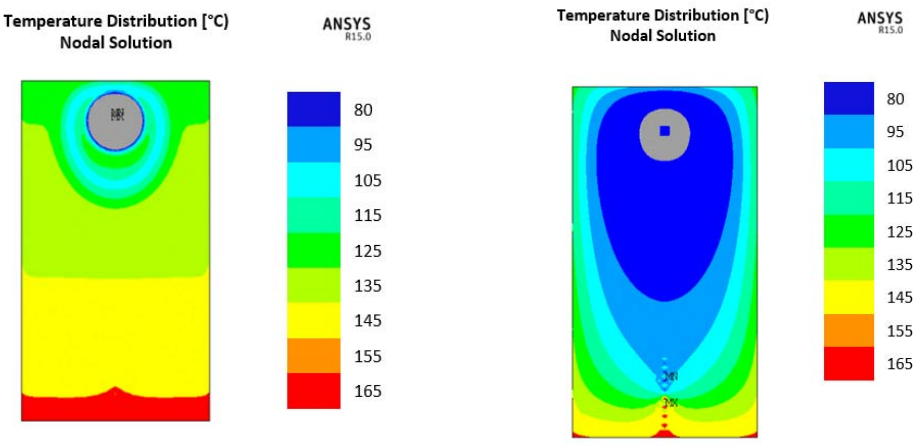

Figure 5.16: Temperature Distribution for unconverged solution due to out-of-plane velocities (left) and oscillations due to inlet-outlet fluxes (right)

These instabilities are caused due to the following reasons :

- **Unconvergent Solution due to Out-of-Plane velocities** - The out-of-plane hydraulic conductivity in the model leads to low velocities in the out-of-plane direction of the fracture network. These low velocities have very low magnitudes when compared to the in-plane velocities. Upon assembling the global stiffness matrix, the condition number becomes high due to presence of low and high velocity components which makes the problem ill-conditioned.
- **Oscillations in Solution due to Concentrated Fluxes** - Velocity fluxes converge to a few elements near the inlet/outlet as seen in figure 5.15. It leads to numerical oscillations as soon as the temperature front reaches the highly concentrated flux region, causing numerical ripples in the model.

The aforementioned problems can be remedied by removing the out-of-plane velocities and using high thermal conductivity for elements near the inlet and outlet instead of applying a convective flux to those elements. Although the workarounds modify the physics of the problem in hand but they do not impact the accuracy of the solution since they are concentrated to 2-4 elements near the inlet - outlet regions whereas the total number of elements $>$ 200,000!

In-plane Velocity Magnitude [m/s]	Out-of-plane Velocity Magnitude [m/s]
0.566E-07	0.736E-12

Table 5.3: In-plane and Out-of-plane Velocity magnitudes

The stability and accuracy of the solution, especially the energy balance, is also impacted with the temperature loading. The temperature of water at the

inlet is applied as a temperature boundary constraint at the inlet nodes. As mentioned earlier, a ramped boundary condition ensures better convergence of the thermal model. Two possible scenarios for such a temperature loading are shown in figure 5.17

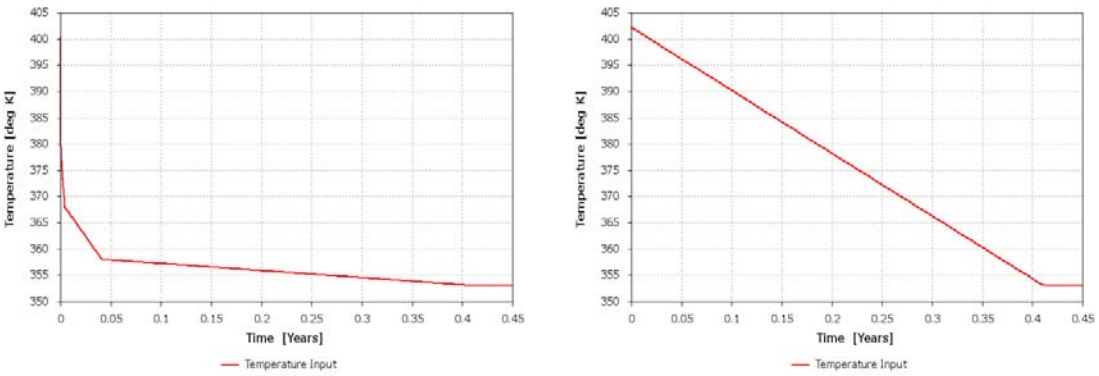

Figure 5.17: Logarithmic and Linear Temperature Loading at Inlet BCs

Both logarithmic and linear ramping of the inlet boundary conditions lead to similar final temperature distribution of the fracture network and outlet temperature curves but the energy distribution in the former case is unphysical since it leads to very high diffusive energy during model initialization. The high diffusive energy in the logarithmic loading case is due to large temperature gradients within the model emnating from the sudden drop of temperature during initial loading. It is illustrated herewith in figure 5.18.

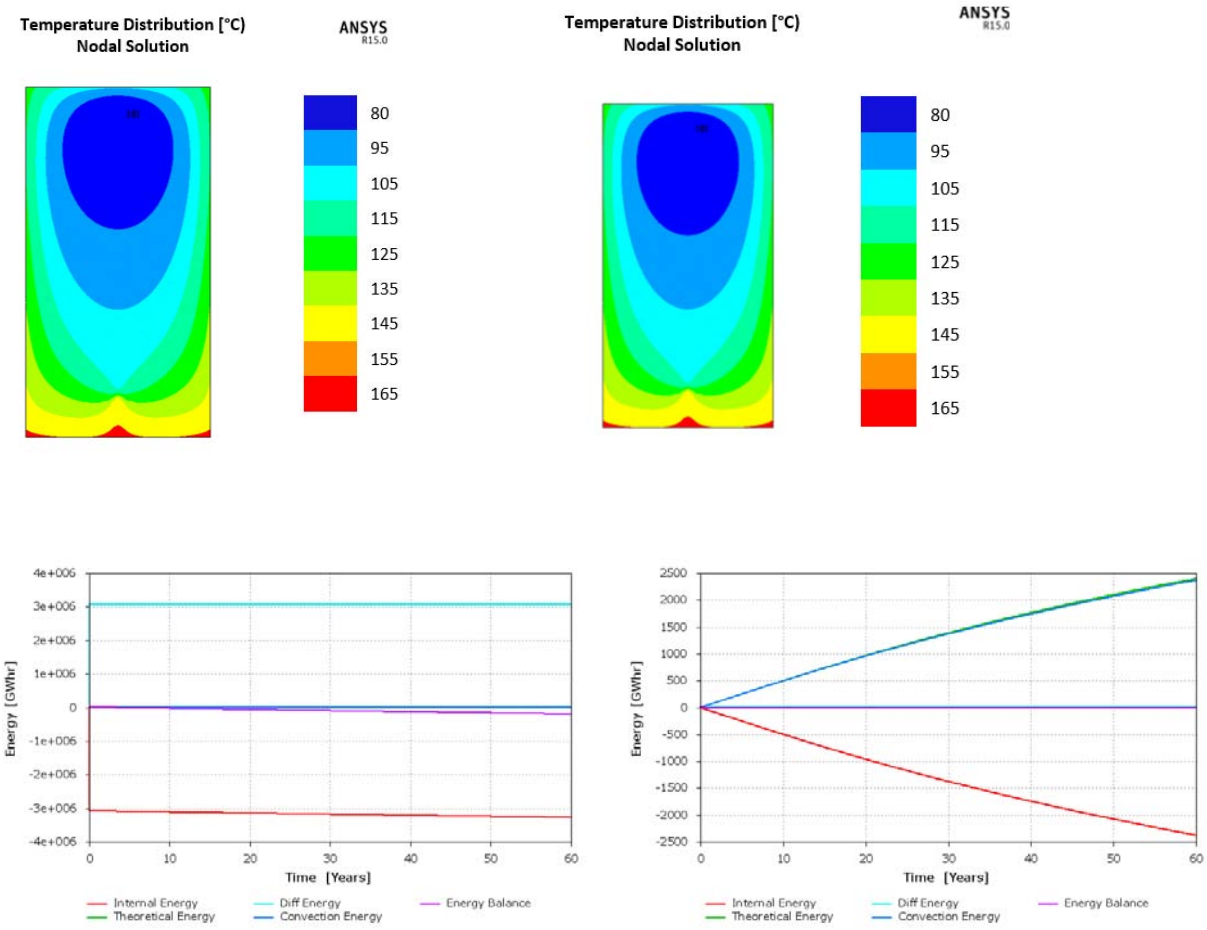

Figure 5.18: Results with Logarithmic loading (left) and Linear loading (right)

Since the application of mass-transport makes the system matrix unsymmetric, the choice of equations solver becomes important. The Pre-Conjugate Gradient (PCG) solver, an efficient and highly used iterative solver provided by ANSYS, cannot be employed since it can only solve symmetric matrices. Instead, a Jacobi Conjugate Gradient (JCG) or Incomplete Cholesky Conjugate Gradient (ICCG) should be used. In the current study, the ICCG solver has been used since it is known to be more robust although it demands higher memory requirements (ANSYS, 14 [10])

5.3.1.3 Results and Discussion

Introduction of stability algorithms and solver schemes and linearly varying ramped loading lead to stable temperature distribution and energy balances. In the current section, the outlet temperature distribution determined using ANSYS - mass transport will be compared with COMSOL - DBI results. As stated in Section 5.3, several assumptions were made by DBI with respect to fracture network geometry, developed velocity profile and heat-tranport physics. A comparison of temperature distribution, along with the outlet temperature development and corresponding energy balance for 10 L/s and 100 L/s are illustrated in figure 5.19.

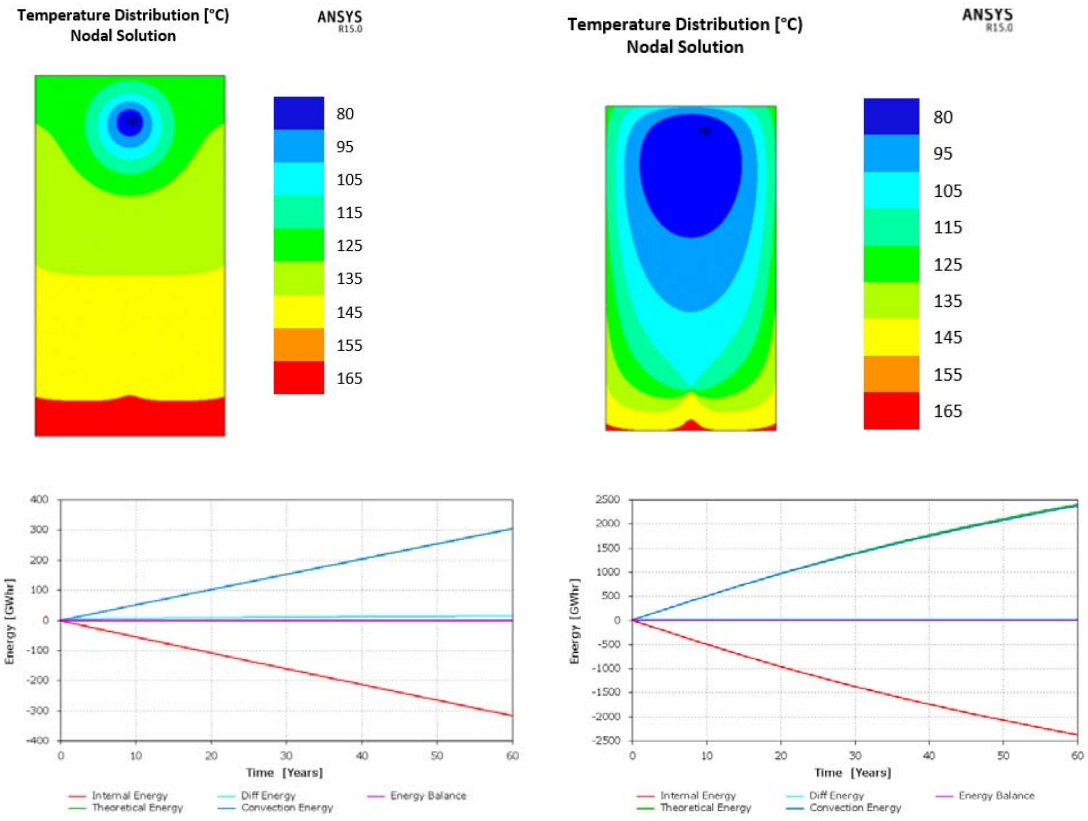

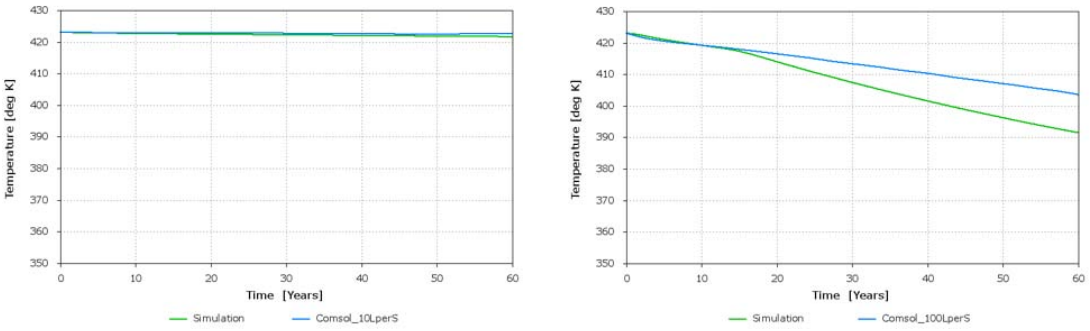

Figure 5.19: Temperature Distribution, Energy Balance and Outlet Temperature for 10 L/s (left) & 100 L/s (right)

The following observations could be made from the analysis of above flow rates

- **Diffusion energy is dominant at low flow rates** - Lower flow rates lead to lower darcy velocities in the model which leads to reduced convective fluxes in the model. Hence, diffusive fluxes at lower flow rates are not negligible and should not be ignored.

- **Oscillations at higher flow-rates** - The minimum temperature for temperature simulation with 100 L/s is slightly lower than the minimum applied temperature boundary condition in the model, i.e. 80°C. This is due to numerical oscillations in the model and can be overcome by using direct sparse solvers or finer spatial discretization.

- **Outlet temperature distribution** - The temperature distribution for both low and high volume flow rates shows deviation with COMSOL results. This is mainly due to the unknown velocity profile (joint opening field, actual hydraulic conductivity) of the fracture network. However, the energy balance in both low rate and high rate scenarios shows accurate physics representation with the employed mass-transport scheme.

As highlighted with the Lauwerier Model (*see Section* 5.2.3.4), the homogenization principle should be supplemented with a Design of Experiments (DoE) study to clearly understand the influence of governing parameters and arrive at an optimized solution. In the current study, a DoE investigation has been carried out only for production parameters such as average pressure change responses and leak off measure.

Chapter 6

Results and Discussion

In the current section, the results of the reference model for the Meiningen-Suhl reservoir is discussed. The extended process chain is shown in figure 6.1. As discussed earlier, the homogenization principle needs to backed by a Design on Experiments (DoE) study considering not only the assumptions in reservoir-modelling but also the uncertainities associated with material and layering data-acquisition. A recommended approach is to supplement a DoE with a sensitivity analysis, which not only illustrates the dependence of parameters on each other but also highlights the most significant parameter to a resulting response. Such a sensitivity analysis could be further used in process optimization and higher system efficiency.

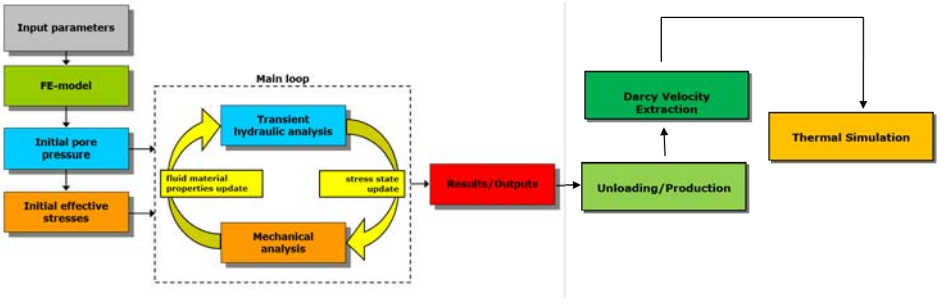

Figure 6.1: Extended Process Chain

6.1 Reference Design

In order to establish a design space with defined parameters and their ranges, a reference design needs to be established. The parameter values for the reference design are based on actual measurements and reliable literature data. *See Table* 3.1 *and* 3.2.

6.1.1 Reference Design - Results

The results of model Unloading and Production for the reference model have been discussed in detail, *see Section* 4. The fracturing or stimulation cycle, is itself a good estimation of the tappable resources in a given reservoir. Moreover, in order to compare the current simulator results with other established well simulators, it is important to develop characterizing dimensions for the resutling fracture network. The characteristic dimensions are used as input parameters to most well simulators which use discrete-element modelling. Such a dimension could be extracted using the fracture distance, illustrated in figure 5.2 (down). Moreover, the fracture core could also be represented using plastic elements generated during fracturing, also shown in figure 5.2 (top). The three smeared faces of elements in the reservoir represents the generated fracture core as a direct result of the fracturing stage. Each block of elements represents a stage which is a pumped over a given time interval. Here, the final representation after 3-stage pumping is visualized. The total distance (figure 6.2 down) represents the equivalent distance of the fracture dimension, based on its horizontal and vertical extension. The plot shows the evolution the total distance of the three fracture over time. In both the cases, plastic elements having opening values larger than 0.1 mm are illustrated since they represent the core of the fracture which have large enough openings to allow water to flow through.

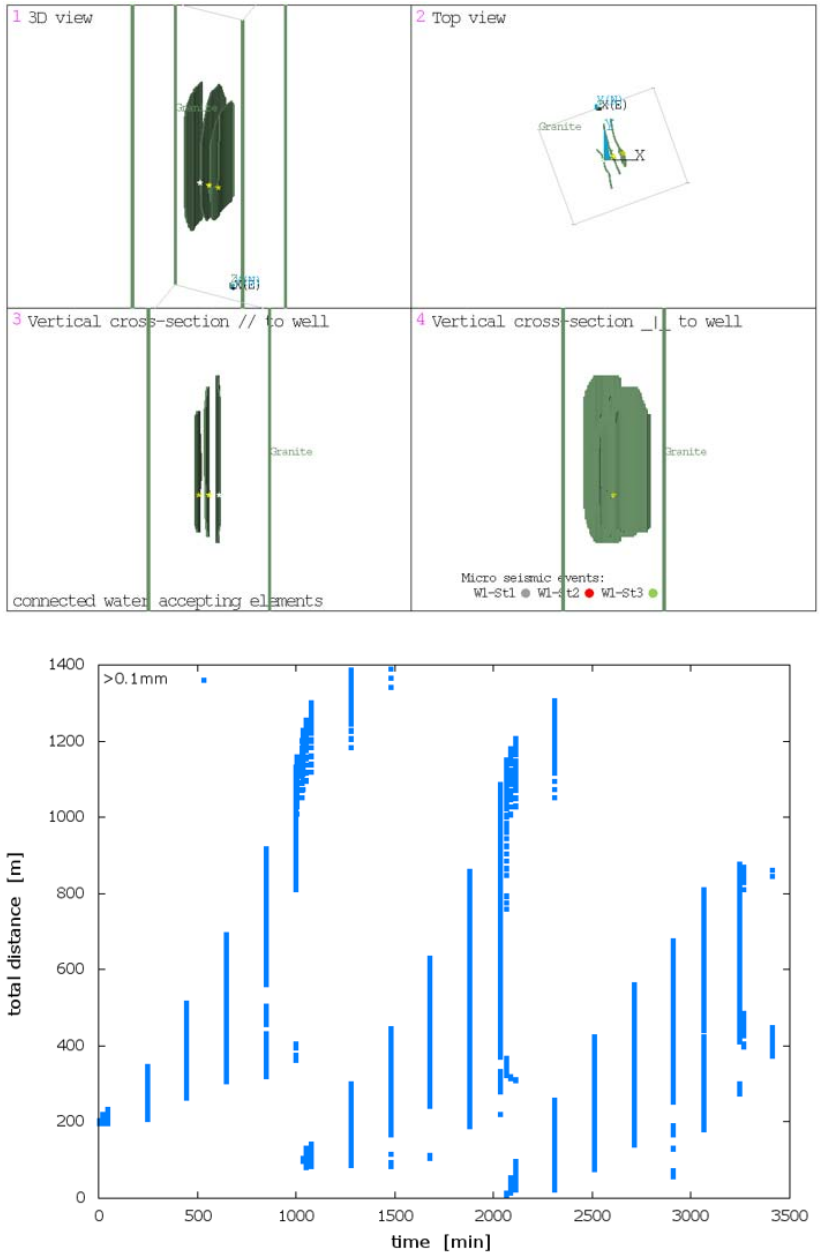

Figure 6.2: Responses of a typical Fracturing cycle - Plastic Volume (top) and Total Distance (below)

Additional post-processing of the reservoir such as hydraulic conductivities, average and maximum opening of individual joint-sets are available in *Appendix A*.

The thermal simulation cycle proceeds the production simulation where the darcy velocity flow field in the fractured elements is used to simulate the thermal-transport problem. The hydraulic model used for the simulation of the production cycle is chosen as the model for the thermal simulation since it contains more elements and is therefore more stable than the corresponding mechanical model. It however reduces the computational efficiency of a given load-step in the thermal cycle. The darcy velocity, imported to the hydro-thermal model is illustrated in figure 6.3.

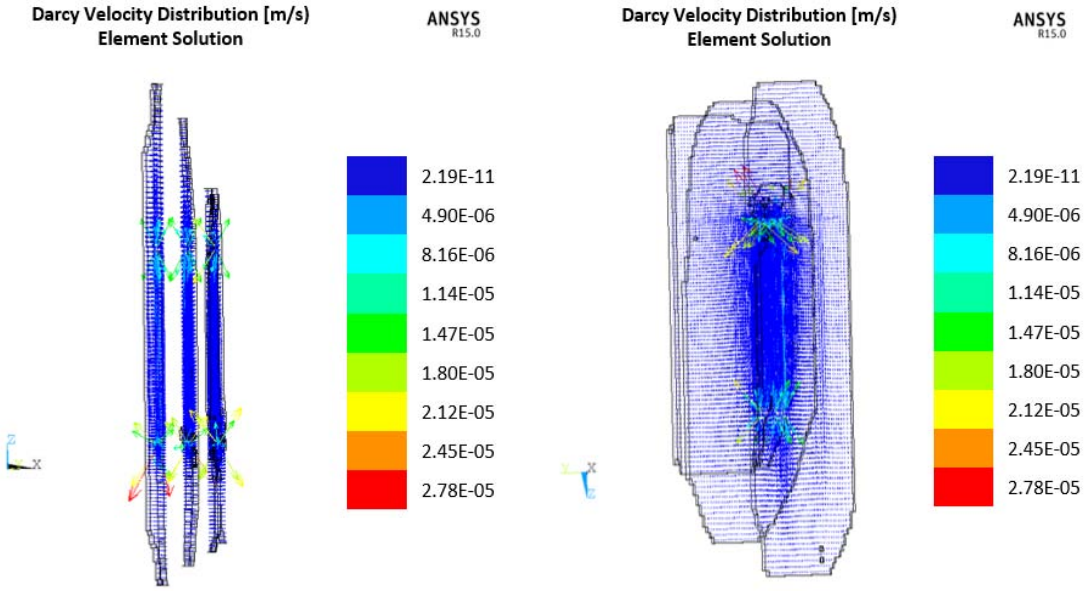

Figure 6.3: Darcy Velocity Flow Field in Reference Model

There are certain modifications made before the hydraulic model, derived from the Production simulation, could be used for the Heat Transport simulation. These include :

- **Element Formulation** : The element formulation needs to be changed to Solid 70 from User 100. Link elements, used as observation/injection wells could be deleted since the boundary conditions for the thermal process are applied directly to the solid model and not the 1D or link elements.

- **Porosity** : The porosity of each fractured element needs to be calculated using eq 5.16. The joint volume is based on the joint activity of the most dominant joint set. Based on the porosity, a homogenous heat capacity and conductivity is calculated using eq 5.11
- **Boundary Conditions** : All fracturing and production boundary conditions need to be deleted and replaced by thermal boundary conditions (*See Section* 5.3.1)
- **Out-of-plane Velocities** - The out-of-plane velocities, as discussed in 5.3.1.2 are removed. In this case, the out-of-plane velocities refer to the plane perpendicular to the most dominant vertical joint set and not the fracture plane itself.

The comparison of the hydraulic model before and after introducing the aforementioned modifications are illustrated in figure 6.4 & figure 6.5

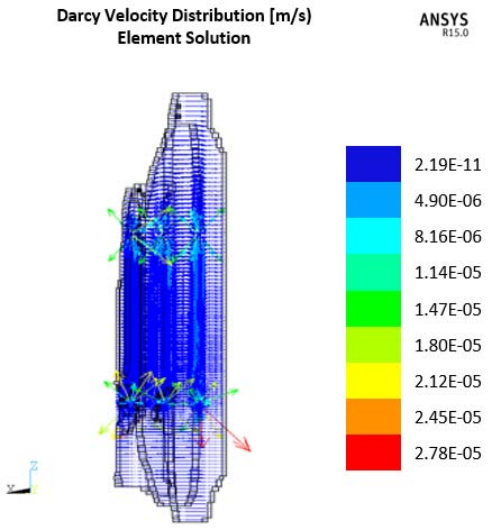

Figure 6.4: Darcy Flow Field before Thermal Simulation modifications

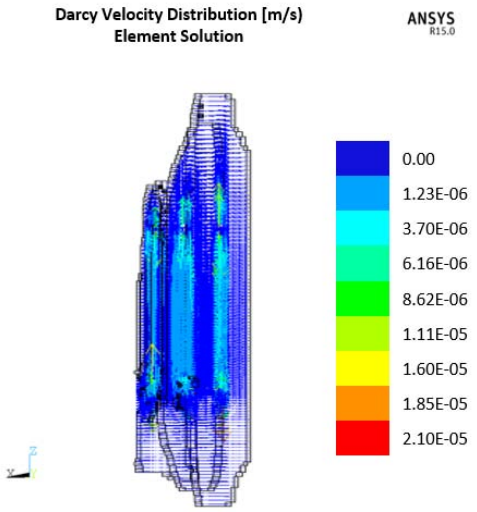

Figure 6.5: Darcy Flow Field after Thermal Simulation modifications

The resulting outlet temperature distribution, energy balance, time-stepping and the temperature profile are higlighted in figure 6.6.

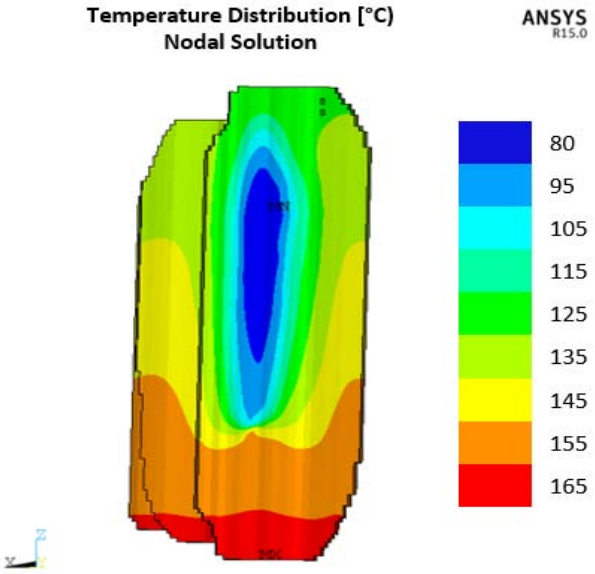

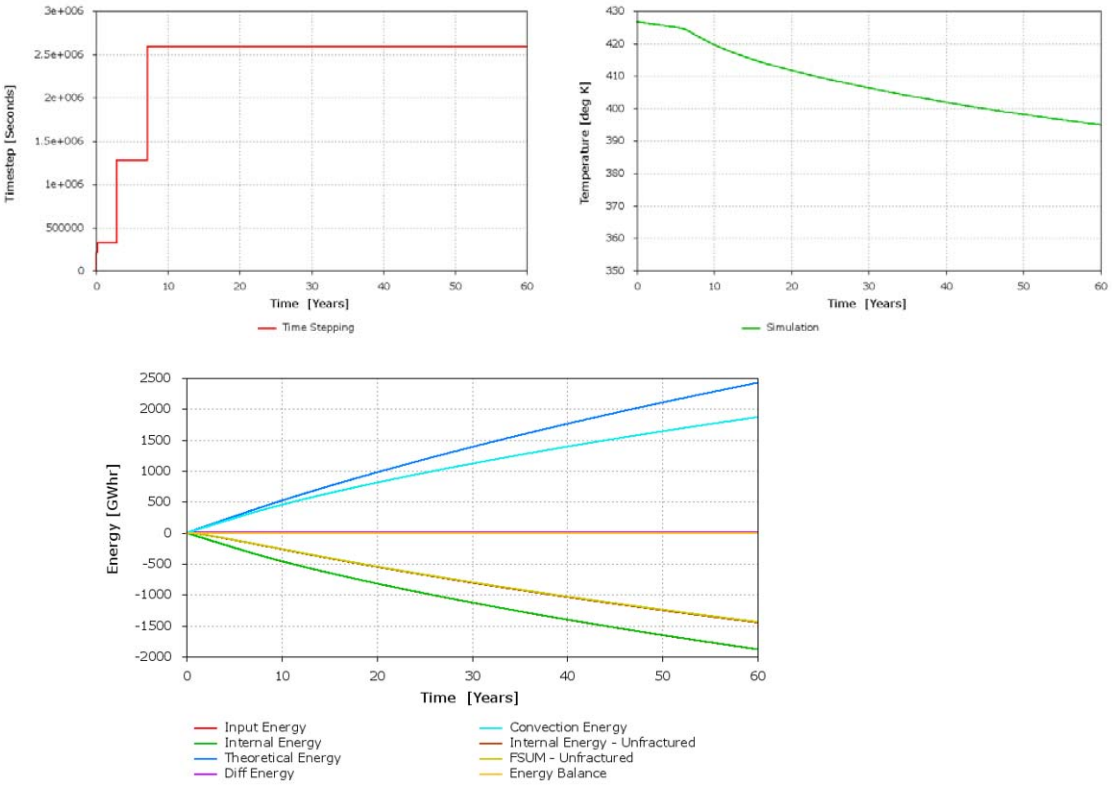

Figure 6.6: Outlet Temperature, Energy Balance, Timestepping and Temperature profile - Reference Model

The simulation process is stable and yields reasonable results for the general unstructured mesh. In order to further validate the simulation process, the methodology is tested for a refined time-stepping scheme. The results are compared and checked for discrepancies.

Moreover, the energy balance has been further detailed to highlight the energy conservation in the model. The individual terms denote :

- **Input Energy & Internal Energy** - Input Energy is the total sum of convection energy and diffusion energy in the model. Based on the conservation of energy principle and neglecting any incurred losses, the input

energy should be equal to the internal energy of the model as illustrated in figure 6.6 (Red & Green).

- **Theoretical Energy & Convection Energy** - The theoretical energy based on the outlet & inlet temperature difference and the heat capacity of the injected fluid should be in balance with the convection energy in the model (Dark Blue & Light Blue). However, due to removal of high magnitude fluid velocities at the inlet and the outlet (for stability), lack of fluid leak-off calculations and the varying temperature of the outlet at every fracture, the balance is not visible.

- **Internal Energy & Diffusive Energy - Unfractured Elements** - The internal energy of the unfractured elements should be in balance with the applied diffusive energy since the unfractured elements do not bear any convection terms. (Yellow & Maroon).

6.1.1.1 Refined Time-stepping Scheme

The maximum time-step in the simulation during flow initialization has been defined using the CFL condition given as :

$$t_{max} \leq \frac{Perforation\ \ Element\ \ Length}{Maximum\ \ Velocity} \tag{6.1}$$

The perforation element length is a conservative estimate of the the distance parameter in eq 6.1 since the perforation element edge is the smallest length parameter in the model. The maximum velocity is the maximum Darcy velocity magnitude in the hydraulic model. As the flow gets established, the time-steps are scaled and the maximum time step in the model during the entire simulation is fixed at 2.59E+06 seconds or 30 days. As a part of a time-stepping refinement iteration, the rate at which the timestep is scaled to the CFL timestep and the maximum timestep of 30 days is reduced. The results are outlined in figure 6.7.

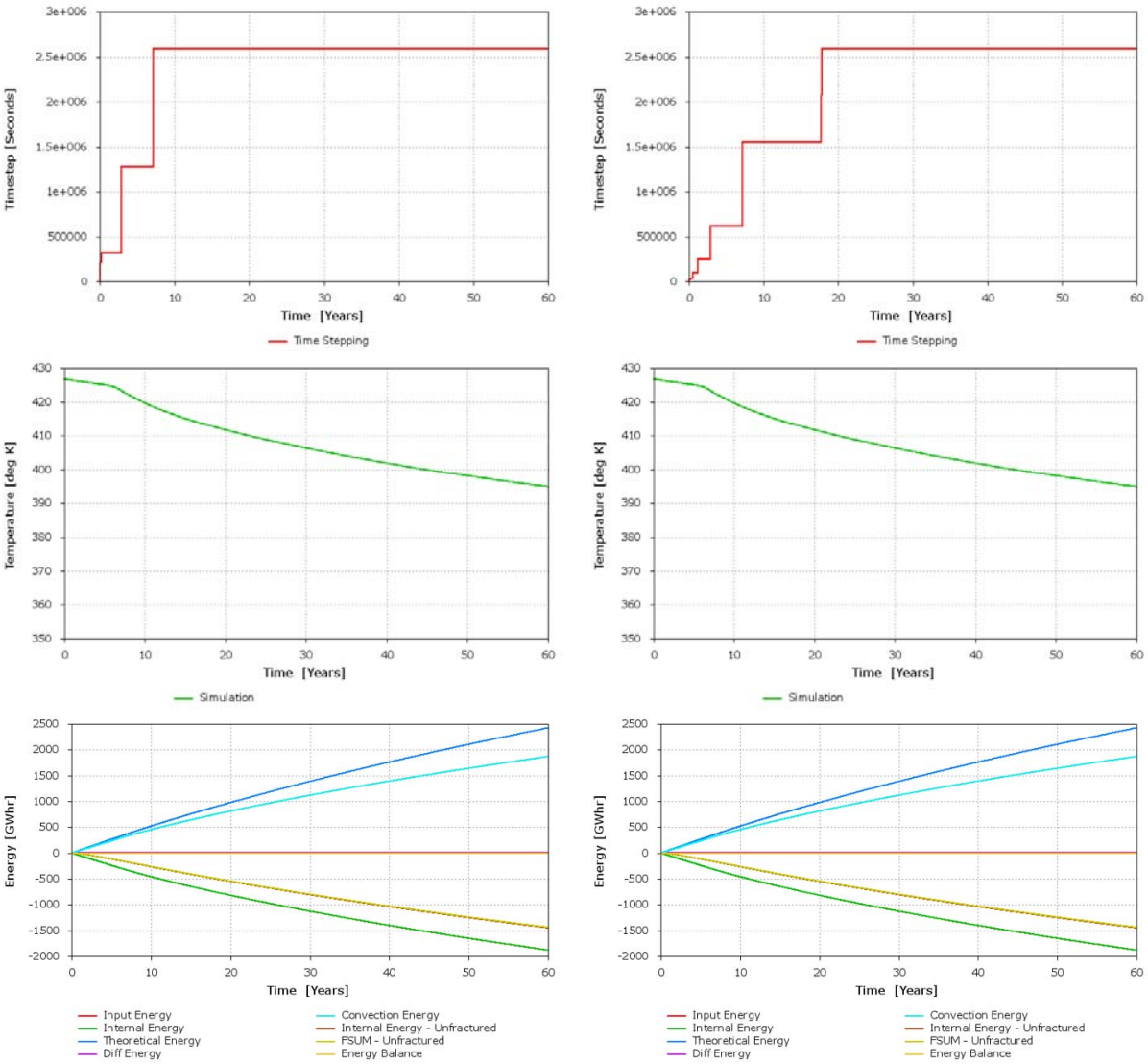

Figure 6.7: Timestep, Outlet Temperature and Energy Balance Comparison - Coarse timestep (left) & Refined timestep (right) scheme

The comparison of the two timestep schemes reveals the independence of the models on the applied temporal discretization. It must be noted that the maximum timestep of 30 days is estimated based on the numerical stability of the model and further scaling might be possible. The total number of steps for the coarse and refined scheme are 1067 and 1832 respectively with each step

requiring ~ 2.5 mins of solver time on an Intel XEON CPU with 72 GB RAM and clock-time equal to 2.40 GHz.

A Sensitivity study involving thermal simulation parameters and process chain could also be carried out in order to investigate the variation of thermal responses and identification of sensitivities of various thermal parameters to the resulting responses . However, the thermal solver and process chain discussed here is not in any form the finished article. However, the objective of the study is to initiate the development of an integrated solver and it has been illustrated that both the production cycle and the thermal simulator work seamlessly with a general 3D unstructured fracturing model.

Chapter 7

Conclusions & Future work

The current study focuses on development of an integrated numerical simulation process chain for a Geothermal operation cycle. A reference model based on reservoir conditions in Meiningen/Suhl, Thüringia, Germany has been evaluated. The simulation technique is a combination of several standalone individual processes, namely, stimulation phase, unloading phase and production phase. The basic building block of the numerical simulator are the 3D Groundwater relations and the general 3D advection-conduction equation. Development of an additional thermal simulator, based on heat transport formulation in ANSYS, has been carried out which has further extended the process chain beyond its original scope. The thermal simulator has been validated with analytical solutions and other commercial numerical models. The stability of the implemented schemes has been verified with varying mesh characteristics and time-stepping schemes. In order to bolster the principle of homogeneity, a Design of Experiments study has been carried out; based on uncertain and reservoir operational parameters. Consequently, the best design parameter set along with the sensitive parameters have been identified.

The development of an integrated solver allows room for further study and improvements which could not be achieved during the stipulated time. Some of these include :

- **Production Well Selection Algorithm** - The Production well algorithm is currently based on assumptions that add numerical noise to the model. Further enhancement to the algorithm could be made based on actual operational practice or improved numerical performance.

- **Thermal Solver Stability** - The thermal solver could be further optimized based on identification of an efficient time-stepping scheme and/or stabilization algorithms. Stability of the model in an unstructured mesh needs to be further investigated and incorporating the out-of-plane velocities with an efficient time-stepping scheme remains a challenge.

- **Sensitivity study for Thermal simulation** - Since the thermal solver is also based on the assumption of homogeneity, a DoE study involving thermal parameters is recommended.

Appendix A

Appendix I

Slurry Rate & BHP - Viscosity Iterations

The results for bottom hole pressure and slurry rate for viscosity iterations are shown below :

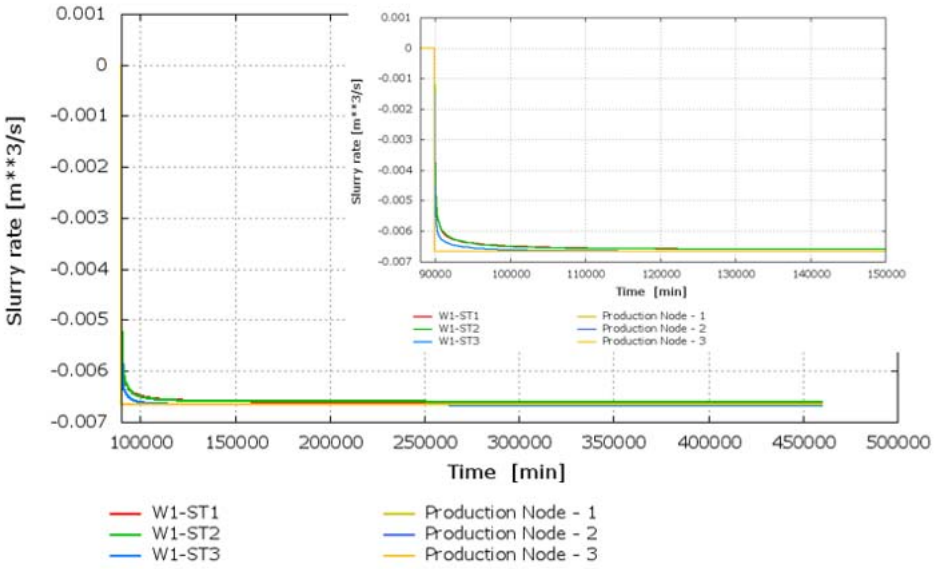

Viscosity 1.5 cP

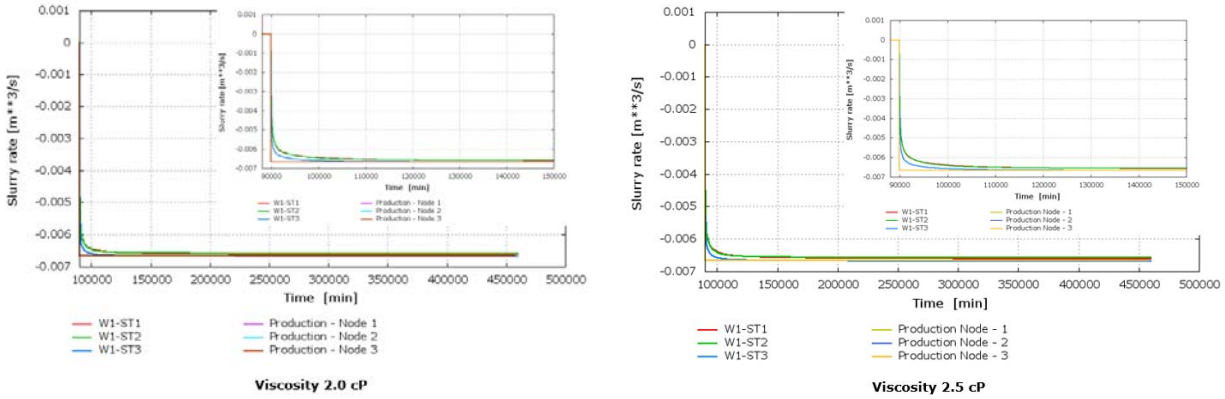

Figure A.1: Slurry Rate Responses - Viscosity Iterations

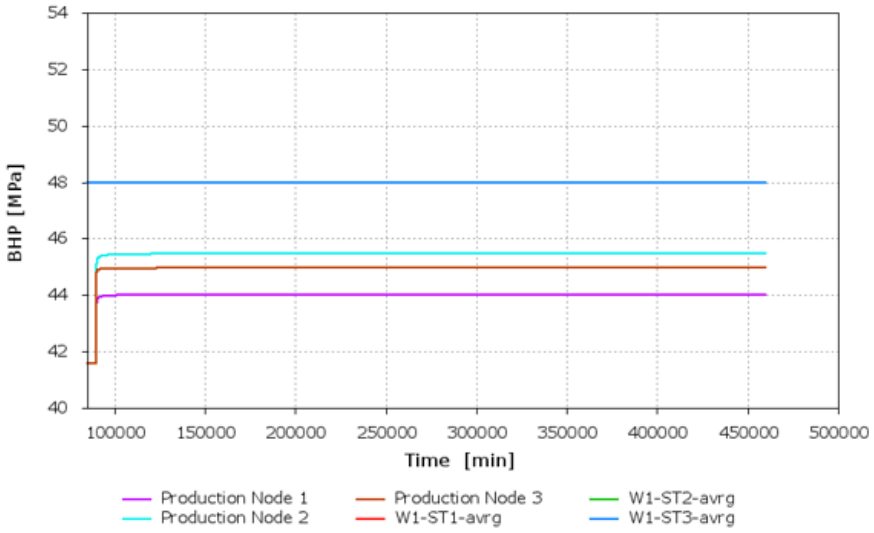

Viscosity 1.5 cP

Avg Δ Pressure = 31.90 bar

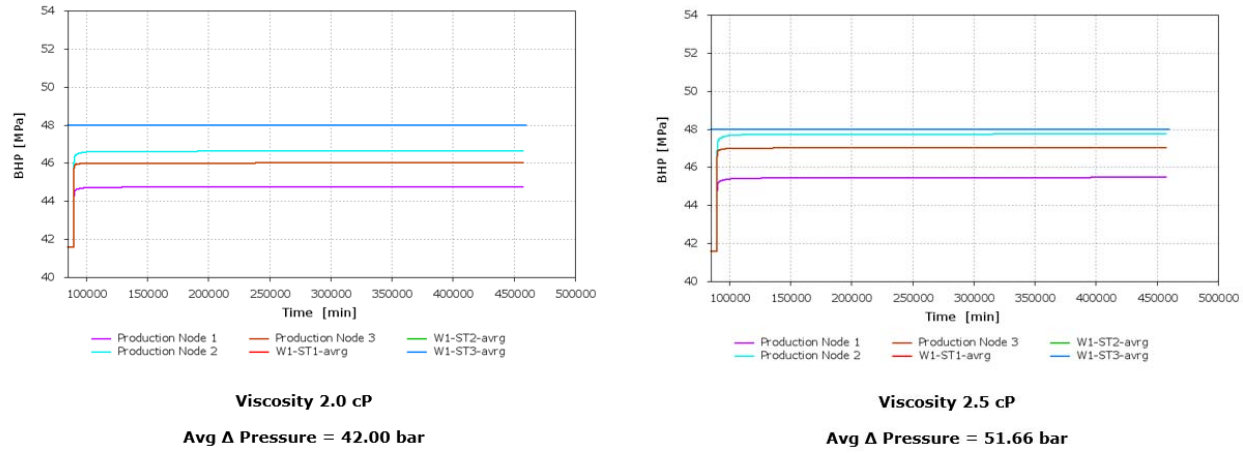

Figure A.2: Bottom Hole Pressure Responses - Viscosity Iterations

2D Lauwerier Simulation

The results for other flow rates have been illustrated in figure A.3

Volume Flow Rate : 20 L/s

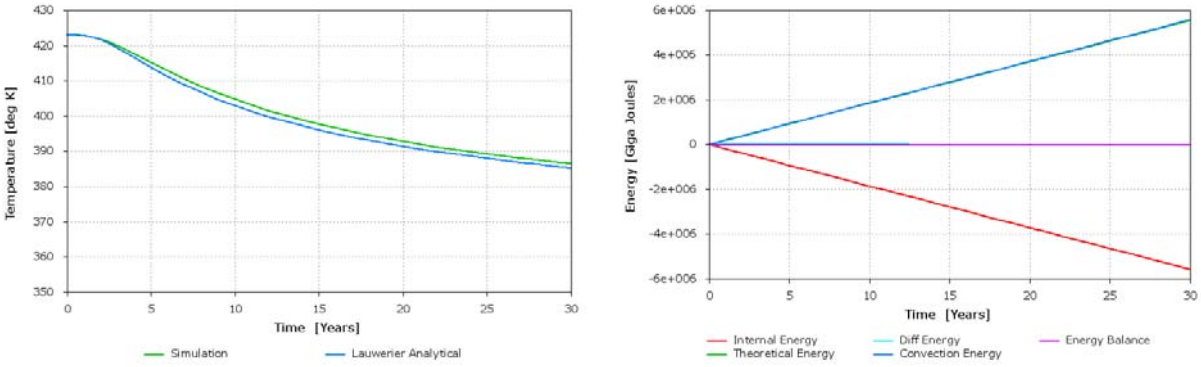

Volume Flow Rate : 30 L/s

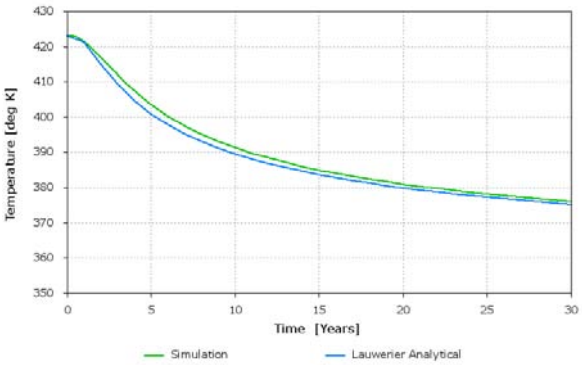

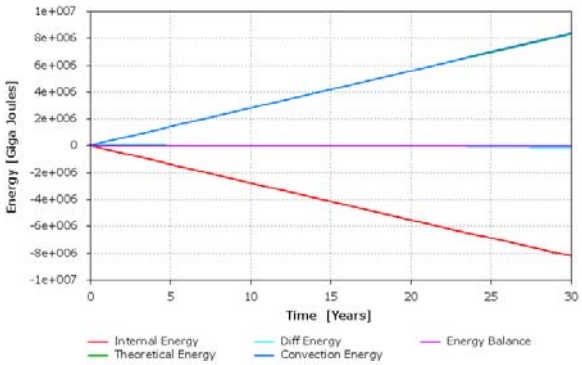

Volume Flow Rate : 40 L/s

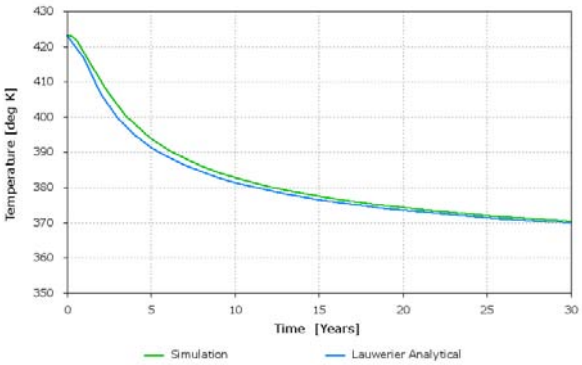

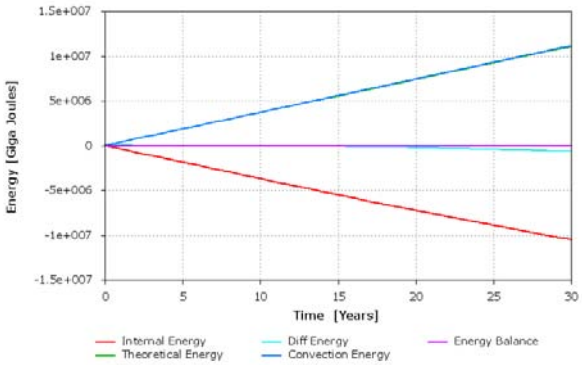

Volume Flow Rate : 50 L/s

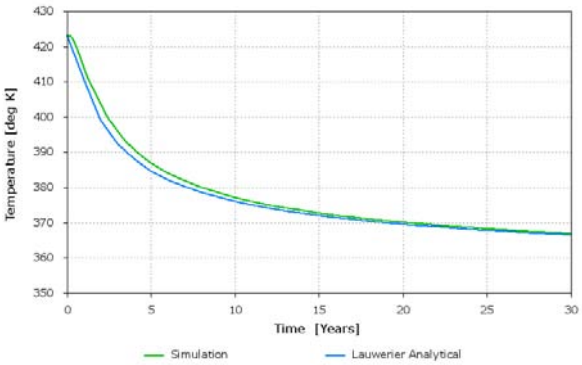

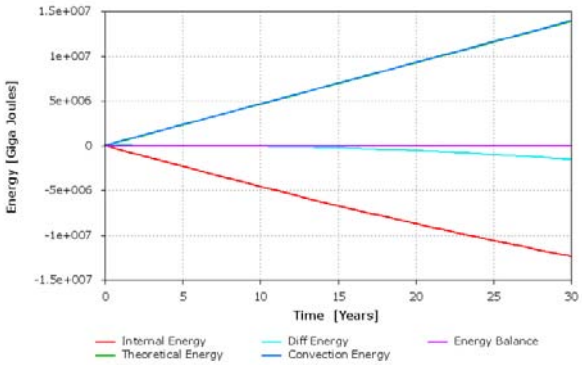

Figure A.3: 2D Lauwerier Simulation - 20, 30, 40, 50 L/s

Hydraulic Fracturing - Conductivity, Joint Opening & Activity

The figures for opening, conductivities and plastic activities have been plotted in figure A.4.

Plastic Activity [m^3] and Plastic Volume [m^3]

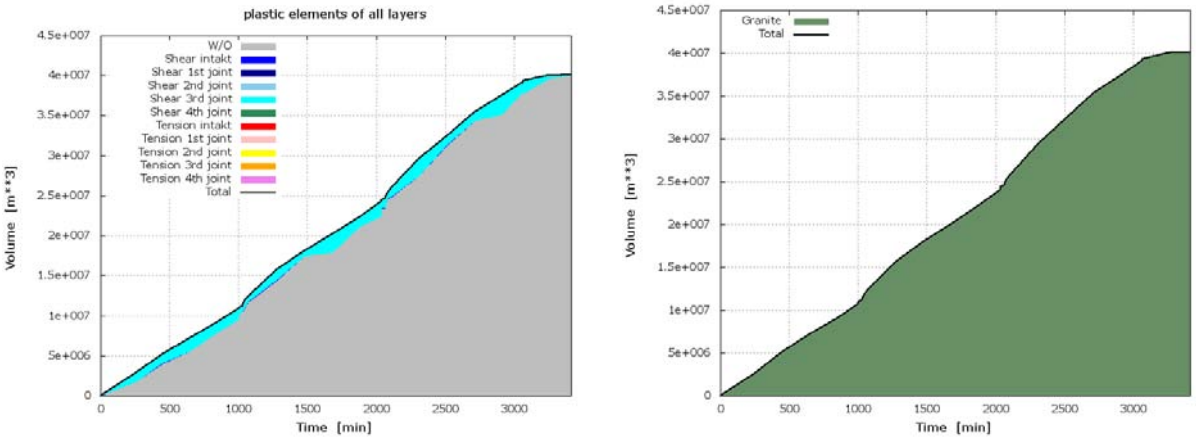

Joint Conductivity [m/s] & Joint Opening [m]

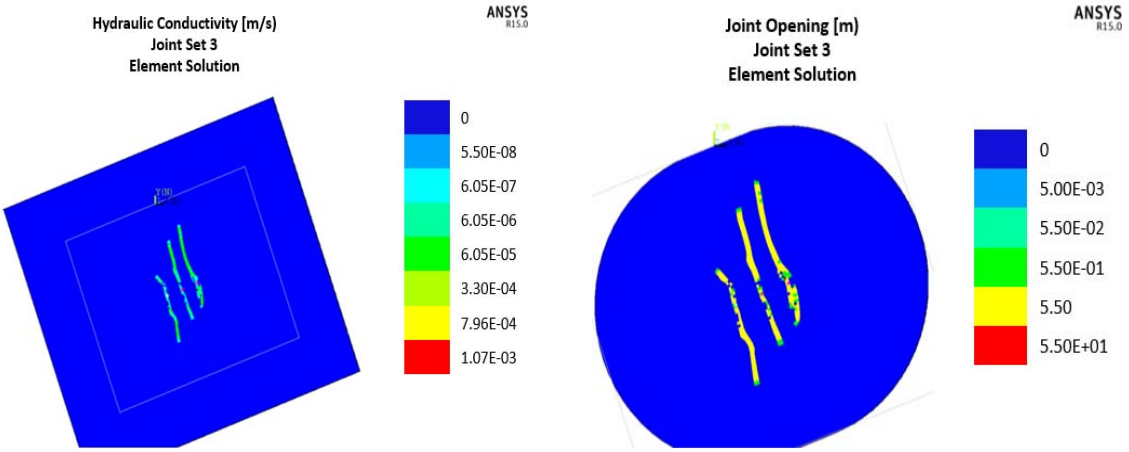

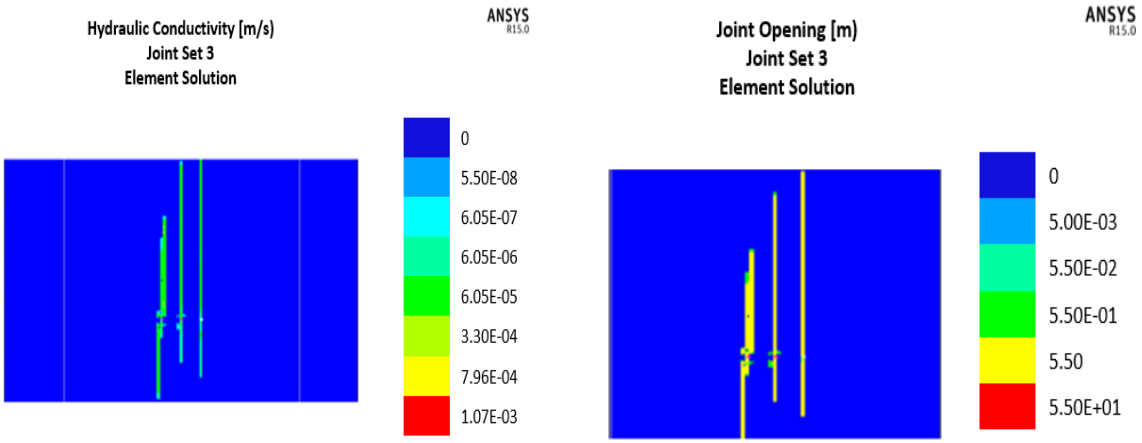

Figure A.4: Plastic Activity, Joint Conductivity & Joint Opening - Active Joint Set

Unstructured v/s Structured Fracturing - Hydraulic Height, Joint Opening Over Fracture Plane

The figures for hydraulic height and joint opening for structured & unstructured mesh have been plotted in figure A.6.

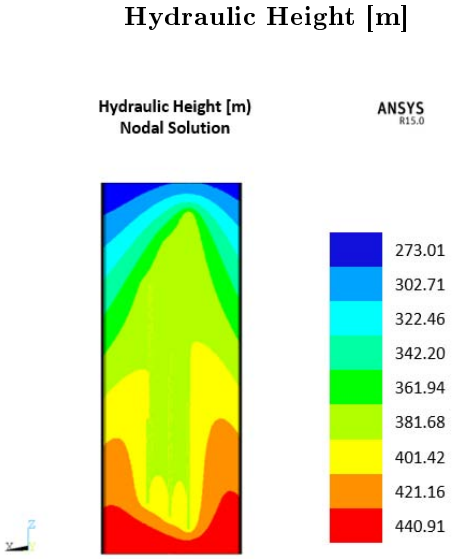

Joint Opening Over Fracture Plane - Stage 1 - Joint Set 3 [m]

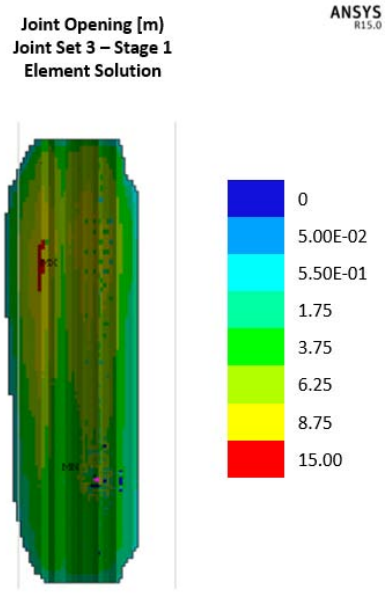

Joint Opening Over Fracture Plane - Stage 2 - Joint Set 3 [m]

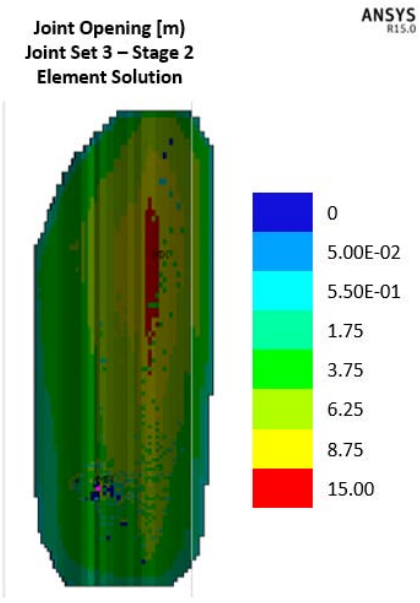

Joint Opening Over Fracture Plane - Stage 3 - Joint Set 3 [m]

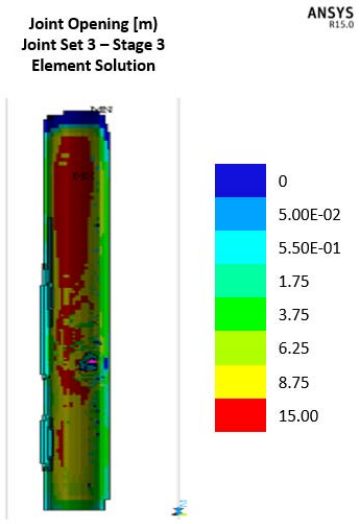

Figure A.5: Hydraulic Height & Joint Opening over Fracture Plane

Total Fracture Characteristics

Total Fracture Characteristics		
Well Connection Scenarios	Surface Area	Connected Height
Connected Surface Area (over and above Perforation – All Stages Connected)	1,239,185 m^2	652 m
Connected Surface Area (over and above Perforation – Two Stages Connected)	918,190 m^2	831 m
Connected Surface Area (over and above Perforation – One Stage Connected)	460,785 m^2	883 m
Active Joint Sets	Vertical Joint Set 2	

Individual Fracture Characteristics

Individual Fracture Characteristics	
Stage 1	
Vertical Extension	1198.11 m
Full Length	426.52 m
Total Surface Area	566,998 m^2
Stage 2	
Vertical Extension	1082 m
Full Length	533.3 m
Total Surface Area	610,905 m^2
Stage 3	
Vertical Extension	848 m
Full Length	513.70 m
Total Surface Area	619,719 m^2

Table A.1: Total & Individual Fracture Characteristics

Additional MOPs

The figures for additional MOPs of vertical extension, joint volume and fluid efficiency for the fracturing cycle have been plotted in figure A.7.

Vertical Fracture Extension [m] & Joint Volume [m³]

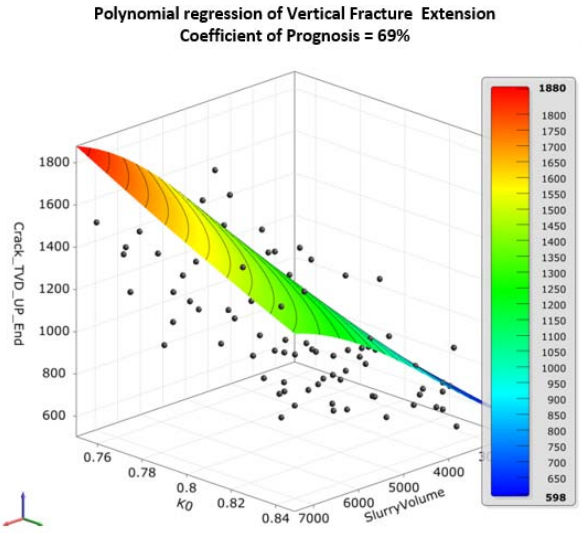

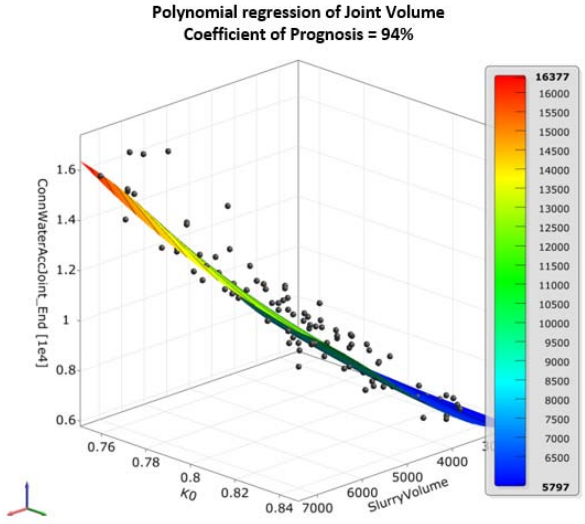

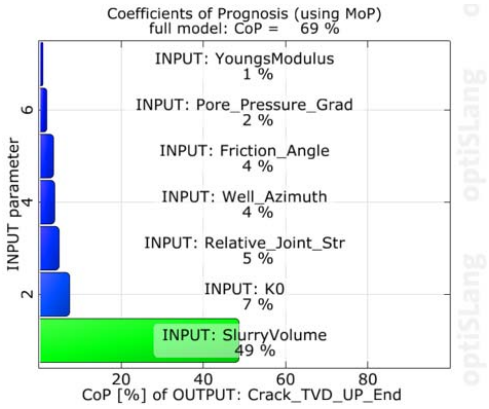

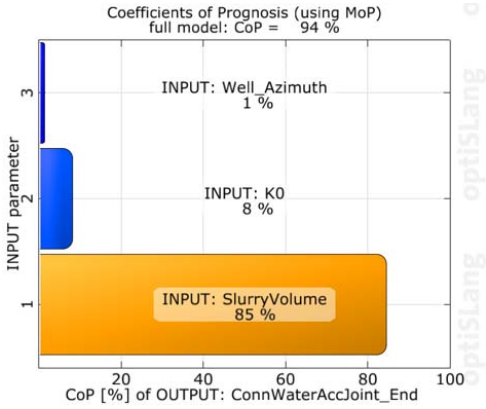

Fluid Efficiency

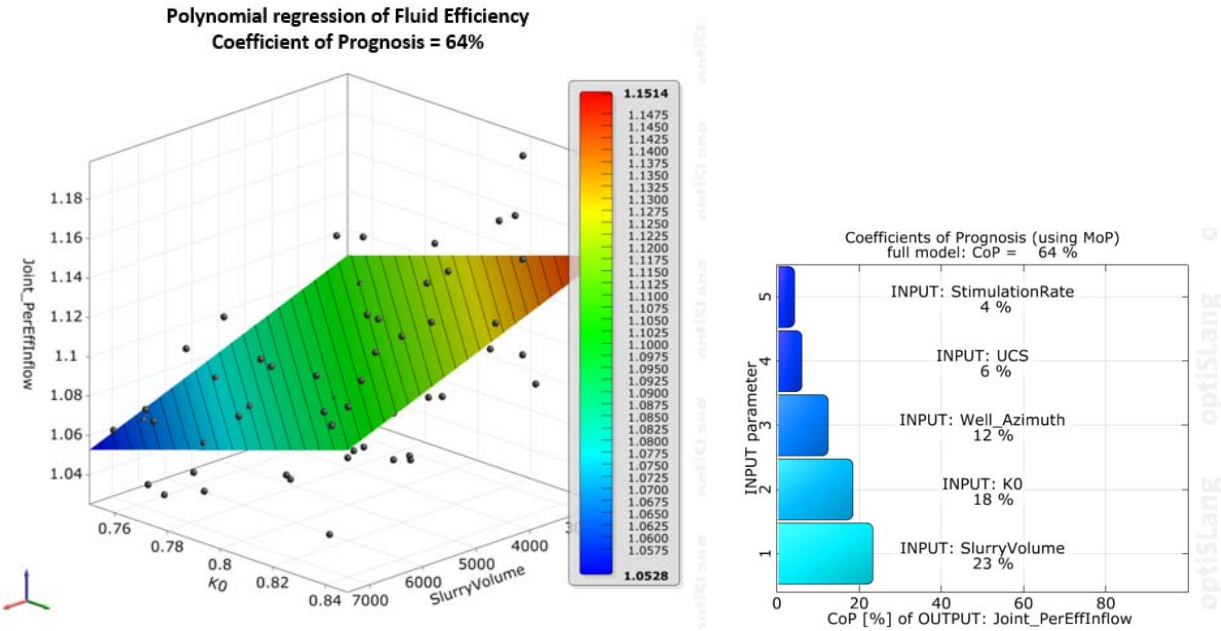

Figure A.6: Additional MOPs - Fracturing & Production

Tectonic Stress Regimes

The various tectonic stress regimes are illustrated in further detail in figure A.8. Compressive Stresses are positive as per geophysical notation where S1>S2>S3. The relative movement of tectonic plates based on the stress magnitude and orientation is also illustrated in the figure below.

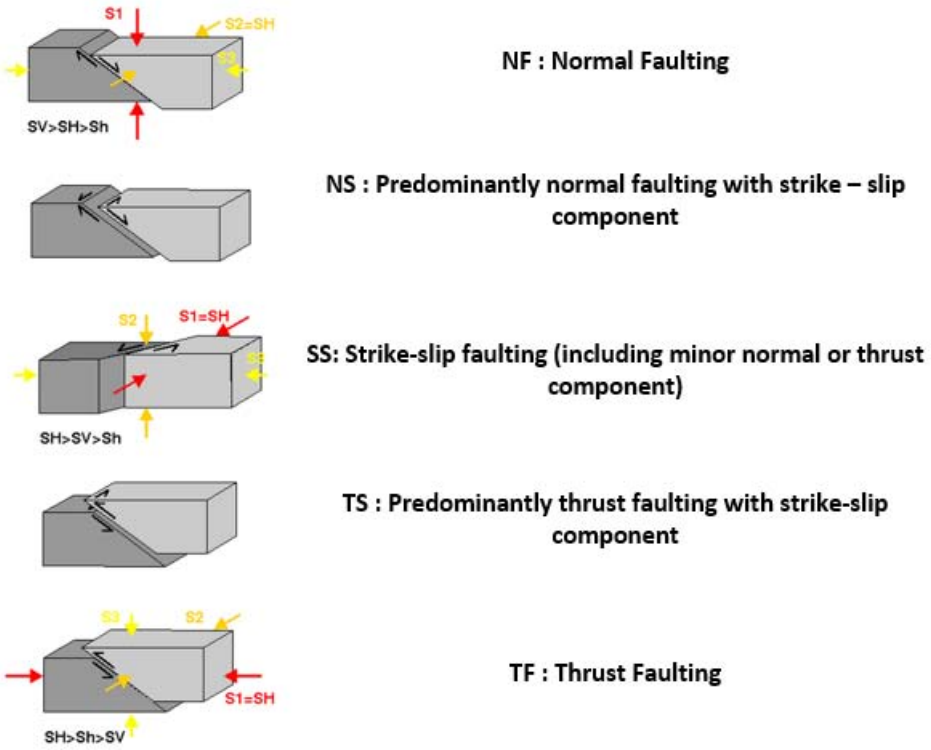

Figure A.7: Tectonic Stress Regimes and Movement of Rocks along Faults

REFERENCES

1. Bendall Betina, Huddlestone-Holmes Cameron, Goldstein Barry, *The Current Status of Geothermal Projects in Australia,* Proceedings of 38th workshop on Geothermal Reservoir Engineering, February 2013.

2. Bertani Ruggero, *World Geothermal Generation in 2007,* Proceedings European Geothermal Congress 2007, Unterhaching, June 2007.

3. *BP Statistical Review of World Energy,* June 2013.

4. Deo Milind, Roehner Richard, Allis Rick, Moore Joseph, *Reservoir Modeling of Geothermal Energy Production From Stratigraphic Reservoirsin the Great Basin,* Proceedings of 38th workshop on Geothermal Reservoir Engineering, February 2013.

5. Ehsan Mohseni Languri and Davood Domiri Ganji, *Heat Transfer in Porous Media,* Heat Transfer - Mathematical Modelling, Numerical Methods and Information Technology, Prof. Aziz Belmiloudi (Ed.), ISBN: 978-953-307-550-1, InTech, 2011.

6. Gangi A.F., *Variation of Whole and Fractured Porous Rock Permeability with Confining Pressure,* International Journal of Rock Mechanics, Mineral Sciences & Geomechanics, pp 249-257, 1978.

7. Glanz James, *Quake Threats Leads Swiss to Close Geothermal Project,* The New York Times, December 2009

8. Gravemeier Volker, *Advanced Computational Fluid Dynamics - Lecture Notes*, Applied Computational Mechanics, ESOCAET, 2015.

9. Heat Flow Fundamentals, *ANSYS - USER MANUAL*, version 14.5, 2014.

10. Iterative Solver, *ANSYS - USER MANUAL*, version 14.5, 2014.

11. Heidbach, O., Tingay, M., Barth, A., Reinecker, J., Kurfeß, D. and Müller, B., The World Stress Map database release 2008 doi:10.1594/GFZ.WSM.Rel2008, 2008.

12. Jelacic Allan, Fortuna Raymond , LaSala Raymond, et al, *An Evaluation of Enhanced Geothermal Systems Technology,* Technical Report - US Department of Energy, 2008.

13. Jirásek Milan, *Numerical Modelling of Deformation and Failure of Materials,* Lecture Notes, December 2000.

14. Kretzschmar H. J., Rafiee M., Schmitz S., *MFRAC – Sensitivität, DBI – Zwischenbericht für OPTIRISS – Modellgruppe.* DBI Freiberg, April 2013.

15. Lauwerier H.A., *The Transport of Heat into an Oil Layer caused by Injection of Hot Fluid,* J. Appl. Sc. Res., Section A, Vol 5, Nr 2-3, pp 145-150, 1955.

16. Louis C, *A Study of Groundwater Flow in Jointed Rock and its Influence on the Stability of Rock Masses*, Rock Mechanics Research Report 10, 90 pp., Imperial College London, London, 1969.

17. Meyer Bruce, Bazan Lucas, *A Discrete Fracture Network Model for Hydraulically Induced Fractures - Theory, Parametric and Case Studies,* SPE Hydraulic Fracturing Technology Conference, Woodlands, Texas, 2011

18. multiPlas – elastoplastic material models for ANSYS, *MultiPlas - USER MANUAL*, version 5.2.0, DYNARDO GmbH, Weimar, 2015.

19. Nemat-Nasser S, Abé H, Hirakawa S, *Hydraulic Fracturing and Geothermal Energy,* Proceedings of First Japan-United States Joint Seminar on Hydraulic Fracturing and Geothermal Energy, November 1982.

20. OnePetro, *Gridding in Reservoir Simulation,* Petrowiki - Society of Petroleum Engineers, 2015.

21. Pierce Brenda, *Goethermal Energy Resources,* NARUC Winter Meeting, February 2010.

22. R. Courant, E. Isaacson and M. Rees, *On the Solution of Non-linear Hyperbolic Differential Equations by Finite Differences*, Commun. Pure Appl. Math., 243–255, May 1952.

23. Report, *Modellsimulation der Petrothermischen Energiegewinnung nach Ausbildung eines Optimalen Risssystems als Geowärmetauscher,* OPTIRISS Petroenergie, Gastechnologisches Institut, DBI Freiberg, January 2014.

24. Saeid S, Barends F.B.J, *An Extension of Lauwerier's Solution for Heat Flow in Saturated Porous Media,* Proceedings of COMSOL Conference Milan, 2009

25. Schlegel Fabrice, *Understanding Stabilization Methods*, COMSOL Blog, May 2014.

26. Simo J C, Hughes TJR, *Computational Inelasticity,* Mechanics and Materials, Springer, 1998.

27. Weijers L, *Evaluation of Oil Industry Stimulation Practices for Engineered Geother-mal Systems*, Report DOE-PS36-04GO94001 from Pinnacle Technologies ,October 2007

28. Will Johannes, Most Thomas, *Metamodell of Optimal Prognosis (MOP) - an Automatic Approach for User Friendly Parameter Optimization*, Weimar Optimization and Stochastic Days, Weimar, 2009.

29. Will Johannes, Most Thomas, *Sensitivity analysis using the Metamodel of Optimal Prognosis*, Weimar Optimization and Stochastic Days, Weimar, 2011.

30. Will Johannes, Schlegel Roger, *Simulation of Hydraulic Fracturing of Jointed Rock,* Proceedings of European Conference on Fracture, 2010, Dresden.

31. Wittke White, Sykes R., *Rock Mechanics : Theory and Applications with Case Histories,* Berlin, Springer - Verlag, 1990.